INVESTIGATION ON ELEVATED TEMPERATURE WEAR BEHAVIOUR OF HVOF SPRAYED AND POST-PROCESSED ALLOY718-Al_2O_3 COMPOSITE COATINGS

Thesis Submitted for the Award of the Degree of

DOCTOR OF PHILOSOPHY

in

MECHANICAL ENGINEERING

By

SUNITHA K

Registration Number: 41900674

Supervised By

Dr. Hitesh Vasudev (24804)

School of Mechanical Engineering

(Professor)

Lovely Professional University, Punjab

LOVELY PROFESSIONAL UNIVERSITY, PUNJAB

2024

DECLARATION

I, hereby declared that the presented work in the thesis entitled "INVESTIGATION ON ELEVATED TEMPERATURE WEAR BEHAVIOUR OF HVOF SPRAYED AND POST-PROCESSEDALLOY718-Al_2O_3 COMPOSITE COATINGS" in fulfilment of degree of Doctor of Philosophy (Ph. D.) is outcome of research work carried out by me under the supervision _Dr.Hitesh Vasudev, working as Professor, in the School Of Mechanical Engineering of Lovely Professional University, Punjab, India. In keeping with general practice of reporting scientific observations, due acknowledgements have been made whenever work described here has been based on findings of another investigator. This work has not been submitted in part or full to any other University or Institute for the award of any degree.

(Signature of Scholar)

Name of the scholar: SUNITHA K

Registration No.:41900674

Department/school: Mechanical Engineering

Lovely Professional University,

Punjab, India

CERTIFICATE

This is to certify that the work reported in the Ph.D. thesis entitled **“INVESTIGATION ON ELEVATED TEMPERATURE WEAR BEHAVIOUR OF HVOF SPRAYED AND POST-PROCESSED ALLOY718-Al_2O_3 COMPOSITE COATINGS”** submitted in fulfilment of the requirement for the reward of degree of **Doctor of Philosophy (Ph.D.)** in the School of Mechanical Engineering, is a research work carried out by Pardeep Singh, Registration No.41900674 is bonafide record of his/her original work carried out under my supervision and that no part of thesis has been submitted for any other degree, diploma or equivalent course.

Dr. Hitesh Vasudev (24804)

School of Mechanical Engineering

(Professor)

Lovely Professional University,
Punjab

ABSTRACT

Power plants and the automobile sector face losses to the components like engine manifolds, turbine blades, and turbocharger housings. For instance, the efficiency of the power generated through the turbocharger in modern vehicles with extra forcing extra air into the combustion chamber, and the temperature of these components is limited by creep and corrosion resistance, which impacts the thermal effectiveness of the system as a whole. Furthermore, continual advances in materials development will demand still higher operation temperatures for such components. The types of degradation phenomena that affect materials used in high-temperature applications can vary greatly depending on the application, including wear, solid particle abrasion, overheating, erosion-corrosion, high-temperature corrosion, and so on. This includes anything from propulsion engines' brief operational times to the weeks, months, or even years required for chemical reactions or the creation of electricity.

The High-Velocity Oxy-Fuel process was utilized extensively amongst processes and is popular as a viable technology for various applications. The HVOF process gained popularity in many industries as it produces coatings of superior quality, flexibility, and cost-effectiveness. The high velocity and moderate temperature in this process result in lower porosity, high hardness, superior bonding between substrate and coating, high abrasion resistance, high density, fine finishing capability as compared to other coating processes, and lower oxide content. The capacity of materials to produce protective oxide scales on the surfaces is directly correlated with how well they operate in high-temperature aggressive situations. The coatings are anticipated to create protective oxides with a modest growth rate during service, which should prevent corrosive species from diffusing into the coating and subsurface of the coated material.

Super alloys and ceramic coatings were extensively utilized to reduce erosive wear at elevated temperatures. The oxidation resistance is given by Alloy718 (A718) matrix whereas the wear resistance is primarily owing to the reinforcement Al_2O_3. The current research is aimed to evaluate the high temperature "sliding wear" and erosion behavior of the GCI (Grey Cast Iron) substrate and seven compositions of coatings viz. Alloy718 (A718), Alloy718-10% Al_2O_3(A718/10AL), Alloy718-20%

Al_2O_3(A718/20AL), Alloy718-30% Al_2O_3 (A718/30AL) deposited by HVOF thermal spray coating process. The coatings viz. Alloy718 (PT-A718), Alloy718-10% Al_2O_3(PT-A718/10AL), Alloy718-20% Al_2O_3(PT-A718/20AL), Alloy718-30% Al_2O_3 (PT-A718/30AL) were further post-treated by using direct-aging (DA) process. The coatings are developed with an aim to enhance the turbocharger casing and engine manifold life by protecting against sliding and erosion wear in the energy conversion systems. The HVOF coatings have been sprayed at M/S "Metallizing Equipment Corporation Pvt. Ltd." (MECPL), Jodhpur, India.

The characterization of the deposited coatings has been carried out using techniques like EDS ("Energy Dispersive Spectroscopy"), SEM ("Scanning Electron Microscope"), XRD ("X-Ray Diffractometer"), OM ("Optical Microscope"), Micro-hardness Tester and Porosity Analyser. The thermal spray process of HVOF was utilized to deposit coatings of different compositions of Alloy718-Al_2O_3 powders on grey cast iron up to the thickness range of 200-230 µm with surface roughness in the range of 0.68 to 0.86µm. The porosity in general, has been found to be less than 2.5% for all the coatings. Alloy718-10% coated samples have shown the least value of cross-sectional and surface porosity in order of 0.50 and 0.86, respectively. The HVOF-sprayed coatings were discovered to have a micro-hardness that was more than the GCI. The PT-A718/30AL coating, which has a hardness of 912±16 HV, has enabled the hardness to be increased to its maximum value. The high micro-hardness for this coating was attributed to the high Al_2O_3 percentage present in the composition and dissolved laves phase within microstructure. The XRD diffraction pattern of the as-coated samples produced using the HVOF spraying approach specified the retained identity of the coating powder used and also showed the formation of low-intensity peaks of NiO observed in XRD analysis. A nearly uniform lamellar structure consisting of typical splat-like morphology was observed in the FE-SEM analysis.

All the HVOF-sprayed Alloy718-Al_2O_3 coatings were found beneficial in increasing the resistance to Sliding and erosive wear.

According to ASTM-G76, erosion testing was done with an air jet erosion tester ("Model: TR-471-800, Make: Ducom Instruments Pvt. Ltd., Bangalore, India"). Additionally, the erosion behavior of uncoated and coated GCI has been evaluated at 800°C at impact angles of 30° & 90°. For both the GCI substrate and coated simple, the "erosive wear rate" (*g/g*)—defined as the ratio of "wear mass" loss in g to the supplied erodent mass in g— has been computed. The eroded samples were examined using the SEM ("Scanning Electron Microscopy") method at both higher and lower magnifications.

The eroded surface's morphology shows the crack arrest by the coatings and micro-cutting and ploughing is responsible for the plastic deformation of coatings at a 30° impact angle, whereas the repetitive effect of erodent particles caused fatigue at a 90° impact angle and showed the brittle mode of erosion. The embedment of sand particles in the substrate was clearly revealed in the SEM micrographs. Based on the erosive wear rate, the erosion rates for the investigated coated and uncoated steel at 90° and 30 impact angles can be arranged in the following order:

As-sprayed: A718/30AL > A718/20AL > A718/10AL> A718>GCI

Post-treated: PT-A718/30AL > PT-A718/20AL > PT-A718/10AL> PT-A718

With the increase in Al_2O_3 content in Alloy718 alloy, the erosion resistance significantly increased and a ductile mode was seen in the case of Alloy718 coating, and for all Alloy718- Al_2O_3 coatings, a brittle mode of erosion was observed.

The sliding wear rate for PT-**A718/30AL** was reduced by 3.2 times and 2.8 from the substrate and as-deposited coatings. Whereas in the case of the **A718/30AL** sample, it is reduced by 2.1, and 1.8 times compared to substrate. The dry sliding wear rate of PT-**A718/30AL** specimens showed a 78% minimum abrasive wear coefficient from the substrate material. The fact that the PT-A718/30AL treated samples had the lowest possible abrasive wear coefficient was caused by the heat treatment, which caused a significant amount of Laves phase to dissolve in the matrix and increase the amount of Nb elements available for strengthening stages precipitation. The sliding wear resistance has been observed in the following sequence:

As-sprayed: A718/30AL > A718/20AL > A718/10AL> A718>GCI

Post-treated: PT-A718/30AL > PT-A718/20AL > PT-A718/10AL> PT-A718

ACKNOWLEDGEMENT

First and Foremost, I am very much heartily thankful to my dissertation Supervisor, **Dr. Hitesh Vasudev**, Professor in School of Mechanical Engineering, Lovely Professional University, for his invaluable guidance and support during the present research work.

I wish to thank **Mr. Shiv Kumar**, in-charge of FE-SEM, Institute Instrumentation Centre, IIT Roorkee.

I would like to thank my friends, **Mr. Bala Ganesh, Mrs. Satyavathi**, and all the fellows who helped me directly or indirectly during the entire period of this work.

I express my profound regards to my parents for their blessings and for being the main source of inspiration to succeed in my endeavours. I would like to express particular thanks to my father **Mr. K. Swamynath,** my mother, **Mrs. Deena Kumari** for her advises, care and love. I would like to express particular thanks to my father-in-law **Dr. K.B. Rajendra Prasad** for his encouragement and financial support to pursue Higher studies, and my beloved Husband **Mr. K. Amar Kumar** for his love and care. I feel blessed for having wonderful daughter **Ms. K. Hithyshi** and thank her for her constant support. I feel proud to my sisters and brother in laws **Mrs. K. Sandhya Selina** and **Mr. S. Karunakar** and younger sister **Mrs. K. Ruth Sucharitha** and **Mr. S. Kishore** for their extensive love and supporting me in my entire life.

I would like to thank everyone who supported me for completing this work successfully and I express my apology that I could not mention everyone individually. Above all, I would like to express my sincere gratitude from the core of my heart to **ALMIGHTY** for giving courage, strength and patience to carry out my research out.

(SUNITHA .K)

TABLE OF CONTENTS

LIST OF TABLES

Description **Page No:**

LIST OF FIGURES

Description **Page No:**

LIST OF APPENDICES

APPENDIX

Model: D8 Advance
Make: Bruker AXS Instruments, Germany
Radiation: Cu-Kα
Scan rate: 0.5 to 1° min−1
Scan range: 20° to 100°

Figure A-1: View of the X-Ray Diffraction Equipment Used for Phase Analysis.

Model: LT 23B
Make: Dewinter, India
Magnification:50 x, 100 x, 200 x, 500 x
Display: Large field
Interface: With USB Digital camera and Image Analysis Software (Dewinter Material Plus, Version 4.2)

Figure A-2: View of Optical Microscope.

Model: FEI Quanta 200
Make: FEG-SEM, Czech Republic
Operating voltage: 2-25 kV
Magnification: 25 x to 100000 x
Gun: Field Emission Gun (FEG)

Figure A-3: Typical View of the Field Emission Scanning Electron Microscope (FE-SEM) Used for Microstructural Investigation

Model: Economet VH–1 MD
Make: Chennai Metco, India
Indenters: Vickers
Test Load: 10 – 1000 gf
Operating Time: 15 s
Min Measuring Unit: 0.05 μm
Hardness Measuring Range: 5~2500 HV
Test Microscope Magnification: 400X (Measuring), 100X (Observation).

Data Output: LCD screen display, Inside Printer, RS-232.

Max. Sample Height: ~100 mm

Figure A-4: Typical View of the Vicker’s Micro-hardness tester

Model: Mettalurgical sample saw MS-10
Make: Ducom Pvt. Ltd, Bangalore, India
Capacity: 240 RPM
Blade Thickness: 200 μm

Figure A-5 : View of the Diamond Cutter Used for Sample C

CHAPTER 1

INTRODUCTION

1.1 SURFACE DEGRADATION

Engineering components used in power plants, gas turbines, and jet engines must work under extreme heat loads, and the effectiveness of these serviceable parts depends not only on the material's attributes but also on its surface properties. This is especially true for wear-resistant components since, in harsh settings, the component's surface must play a crucial role. Therefore, material behavior is solely dependent upon the material surface under which the material operates.

Ni-based coatings are highly common for applications involving wear and corrosion at elevated temperatures because they offer strong resistance to wear, effect, corrosion, and fatigue at these temperatures and are relatively less expensive. The alloy has good wear resistance owing to the elements' promotion of the development of hard phases. The alloy has high-temperature corrosion resistance due to chromium and nickel. In addition, many researchers, including Zikin et al., Guo et al., Serres et al., Rodriguez et al., and Gonzalez et al. examined the various steel substrates noted the improved performance of coated samples. Additionally, it was noted by Ahn et al. and Garca et al. that adding hard reinforcement particulates like VC, SiC, TiC, Cr_3C_2, NbC, and WC to a Ni-based matrix improved wear performance. Al_2O_3 is a commercially accessible hard coating that is most frequently utilized for wear-resistant uses owing to its beneficial qualities including low coefficient, “high melting point”, and high hardness of thermal expansion. Different authors such as Shu et al., Dhakar et al. Molina-Claros et al., and Yao, Bolleli et al., examined the that coatings with hard-formed phases had superior wear resistance compared to Ni-based coatings alone.

Galedari et al. evaluated the wear characteristics of several materials and indicated that owing to its composition, super alloy (Inconel-718) must be taken into consideration for providing wear resistance. Therefore, composite coatings made of superalloys as well as thermally stable reinforcing particles are a promising option for use in hostile environments where wear and corrosion protection is required. Tungsten carbide (WC), titanium oxide (TiO_2), silicon carbide, chromium carbide (Cr_3C_2), aluminium oxide (Al_2O_3), etc. are all examples of hard phases that may be utilized as reinforcement additives.

1.2 ROLE OF POST-HEAT TREATMENTS.

However, owing to flame temperature and rapid cooling, unwanted residual stresses occur due to the formation of cracks and pores in microstructure which in turn weakens the developed coating’s strength. The thermal spraying method known as HVOF ("High-Velocity Oxy-Fuel") operates in the middle-temperature range. Therefore, HVOF sprayed coatings need to be appropriately heat treated or post-processed to improve adhesion among splats and reduce porosities. Heat treatment of Ni-based coatings established with the process of HVOF was conducted and authors reported significant enhancement at the micro-structure level in the form of decreased levels of porosity, hard phases’ uniform distribution, and also there was a reduction in micro-cracks and un-melted particles.

1.3 HIGH-TEMPERATURE EROSION.

The erosion of the surface takes place owing to the striking of abrasive particles on the surface and this produces craters, pores, and detachment of material from the working area. Praveen et al. (2015) reported the formation of cracks and erosion at the surface of SS-304-graded stainless steel. Moreover, the different failure mechanisms have been studied at several impact angles. The unburned carbon and oxide particles at high temperatures strike the material’s surface and this results in the surface failure of the component. A higher maintenance cost is required there and sometimes replacement of components is needed. These are stringent problems in industries and researchers have been continuously developing new materials for high-temperature applications.

The failure of the surface due to oxidation and erosive wear can be found in engineering components used in automobiles, aerospace, production lines, and the petrochemical industry. Corrosion and erosive wear both are common forms of surface degradation of engineering components.

Erosive wear is owing to the striking of hard particles on the surface (Finnie, 1960). The protection of surfaces is therefore required which can provide wear resistant in the type of coating and is a good solution to prevent the surfaces from wear (Ma et al. 2014; Balla et al. 2010; Gupta et al. 2011 and Oladijo et al. 2012).

1.4 PREVENTIVE MEASURES .

The prevention is necessary for the prolonged life of components. However, corrosion and wear cannot be terminated completely but can be reduced to the extent that their costs could be reduced.

Many protective techniques are used by industries to combat this problem and still research is going on, especially for high-temperature applications. Some methods can help to reduce high-temperature wear and corrosion:

- One method is to change the bulk material with some material that can withstand highly aggressive environmental conditions. The whole component needs replacement in this method and therefore the protection of the surface can be achieved.
- Another way is a surface modification of material by using a coating to combat the problem of failure of materials at high-temperature applications. Since composite coatings can provide a multiset of properties cheaply and easily utilizing coating techniques and the material can provide good mechanical strength against erosion and sliding wear (Li et al. 2003; Liu et al. 2001; Sidky and Hocking, 1999).

The researchers have focused continuously on the development of new coating techniques and have given importance to surface degradation problems in engineering applications. The use of the coating in any of the products can increase its value by 10% in terms of its cost (Matthews et al.1998). Some methods can avoid the failure of material surface and are advisable such as shielding of material, design of types of equipment, alloy selection, and protective coatings for the materials in aggressive environments (Stringer, 1987 Heath et al. 1997). Coatings techniques can provide numerous options for materials from polymers to ceramics and mechanical, thermal, and electrical properties can easily be achieved for protection (Sidky et al. 1999; Sidhu et al. 2005 and Chatha et al. 2012).

1.5 COATING TECHNIQUES .

Coatings are utilized for room and high-temperature applications and even for aqueous conditions like seawater. The various classes of coatings that have been used for the deposition of engineering components are given in **Fig. 1.1** (Goyal et al. 2010).

The life of the material can be increased by using these techniques to prevent the formation of scales (Bala et al. 2009). Amongst the all coating processes a thermal spray is an emerging technique to use with any class of engineering materials to achieve the relationship between multiple sets of properties.

1.5.1 Thermal spray coating methods .

In the early 19^{th} century, a scientist in Switzerland called Dr. Max Schoop designed a thermal spray process. He got this idea in mind after observing his little son who was playing with toy cannon. Mr. Schoop after watching his son found that an idea if metal can be melted and then predicated in the form of spray could eventually build up and stick with that material.

In the 1970s, new techniques come in the area of thermal spray process to produce and develop high-temperature and wear-resistant materials due to the increase in demand of industry (Knotek, 2001). The thermal spray coating approach is a widely utilized technique for surface modification in the form of coatings with a thickness even in microns.

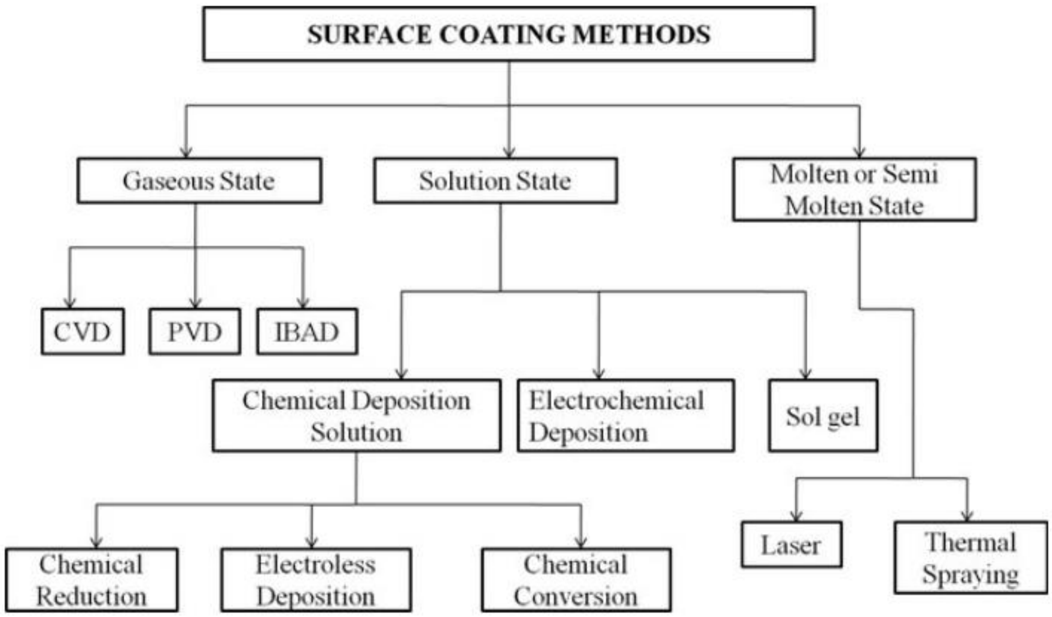

Fig.1.1. Various classes of coating techniques used for engineering applications (Goyal et al. 2010) .

The components under erosive wear, oxidation, abrasive wear, and corrosion can be coated and protected using this technique (Ishikawa et al. 1993; Singh et al. 2015; Kumar et al. 2015; Goyal et al. 2012; Marceau and Adjorlolo; 1995; Groshart, 1995). Thermal spraying is a method for depositing any substance that does not disintegrate, or dissociate when heated, evaporate, or sublimate. The metallic and non-metallic classes include polymers, alloys, metals, ceramics, and cermet's can be sprayed by the process of thermal spray. The feedstock material is mostly used in the form of powders from nano to micron sizes. In the process of thermal spray, the feedstock material is heated and then sprayed to deposit on the semi-molten in substrate material state or molten, and on cooling this is plastically deposited on the surface in the type of splats. This approach is extensively utilized in high-temperature uses like in aerospace engineering, manufacturing processes, and space exploration (Nicoll, 1992; Nakagawa et al. 1994; Thakur et al. 2013). In particular, HVOF-sprayed coatings are utilized in engineering components for corrosion and wear resistance including engine and machine tool casings, superheaters, boiler steels, pump impellers, and pipe fitting applications (Tan et al. 2005). The thermal spraying coating techniques that are used for the deposition of the coatings for corrosion and wear resistance are given below and were reviewed by (Heath et al, 1997):

- HVOF
- Spray and fuse method
- D-Gun (Detonation Gun) spray
- Cold spraying (CS)
- Air and Vacuum plasma spraying
- Flame spraying with a wire or powder.

There are various spraying parameters of the HVOF process including particle speed, temperature of the flame are presented in **Fig.1.2.** The comparison shows that the PS ("Plasma Spray") has a maximum temperature while cold spray has a minimum temperature. The HVOF covers both characteristics of high velocity and sufficient temperature for the coating deposition. The bond strength is achieved by good particle velocity and this results in good hardness and a coating with less porosity. HVOF was most effective for depositing cermet materials and especially corrosion-resistant alloys (hydroxyapatite, aluminium, nickel-based, stainless steels, and so on (Kuroda et al. 2008).

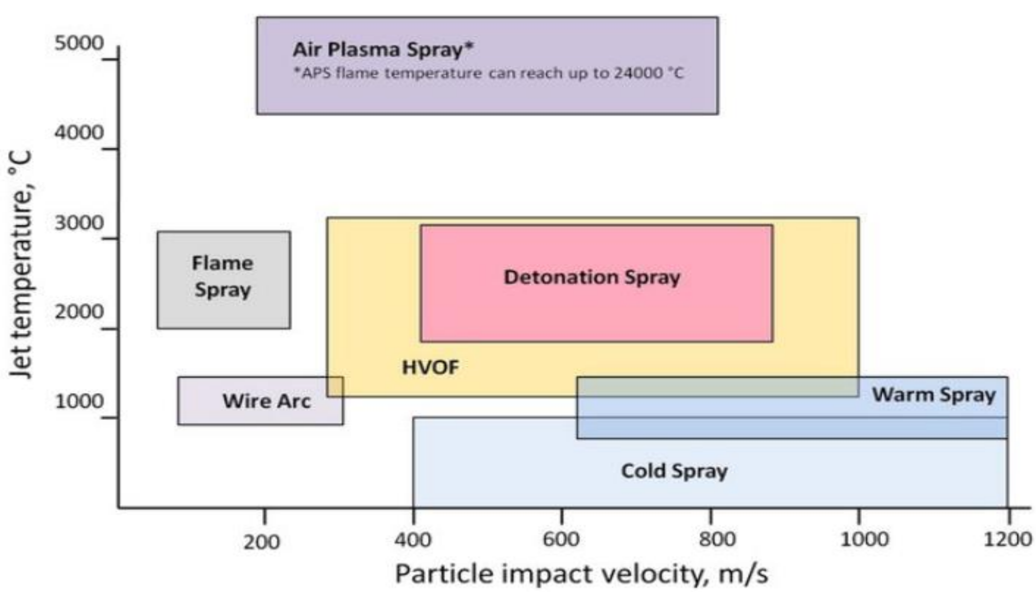

Fig.1.2. Comparison of various thermal spray processes (Tokarev, 1996).

1.5.2 HVOF process.

In a family of thermal spraying, a new technique called HVOF was introduced in the 1980s. A schematic diagram of the HVOF process is revealed in **Fig. 1.3** along with the built-up mechanism of coating. In the HVOF, O_2 and liquid of gas fuel are burnt and combustion takes place to generate a flame this flame is accelerated with feedstock powder and sprayed on the substrate to be coated. The hot gas at very high pressure near about 1 MPa flows via a nozzle having a converging-diverging cross-section. The powder particles' velocity or jet velocity reaches up to 1000 m/s. The feedstock powder is injected and it achieves a velocity of 800 m/s. The jet of powder and hot gas then mixes and accelerates toward the substrate materials. The jet of powder and gas strikes with the substrates then it forms splats and is finally plastically deposited on the substrate with mechanical bonding. The HVOF process produces a coating with very less porosity and higher bond strength [Brandt, 1995]. Bonding occurs mostly as a function of kinetic energy rather than thermal energy. The difference between HVOF from other spray processes is revealed in **Table 1.1.**

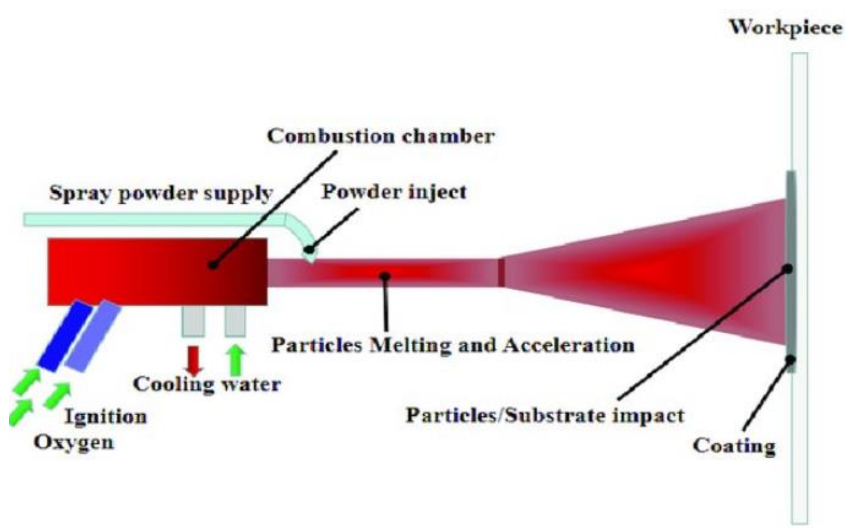

Fig. 1.3. Schematic representation of the HVOF process and built-up mechanism of coating (Mattews, 2004) .

In thermal spray coating approaches HVOF technique is gaining popularity for coating material, high velocity produces higher bond strength, lower porosity content, and dimensional restoration (Gill and Staia, 1999). The coating was used in this method, which can reach 1000 m/s (Lugscheider et al. 1998). Furthermore, the excellent coating quality (Liu et al., 2003 Sidhu et al. 2010) can be achieved. Compared to conventional thermal spray coating methods, the HVOF process can deposit coatings with higher levels of hardness, extremely low levels of oxidation, strong abrasion resistance, reduced porosity levels, and higher levels of erosion resistance (Liu et al. 2003; Zhao et al. 2002; Mann et al. 2001; and Lee et al. 2000).

HVOF process can provide lower oxidation during the coating process owing to high velocity, high hardness of coating due to good bond strength, and high resistance to corrosion due to less porosity (Bala et al. 2010; Sidhu et al. 2006; Guilemany et al. 2006; and Matthews et al. 2004). High bonding coatings that have better hardness, reduced porosity, and higher density may be deposited thanks to high velocity's unique properties. The process of HVOF is a member of the family of thermal spraying techniques and can provide coatings with fewer pores, greater hardness, improved bond strength, as well as less decarburization as compared to thermal spraying techniques.

Table 1.1 Attributes for various thermal spray processes (Pawlowski, 1995) .

Process of Coating	**Heat Source**	**Feedstock material**	**Feedstock powder temp (°C)**	**Powder Velocity (m/s)**	**Deposition rates (Kg/hr)**
Flame spray	Oxy-acetylene	Powder or wire	3100	40	2-5
Plasma spray	Plasma arc	Powder	10000	200-400	3-8
LPPS	Plasma arc	Powder	11000	200-400	3-8
Detonation spray	O_2 acetylene-N_2+gas detonation	Powder	4700	800	0.6
HVOF	Oxyfuel combustion	Powder	3000	800	2-4

The fuel combustion takes place in a “combustion chamber” in the HVOF process and the burning of liquid with oxygen produces intense heat along with high pressure. In the case of the HVOF process, there is a feature of high velocity with a moderate temperature range which helps in the deposition of coating with lower porosity and produces a coating with good properties. This method is extensively utilized for nickel deposition-based alloys. This is also used for depositing carbide coatings and stainless-steel feedstock powders.

Characteristics of the HVOF process

The main factor in HVOF's success is the extremely high kinetic energy created and transmitted utilizing space-age rocket propulsion technology between the HVOF unit and the substrate, finally leading to the high-velocity particles when practically embedded with substrate and forming an excellent coating with the required following features of a coating:

The HVOF coatings in comparison to the other thermal spraying methods have a higher erosion resistance, fewer porosity levels, higher abrasion resistance, very low oxidation, and high hardness (Liu et al. 2003; Zhao et al. 2002; Mann et al. 2001; and Lee et al. 2000). These characteristics of HVOF coatings result in the formation of erosion, corrosion as well as wear resistant coatings.

a. During the HVOF-spraying process, powder particles commonly consist of three regions which are fully melted, partially melted as well as unmelted zones. This results in the exhibition of characteristic splat such as layered morphologies owing to deposition as well as molten or semi-molten powder particles’ re-solidification (Dent et al. 2001; Kong et al. 2003 and Zhang et al. 2003)
b. Dense coatings offer better “corrosion resistance” as compared to porous coatings because pores can reduce a coating's ability to resist corrosion over time (Guilemany et al. 1997 and 1998; Zhao et al. 2004 and 2005). The coatings applied by the HVOF-spraying technique are extremely dense and have low porosity levels because of the high velocity and strong impact of the sprayed powder particles.

This is the important reason for the application of deposition of hard metals and cemented carbides such as WC/Co and Cr_3C_2-NiCr since these have high density and extreme wear resistance (Chidambaram, 2003).

. Liu et al. examined the mechanical characteristics, microstructure, as well as abrasion wear resistance of titania/ alumina ceramic coatings made of nano- and micro-structured powders that were applied using the HVOF and PS ("Plasma Spray") techniques (2003). The authors concluded that HVOF deposition resulted in very thick ceramic coatings with hardness as well as fracture toughness that were greater.

Advantages of the HVOF process

- High-velocity results in low porosity levels.
- Hard and tough coatings provide high wear resistance.
- Less porosity gives the surface better corrosion resistance.
- Mechanical bonding and plastic deformation of sprayed feedstock provide high strength
- Less exposure time due to high velocity restricts oxide content.
- Retention of powder chemistry due to reduced time at temperature.
- A wide range of feedstock powder from nano to conventional sizes can be sprayed and smooth coatings can be obtained.

Applications of the HVOF process

- There are several advantages that make this process very promising for repair and for producing a wide range of industrial components. There are many examples like pipelines in oil refining industries, blades in turbines, cylinders, and rings; and bearing-related components, pump elements, pistons, sleeves, valves, shafts, and seals.
- This process has many applications for protection against corrosion and the lack of process-induced oxidation offers enhanced properties.
- In the electrical & thermal engineering field, there is an absence of process-induced oxidation and it offers enhanced conductivity in the coatings.
- This process is also used in the aerospace engineering field and it is mostly used for coatings in gas turbines and in the form of aluminium and coatings of its alloy.

- Retrieval and repair of the parts and the plate stocks that are mostly used in aircraft structures.
- Repair and maintenance of worn surfaces can be done for wear resistance and corrosion resistance coatings can also be produced.

1.6 SUPERALLOYS.

In this modern era, advanced engineering applications come into the picture like machinery operated at high temperatures including rocketry, aerospace engine parts and dies, etc. The material required for these applications has to withstand raised temperature ranges from 200-1200°C. The properties that can be retained at these temperature ranges are the prior requirement of the material to be used in these applications. Superalloys are heat-resistant nickel-based alloys and iron-nickel alloys that can withstand 1000°C. These materials exhibit strength, resistance, and creep resistance and can bear thermal cycling due to their metallurgical stability (Davis, 1997; Ramesh et al. 2011).

In general, nickel-based alloys are utilized in high-temperature engineering apps and then iron-based alloys are also used. The extensive use of nickel-based alloy is due to its metallurgical properties. The nickel-based alloy has a face-centered cubic (FCC) structure at room temperature and this structure does not change even at high temperatures while in the case of iron and cobalt, the structure changes after transformation temperature. Therefore, due to the stability in the structure of nickel-based alloys, these are preferred for high-temperature uses. The superalloys have a surface stability of up to 85% of their melting points temperature (Metal Handbook, 1961).

The desired properties required for high-temperature applications can be achieved by the use of composite coating combinations. In composite coatings, usually, a hard reinforcement like Al_2O_3, WC, SiC, TiO_2, and Cr_3C_2 is embedded in the softer matrix such as Ni, Cr, and Co. Initially, Ni-20Cr coating was deposited with HVOF for wear resistance and it showed good performance up to 650 °C. However, the Fe diffusion from the workpiece to the coating took place. Furthermore, the Ni-50Cr coating reduced the problem of Fe diffusion to the substrate (Sundararajan et al., 2004). These both coatings belong to the category of mnemonics and are widely used for high-temperature oxidation resistance. In certain applications, such as gas turbine blades, turbochargers, rocketry components, and machine apparatuses, protection against "erosive wear" is also necessary in addition to oxidation resistance (Kaushal et al., 2011). Hence, a requirement of hard phase became the secondary requirement. Optimum combinations of properties are necessary for high-temperature applications, and composite coatings may be able to provide them. The use of composite coatings with Ni as a matrix and alumina as a reinforcement showed better resistance against slurry erosion up to 2.5 times (Grewal et al., 2014). The various Ni-Cr, NiCrTiC, and NiCrTiCRe coating combinations that were applied using the CS ("Cold Spray") technique demonstrated oxidation resistance up to 700°C (Bala et al., 2011). In comparison to NiCr-Cr2C3, Ni-Cr coatings showed superior resistance against cyclic oxidation, followed by WC-Co applied using the HVOF technique (Sidhu et al., 2005). Superalloys are the most popular alternative to these coatings, particularly for fatigue, mechanical, as well as creep strength at greater temperatures. These are nickel-based alloys with closely packed structures and retain their properties at elevated temperatures (Fecht et al., 2000). The Alloy718 coating deposited through Plasma spraying (PS) mild steel resulted in an improved performance against slurry erosion (Ramesh et al., 2011). However, studies of HVOF-sprayed Alloy18-Al_2O_3 composite coating for high-temperature wear are scarce within literature.

The current work investigates the evaluation of sliding wear at higher temperatures and high-temperature erosive wear of substrate material, namely GCI and three different compositions of coatings viz. Alloy718, Alloy718-10% Al_2O_3, Alloy-20%Al_2O_3, Alloy718-30%Al_2O_3, deposited by HVOF spraying process. The standard post-heat treatment (Direct ageing) was used for super alloys-based coatings to enhance their mechanical and metallurgical properties and the main objective is to enhance the performance of substrate against the high-temperature erosive wear and sliding wear. The air jet erosion test is carried out at high temperatures for uncoated and coated material. Moreover, the sliding test was also conducted to know the behaviour of coatings and substrate. The weight change data were analysed for comparison of various coating compositions. The weight change data after air jet erosion testing and sliding wear provides information on volume loss and hence the erosion resistance of the coating was calculated.

CHAPTER 2

LITERATURE REVIEW

This chapter offers a comprehensive study of the literature with a focus on the performance of engineering materials used in high-temperature applications. The different techniques of the coatings on the working surface and the effect of the surrounding environment were studied. The HVOF spraying process has been studied and discussed with regard to wear resistance and air jet erosion at high temperatures. The wear and erosion resistant coatings for elevated temperature with Nickel based powders, Nickel plus various reinforcements, and also post-heat treatments of the developed coatings. The high temperatures is a subject of study that is now undergoing a lot of research. The relevant review literature by numerous researchers had been reviewed and particularly for the substrate material used and for Nickel based alloys and other applications. The problem has been formulated and objectives were defined after a critical review of the literature survey.

2.1 MATERIALS FOR HIGH-TEMPERATURE APPLICATIONS.

New challenges in engineering have been introduced with the invention of gas turbine engines (Furrer and Fehct, 1999). The high-temperature capabilities were the requirements for this engine. The use of iron base alloys had been replaced by nickel-based alloys. These nickel-based alloys have special properties to withstand high-temperature conditions. The further advancement in high-temperature resisting materials allowed the aircraft industry to produce engines for small, intermediate, and commercial aircraft (Fulton, 1994; Gunston, 1996). The temperatures in rim sections of gas turbines vary to a high range from 760°C to 815°C (DeMania et al., 1996). Therefore, such materials are required for these ranges, and at the same time cost is required to be more economical (Noel et al., 1997). The new nickel-based materials are much more efficient and are a compromise between economics and performance (Williams, 1996).

To meet the requirements of high-temperature wear-like problems, superalloys can be used. The demand for good mechanical performance at 650°C temperature is accomplished by the use of superalloys and particularly the Inconel series of Ni-Cr-Fe alloys (Thomas et al., 2006). Inconel series alloys belong to the class of Ni-Cr-based alloys and it covers a range of mechanical properties and compositions. At high temperatures, Ni and Cr provide resistance against oxidation, corrosion, carburizing, and other damage mechanisms.

Alloy-718 is a recent alloy used ad has adopted by industries in 1965. This is particularly used in rocket engines, gas turbines, and extrusion dies and containers.

2.2 PROTECTIVE COATINGS.

A material has to withstand aggressive conditions when working at high temperatures and is subjected to oxidation, erosion, and corrosion. The material fails due to these failures and therefore requires some surface modification to prevent the material from surface degradation (Pawlowski, 1995).

Many properties are required at the same time to avoid the failure of the material and the use of some combination of elements or different classes of coatings like composite coatings can fulfill this requirement and a coating enhances the service life of the component. They can be deposited and sometimes used for decoration purposes to the component from an aesthetics point of view. The primary advantages of coatings were summarized by Heath et al. (1997) and are given below:

- Any material from polymer to metallic could be coated with coating processes. Material selection can be optimized according to particular conditions under which a particular component has to work like corrosion and erosion. Surface properties can be different from the bulk material property.
- Functionally graded materials could be by combining for required corrosion and erosion resistance. Multi-layered coatings can also be helpful in some applications. For instance, a bond coat is used between the top coat and substrate to avoid the mismatch

of the thermal coefficient of expansion for two different materials. Therefore, coating materials can be tailored according to the particular requirement for any material.

- Unique microstructures and alloys can be achieved with thermal spray techniques which are impossible with bulk materials. These comprise composites and coating corrosion-resistant phases.
- The coating cost is lower than the bulk material and a coating provide improved service life of a component. Therefore, the cost/performance ratio of the coating in thermal spray coatings is interesting.
- The thermal spray coatings can even use on-site for repair and maintenance purposes with equipment. Hence, this technique has gained popularity for surface protection against corrosion or wear rates.

2.3 PROBLEMATIC AREA OF SURFACE FAILURE.

The basic reason behind the selection of this material was its broad use in the production of turbocharger housings, cases, furnace parts, and engine manifolds. The review of the literature was a critical stage for formulating the research problem and surface degradation of cast iron at elevated temperatures has been formulated after extensive review.

The erosion and sliding wear of the surface is a serious problem for the surface of turbocharger housings and engine manifolds made of cast iron. Cast iron is frequently utilized in the manufacture of turbocharger housings in addition to this, cast iron is commercially used in furnace parts, manufacturing of molds, brake shoe materials, and engine manifolds.

These all-engineering applications are subjected to elevated temperatures. In a cyclical and repeating way, hot air impacts the components’ surface, and the air include “dust particles”. The harsh climate are the main causes of the erosional deterioration of the surface. This research will focus on the prevention of surface by depositing nickel base superalloy in combination with ceramic phase (Alloy718-Al_2O_3) which would help the material against such failures.

2.4 POST-HEAT TREATMENT.

Alloy-718 is strengthened owing to precipitation of Ni_3 (Al, Ti, Nb) coherent precipitates: known as a) $\gamma^{/}$, b) metastable Ni_3Nb phase termed as $\gamma^{//}$ and, c) also the blocky MC carbides in Ni-Cr matrix. The metastable precipitates (Ni_3Nb) $\gamma^{//}$ are produced in the Alloy-718 after annealing across a long period within the temperature range between 550-850ºC [76].

Hence, following the heat treatment is to be performed on Alloy-718+Al_2O_3 coated samples. The standard post-heat treatment (Direct ageing) is used for superalloys to enhance their mechanical and metallurgical properties and the details of this heat treatment are as follows:

Heat the sample to 720°C and hold it there for 8 hrs further kept at 620°C for 8 hrs and then cool it in the furnace.

2.5 SOME EMERGING METHODS TO CONTROL HIGH-TEMPERATURE WEAR RATE .

There are various techniques that have been used for the surface modification process and they can help to attain the desired properties at the surface. Some of the techniques are discussed in this section.

2.5.1 Thermal spray coatings

This process has many variants which are HVOF, plasma spraying, and detonation gun spray. These processes can easily provide very hard, dense, and smooth coatings with accuracy and these processes are used for high-precision components like aeronautical components, steam turbine blades, and die (Holmberg and Mathews, 2009). The schematic illustration of this process is revealed in **Fig. 2.1.**

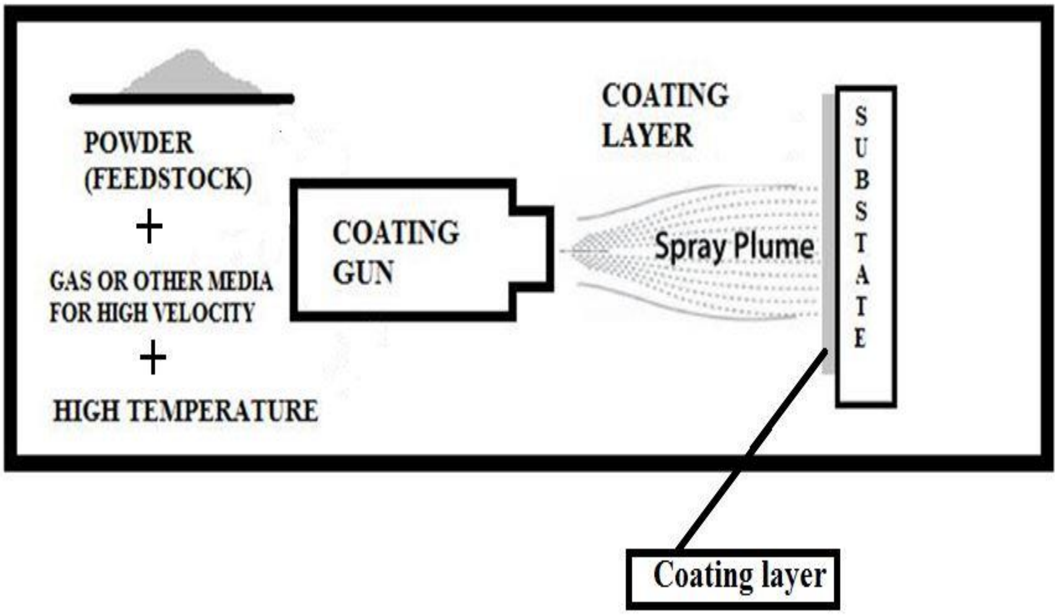

Fig.2.1. Schematic presentation of Thermal Spray Coating Process (Pawlowski,1995) .

TiO_2-13Al_2O_3 coatings were used for resistance against wear corrosion with the plasma spray. In this process, the powder is sprayed in the form of liquid droplets on the substrate and this finally plastically deformed after condensation. These coatings provide higher bond strength. The plasma spraying technique is used for ceramic coating due to the high temperature which completely melts at high velocity prevents the decomposition of powder particles they do not interact with the oxygen and unwanted phases are avoided (Priyantha et al., 2003).

Composite coatings provide some phases which prevent the surface of the cast iron (Hock et al., 2003) Zirconia coatings with plasma spraying technique have been used on gas engine components for increasing their strength at high temperatures (Liang and Ding, 2005) Zirconia is a light element and it goes into the grain boundaries and makes the structure denser.

Grain boundaries are open-structured and when zirconia diffuses it provides a barrier for the dislocations to move. It has also a great role in Ni_3Al single phase when added to it provides strength. Ni_3Al single phase not only provides strength to the coating but also decreases the corrosion rate. For this purpose, Ni_3Al plasma sprayed coatings were used on boiler steels. This coating showed very effective results against high-temperature corrosion (Sidhu and Prakash, 2003). Apart from zirconia, there are some other light elements like carbon and boron that can be used with Ni_3Al single-phase coating to increase its strength.

The actual environmental conditions in the case of boilers in thermal power plants are not very different from the die used for glass manufacturing. In thermal power plants, steam is generated through boilers and that is obtained by heating water with the help of coal. Heating of coal produces ash particles known as soot and which is in the form of black powder it contains similar elements which are present in glass material like silica, alumina, and magnesia and this further contains carbon and oxygen to form gases that rapidly damages the surface of heat exchanger walls, soot blowers' regions and the boiler surface of heating zone surface area.

The presence of these constituents accelerates the corrosion rate and results in premature failure of the surface of components. The ni-20Cr coating has been applied with a high-velocity oxy-fuel technique on boiler steels and thermal power plant (Sidhu et al., 2006). The use of such coatings provides wear and corrosion resistance at high-temperature conditions.

2.5.1.1 Powder thermal spray coatings

The study of high-temperature coatings reveals that nickel-based coatings have a great effect on the working surface's performance. Conventional powders having an size of 74 microns & nanopowders having size of 67 nm were deposited by a thermal spray coating technique called cold gun spray method and their results have shown a higher resistance to wear and increase in hardness as well (Kaur et al., 2015).

Thermal spray coatings techniques have shown good results for high wear resistance which also include the Cr_3C_2-NiCr and WC-Co coatings sprayed with the detonation gun spray method and this coating showed good adhesion to the base metal in high-temperature wear with no evidence of spalling and the oxide scale that forms in this aggressive environment (Kaur et al., 2011).

2.6 PERFORMANCE OF DEVELOPED COATINGS ON GCI.

Ni-based superalloy powder coatings provide protection against surface deterioration, although they aren't indestructible. In spite of this, the strength of the produced coating is diminished because of the flame temperature and quick cooling, which leads to the production of holes and fractures in the microstructure. When compared to other thermal spraying methods, HVOF operates in a more moderate temperature range. Therefore, proper heat treatment or post-processing of HVOF sprayed coatings are necessary to improve the adhesion among splats and to minimize porosities. Authors indicate considerable improvement at the micro-structure level after heat-treating Ni-based coatings created using the HVOF technique, including lower porosity, more uniform distribution of hard phases, and lower micro-cracking. Heat treatment of Ni-based coatings established using the process of HVOF was performed and authors reported significant enhancement at the micro-structure level in the form of decreased levels of porosity, hard phase's uniform distribution, and also there was a reduction in micro-cracks and un-melted particles. Hence, the focus of the current research is to investigate the corrosion and wear resistance of as-sprayed as well as post-processed Alloy-718+30%Al_2O_3 coatings.

2.7 BEHAVIOUR OF COATINGS AT HIGH-TEMPERATURE SETTINGS.

This aims the review the latest wear resistance coatings for elevated temperature by using the HVOF technique with Nickel based powders, Nickel plus various reinforcements, and also post-heat treatments of the developed coatings.

Parveen et al. [2015] examined a 60-weight percent NiCrSiB-40 weight percent Al2O3 composite coating that was applied via atmospheric plasma spraying on AISI 304 substrate material. SEM, an optical microscope, and an XRD have been utilized to analyze the coating surface. We assessed the coating's density, porosity, microhardness, and surface abrasiveness. An adhesion tester that pulls off was used to gauge the coating's adhesive strength. At 30° & 90° erodent impact angles, the erosion rate of samples that were coated and uncoated was assessed. To analyze the erosion mechanism, eroded sample SEM images were collected. According to the test findings, the coating shields the substrate from impacts at both 30° and 90° .

Premkumar. K, et al. [2018] examined the behavior of nanocomposite coatings. HVOF sprayed nanocomposite and traditional 27% Cr_3C_2 to 23% Ni- 50% Cr coatings were deposited onto SA 210 Gr C. Erosion experiments were performed at temperatures 450˚C and impact angles 30, 60 & 90˚. It was concluded, nanocomposite was better than conventional & uncoated substrate due to the incidence of a Cr_2O_3 layer that acts as a protective barrier against incoming erodent particles. Less porosity of nanocomposite was also found to be the reason for low erosion rates. At oblique angles erosion rate was higher for all materials showing ductile behavior. Moreover, both nanocomposite & conventional coatings provide 7.5 times & 3.5 times better erosion resistances at bleak (30˚) impact angle in comparison to the uncoated substrate.

H. Vasudev et al. [2019] used the HVOF method to integrate a bilayer of the 718 alloys into the NiCrAlY coating. The behavior of coated and naked samples under high-temperature oxidation as well as erosion was investigated. According to the authors, alloy-718 is more resistant to erosion and corrosion. High hardness and the development of stable oxides ($Al2O_3$ & $Cr2O_3$) are linked to improved resistance.

Vasudev. H, et al. [2019] in another investigation examined the impact of the microwave post-processing technique on the microstructure and "mechanical properties" of alloy-718 coating that is deposited using HVOF approach. The authors reported that there was a significant improvement in microstructure as porosity and micro-cracks were healed after post-processing. SEM micrographs of sprayed coating exhibit the existence of un-melted particles and pores but after post-processing healing of pores takes place owing to the flow of material in microwave processing. Furthermore, micro-hardness, fracture toughness, and surface roughness also improved.

Daram. P, et al [2019] also examine the effect of post-treatments on corrosion and microstructure performance of NiCrMoAlY alloy coating. The authors concluded that there is a reduction of pores after "heat treatment" that results in enhancing corrosion resistance.

Singh, et al. [2019] investigated the high-temperature tribological performance of a 65 percent ("NiCrSiFeBC")-35 percent (WC-Co) coating sprayed at high velocity with Oxyfuel at temperatures ranging between ambient to 800°C. The coating has been created on the "AISI H11" and "AISI H13". The as-sprayed coatings' microstructural properties, microhardness, porosity, surface roughness, as well as bond strength were assessed. Pin-on-disc tribometer tribology examination was carried out. The outcomes showed that the created coating performed significantly better than the untreated specimens, exhibiting decreased porosity and increased microhardness. At normal temperatures, the coated specimens wore mostly by abrasive processes. The predominant processes at high temperatures were found to be adhesive and oxidative wear.

Praveen. A. S, et al [2020] In another investigation authors deposited two weight compositions 1.4wt & 0.17wt % of nano Al_2O_3 with NiCrSiB by HVOF technique. Authors reported that with the addition of 1.4wt percent nano Al_2O_3 micro hardness increases from 576 Hv to 748Hv.

Chabbra et al [2020] Wear and surface degradation of tools ("die materials") in the sector of hot metal forming is a key issue that has a negative impact on the process economics. Interaction between the tool along with workpiece at greater temperatures causes the issue. Nevertheless, there is still a lack of data regarding the wear & friction of dies. The goal of the current inquiry was to investigate the potential of "Cr_3C_2-NiCr" surface coating using tribological (wear and friction) experiments. The coatings were made using an HVOF spraying process. The coated specimens' microhardness, bond strength, surface roughness, and porosity were discovered and examined. The uncoated and coated samples were then studied in the lab for elevated-temperature wear and friction. 25 N & 50 N loads were used in the investigation. At all test parameters, the coated samples demonstrated an improvement in wear resistance. At 400 °C, the coated sample indicated the lowest COF value and specific wear rate. The SEM method was used to investigate wear processes. The wear processes for the Cr_3C_2-NiCr-coated samples were found to be adhesive at room temperature and a mix of adhesive/ oxidative/abrasive at greater temperatures.

Chabbra et al [2020] focused on analyzing the wear and friction properties of Cr_3C_2-NiCr coatings used on the die steel material's surface by atmospheric plasma spraying. The specimens that had been sprayed were described. We assessed the microhardness, bond strength, and coating porosity values. At room temperature, 400°C, & 800°C under 2 loads of 25N & 50N, wear tests on the high-temperature "pin-on-disc" tribometer were conducted in the laboratory. The SEM method was used to examine the wear processes of each worn-out sample. Analysis was done on the particular wear rates along with friction coefficient values. The newly created coating outperformed its uncoated equivalent in terms of wear resistance. At high temperatures, the "friction coefficient" values for coated specimens declined. The wear mode has been seen to be adhesive at room temperature, and at higher testing temperatures, it was seen to be a mix of oxidative, adhesive, as well as abrasive.

Sun et al., [2021], studied atmospheric plasma sprayed NiAl-20 wt% Bi_2O_3 coatings with varying Cr_2O_3 contents. The findings revealed that Cr_2O_3 greatly improved the coatings' mechanical strength without compromising their plasticity. In addition to this Cr_2O_3 also improves the wear coatings behaviour owing to high hardness and plastic deformation resistance.

Dhzurinskiy et al., [2021], In the research plasma, sprayed Cr_3C_2-NiCr-based coatings have been deposited on "SS-304" L substrate and investigated its erosion performance. The coating developed features a dense microstructure with few flaws like micro-cracks and pores, as well as high hardness and toughness. Enhanced erosion resistance will be attributed to the high value of fracture toughness and hardness in developed coatings.

. Thermal spray coatings are now-a-days being used extensively by the manufacturers of machine tools, heavy machineries, power plants and automobile sector (Praveen et.,2015; Grewal et al., 2015). These techniques are very much reliable in terms of producing wear and corrosion resistant coatings. It has been reported that the coatings consisted of the Ni-based superalloys powders are effective for providing the surface failures caused by wear (Bala et al.,2015). However, the presence of micro porosities and formation of cracks in the thermal spray coating processes (plasma spraying, high velocity oxy-fuel and flame spraying) have been reported by many researchers (Afzal et al., 2014; Sidhu et al., 2005; Zafar et al., 2017). Such defects on the surface of the coatings can even deteriorate the sub-surface region. The WC-Co-Cr and Al_2O_3-40TiO_2 coatings were deposited using D-Gun spraying technique were used for the enhancement of abrasion resistance. It is concluded that phase changes could be induced in the microstructure of as-sprayed coatings by selecting appropriate post-processing conditions of the coating surface. Heat Treatment of HVOF deposited WC and Ni-based coatings were carried out with two major objectives. The first one is to relieve the strains generated during the rapid solidification of the coating and then allow the densifications to take place to minimize porosity levels. The second objective is to promote favourable phase transformations for enhanced wear and corrosion performance. However, some researchers also concluded that thermal post-treatments cannot enhance the corrosion resistance of HVOF sprayed coatings. On the other hand, the in-flight particle shrouding with an inert gas atmosphere decreases the amount of oxide content in the coating (Sidhu et al., 2005). In addition to this, annealing can be used to promote limited inter-diffusion among the coating and substrate for enhancing the bond strength of coating without deteriorating the properties of the substrate. Lee et al, while investigating the corrosion properties of Ni-Cr-W-Mo-B coating sprayed by HVOF, noticed that annealing of the coatings conducted in a vacuum furnace at temperatures 550, 750, and 950 °C for duration 2 h enhances the corrosion resistance (Lee et al., 2000). This may be attributed to increased chemical and microstructural homogeneity, decrease in porosity level, and reduction of the eutectic phase. In 2001, Guilemany et al had examined the effect of thermal treatments on the electrochemical corrosion performance of HVOF sprayed Cr_3C_2-NiCr coatings (Guilemany et al., 2001). Initially, a few coating layers were sprayed, thereafter, thermal treatment was given using the spray gun, and finally, the remaining layers of coatings were sprayed. Results revealed that the thermal treatment with the gun during the spraying process increases the protection of coatings against the passage of electrolytes. Guilemany et al., 2002 have further reported that the sliding wear resistance of the Cr_3C_2-NiCr coating can be improved by adequate HT (1 h at 760 °C) in an inert atmosphere. Small and well-distributed Cr_3C_2 produced by HT at 760 °C (inert atmosphere) greatly enhances the wear resistance of the coating.

2.8 PROBLEM FORMULATION.

The review of the literature was a critical stage for formulating the research problem and surface degradation of cast iron at elevated temperatures has been formulated after extensive review. The erosion and oxidation of the surface are serious problems for the surface of turbocharger housings and engine manifolds made of cast iron. Cast iron is frequently utilized in the manufacture of turbocharger housings. In addition to this, cast iron is commercially used in furnace parts, manufacturing molds, brake shoe materials, and engine manifolds. These all-engineering applications are subjected to elevated temperatures. In a cyclic and repeating way, hot air impacts the component's surface, and this air includes some undesirable dust particles. The severity of such particles and the harsh climate are the 2 main causes of surface deterioration caused by erosion and oxidation. Some stringent steps were required to combat these problems. So, there is a need to use some protective method to avoid the failure of the surface.

2.9 OBJECTIVES OF THE RESEARCH WORK.

The following are the objectives of the current study:

1. To develop Alloy718-Al_2O_3 composite coatings on GCI through HVOF thermal spray coating.
2. To examine the as-sprayed and post-treated Alloy718-Al_2O_3 composite coatings for comparison in terms of mechanical and micro-structural characteristics.
3. To characterize the as-sprayed and post-heat-treated coatings for the high-temperature sliding wear performance.
4. To characterize the as-sprayed and post-heat-treated coatings for the high-temperature erosive wear performance.

CHAPTER 3

EXPERIMENTAL EQUIPMENT AND PROCEDURES

In this chapter, the deposition method of the coatings has been reported along with the process parameters of the equipment used for depositing the coating. The various tools used for the characterization of uncoated & coated samples at different stages of the research work have been described. The procedures of sliding wear tests and erosion tests at elevated temperatures have also been mentioned. The various characterization techniques utilized for erosion and corrosion analysis formed during various tests.

3.1 SELECTION OF SUBSTRATE.

GCI ("Grey Cast Iron") was chosen as a substrate material for the present research study. This material is widely used for turbocharger housings, exhaust manifolds, as well as furnace parts for high-temperature applications. This material is also used for lathe machine slides and beds, and manufacturing tools used for forming processes like dies. The substrate material was procured from Allied Engineering Industries Pvt. Ltd, Limited, Ludhiana, India. This industry manufactures turbocharger housings and supplies to reputed automobile industries in India. An optical spectrometer was used to determine the GCI substrate's chemical composition (Make: "Metal Vision, Model: 1008i"). Actual and nominal compositions of the substrate are given in Chapter 5.

3.2 DEPOSITION OF COATINGS.

3.2.1 Preparation of Substrate Material.

GCI was originally cast as the substrate material, and it was afterward formed into a flat plate with measurements of 300×200×5 mm^3. Then the plate has been further cut using WEDM ("Wire-Cut Electro Discharge Machine") to obtain the substrate sample for the oxidation (20×15×5mm^3) and "air-jet erosion" (25×25×5mm^3) tests. After that, the specimens were polished using alumina powder particles on a polishing machine until they reached a grade of 1200 emery paper. The polished samples were subjected to abrasive grit blasting using virgin brown alumina grit of a 16-mesh size. The tools and media used for grit blasting are shown in **Fig.3.1.**

Fig.3.1. (a) Front and (b) side view of shot blasting m machine and, (c) Blasting medium (Virgin alumina).

This was done to reduce the differential in mechanical and thermal characteristics between the GCI substrate and the Alloy 718 coating. Using a “Hipojet-2700 gun” (Make: “M/s Metalizing Equipment Corporation, Jodhpur, India”), Alloy 718 feedstock powder was HVOF sprayed.

3.2.2 Coating Powder.

There were seven different combinations of powders consisting of Alloy718 and alumina that were deposited using the HVOF process on GCI substrate. The various powders combinations are Alloy718, Alloy718+10%Al_2O_3, Alloy718+20%Al_2O_3, and Alloy718+30%Al_2O_3, the morphology and particle powders size and their compositions have been given in chapter 4 of the present study.

3.2.3 Deposition of Coatings.

HVOF spraying has been performed for the deposition of coatings with Hipojet-2700 gun at “M/s Metalizing Equipment Corporation, Jodhpur, India”). As the HVOF process involves a very high velocity of around 1000m/s, therefore the samples were held by using different fixtures according to the different sizes of the samples. The main advantage of a fixture is that the uniformity of the coating is maintained. The fixtures are sample-holding devices used during the process of deposition to ensure the quality of the coating. The parameters of process in coatings are listed in **Table 3.1.** The same parameters of process have been adopted for the deposition of all powder combinations. However, the skilled and experienced operators performed the coating operation. The deposition of coating includes the initial trails in the form of some passes. The average particle size of the feedstock powder and the number of passes decides the approximate coating thickness to be deposited. Therefore, the deposition of coating with 40 µm average particle-sized powder requires approximately 6 passes for 200µm thickness of the coating.

Table 3.1 Process parameters used for the HVOF spraying process.

Process parameters for spraying	**Units**	
Stand-off distance	Mm	200
Fuel gas (LPG) pressure	Bar	7
Fuel gas (LPG) flow rate	LPM	50
Powder feed rate	g/min	65
Oxygen flow rate	LPM (Liquid per minute)	275
Oxygen pressure	Bar	11

3.3 POST HEAT TREATMENT.

Alloy-718 is strengthened owing to the precipitation of Ni_3 (Al, Ti, Nb) coherent precipitates: known as a) $\gamma^{/}$, b) metastable Ni_3Nb phase termed as $\gamma^{//}$ and, c) also the blocky MC carbides in Ni-Cr matrix. The metastable precipitates (Ni_3Nb) $\gamma^{//}$ are formed in the alloy-718 after annealing over a long time at a temperature range between 550-850ºC**.**

Hence, following the heat treatment was performed on Alloy-718+Al_2O_3 coated samples. The standard post-heat treatment (Direct ageing) is used for superalloys to enhance their mechanical and metallurgical properties and the details of this heat treatment are as follows:

Heat the sample to 720°C and hold it there for 8 hrs further kept at 620°C for 8 hrs and then cool it in the furnace.

3.3.1 Preparation of Specimen.

The slow-speed metallurgical diamond saw ("Model: MS-10, Make: Ducom Instruments Private Limited, Bangalore, India") was used for cutting. The speed of the diamond saw was maintained at around 200 RPM. The detail of the diamond saw is presented in Appendix A (Fig. A-6). The samples were then polished with 200,400,600,800,1000 & 1200 grades of emery paper followed by polishing with the finest emery papers to the 4/0 grade and finally, the mirror-like images were obtained using cloth polishing with diamond paste. The specimens were ultrasonically cleaned and dried in air for moisture removal. The detail of the ultrasonic cleaner is presented in Appendix A (Fig. A-5).

3.3.2 Coating Thickness Measurement.

The thickness has been measured in the deposition process using a thickness gauge used for thin films (Model: Minitest 2000; Make: "Elektro-Physik Koln Company, Germany"), having a precision of±1 µm. The measured values of thickness were further verified by mounting and sectioning of deposited coatings according to the procedure given in section 3.3.1.

A FE-SEM ("Field Emission Scanning Electron Microscope") (Make: JEOL, Japan; Model: JSM-6610LV) equipped with an EDS ("Energy Dispersive Spectroscopy") was used for obtaining the cross-sectional BSE ("Back Scattered Electron") images. The detail of the SEM equipment is presented in Appendix A (Fig. A-3). The average coating of the thickness was obtained and seen from the BSE images. The values of the deposited coatings' average thickness from the cross-section are given.

3.3.3 Measurement of Surface Roughness and Porosity

The HVOF-sprayed samples were polished prior to the measurement of porosity. The as-sprayed coating surface has been polished down to emery papers of 1200 grit size for microstructure analysis. This involved the measurement of porosity on Dewinter inverted optical microscope (Model: LT-2B, Make: Chennai metco Pvt. Ltd, Chennai, India) using image analyzer software (Dewinter Material Plus, Version4.3) according to STM B276 standard. The detail of the Dewinter inverted optical microscope is presented in Appendix A (Fig. A-2). Ten values of porosity were taken and their averages have been reported. The porosity values and surface roughness of the deposited coatings are the average of the ten measurements and are given in Chapter 4 of the current research study.

3.3.4 Measurement of Micro-hardness

The coatings' micro-hardness has been found with Vickers's micro-hardness tester (Model: Economet VH1 MD, Make: Chennai metco Pvt Ltd, Chennai, India) at 300g load with a dwell time of 10s. The detail of Vickers's micro-hardness tester is presented in Appendix A (Fig. A-4). The sample with the sprayed coating's micro-hardness was measured along the layer thickness. A total of 10 indents were made at two separate locations over the coating's cross-section. Five indentations were taken along the layer thickness at each place. Finally, their average value is reported and the distribution of micro-hardness values is presented in Chapter 4 of the current study.

3.3.5 XRD Analysis

The feedstock powder and as-spayed coatings' XRD patterns were taken. The XRD patterns of the surfaces after exposure to various tests were also reported to analyse the phases created on the surface of the coated and uncoated samples. XRD was conducted with a scanning rate of 1°/min and a step range (2-θ range) of 10°-100° on Bruker AXS diffractometer. The XRD has been conducted with a "Cu-Kα radiation" source formed at 40mA & 40kV. The detail of XRD is presented in Appendix A (Fig. A-1).

3.3.6 FE-SEM and EDS Analysis

3.3.6.1 Surface Morphology /Cross-sectional Analysis/EDS Analysis

An FE-SEM ("Make: JEOL, Japan; Model: JSM-6610LV") acceleration with a voltage of 15kV and equipped with an EDS has been utilized for the study of the morphology of the powders and as-deposited coatings. The coated specimens were initially silver pasted between the samples and stub for having conductivity, thereafter, gold coated for obtaining elemental maps for the analysis of different elements present. The as-sprayed coatings have been studied to comprehend the coatings' surface morphology and for the identification of melted splats, partially melted, un-melted particles, as well as pores formed on the surface of as-sprayed coatings. The EDS analysis provides the elemental compositions (weight %) at the selected region in the form of point and line analysis were taken at any region of the coating. Samples were made according to the process presented in section 3.3.1 for the cross-section analysis of the coating before and after the testing. The SEM/EDS analysis was conducted using an FE-SEM equipped with an EDS attachment. EDS study has been performed for the composition of elemental across the cross- at different regions of the substrate, bond coat, and top coats as well. SEM/EDS study of the as-coated and uncoated sample was presented in Chapter 4 of the current research work study.

3.3.6.2 Elemental Mapping Analysis

The different elements represented in the feedstock powders and their proper distribution were obtained by EDS maps and for this; the specimens have been cut over the cross-section and then further polished to achieve the elemental mapping. The procedure for sample preparation is already given in section 3.3.1. The coated specimen was sectioned, and polished, as well as silver was pasted between the samples & stub for conductivity, thereafter, gold for obtaining an elemental-mapping study of several elements represented on the as-sprayed and across the coating's cross-section. The selected area represents the regions which are the substrate, bond coat, and coating regions. Elemental mappings for all deposited coatings were reported in this research study. The mappings give information about the elemental distribution in the deposited coatings. It concentration of the elements in the coatings can easily be seen with the help of X-ray mappings of deposited coatings. The cross-section of all coatings can give the distribution of elements and also helps to understand the difference between all coatings.

3.4 HIGH-TEMPERATURE WEAR BEHAVIOUR.

3.4.1 Erosion Analyses in Air Jet Erosion Test Rig.

An air-jet erosion test at high temperatures was carried out. The erosion testing has been carried out with an air jet erosion tester ("Model: TR-471-800, Make: Ducom Instruments Pvt. Ltd, Bangalore, India") available in Research and "Manufacturing Lab at Guru Nanak Dev Engineering College, Ludhiana, India". The detail of the air jet erosion tester is given in **Fig 3.2.** Test conditions for air-jet erosion at high temperatures are detailed in **Table 3.2.** After each experiment, the specimens were weighed again on a weight scale accurate to within 0.01mg.

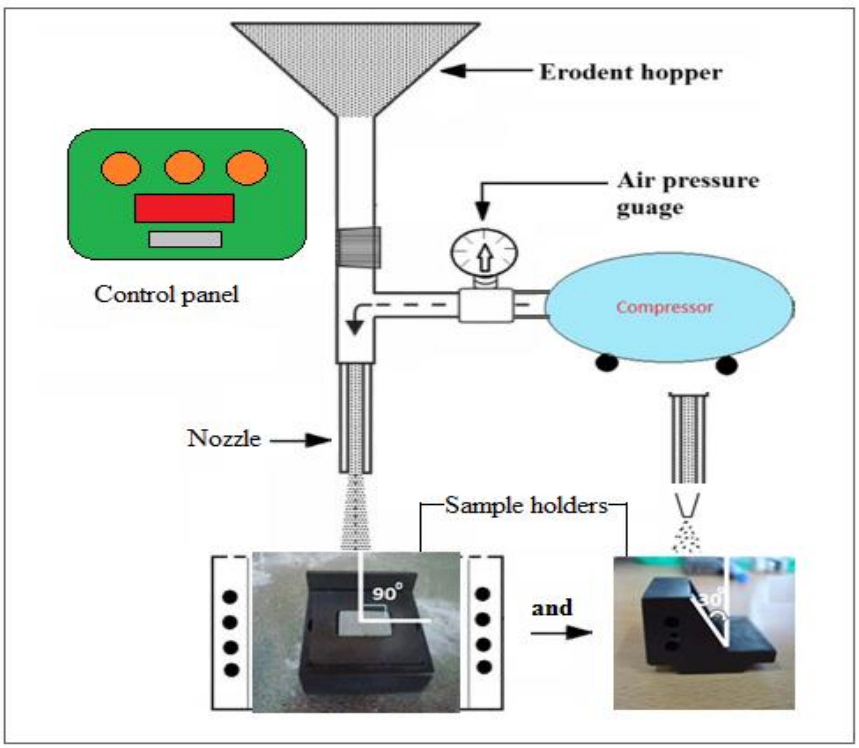

Fig.3.2. (a) Airjet erosion test rig (b) Panel of Airjet erosion test rig.

Table 3.2 Air-jet erosion test parameters.

Parameters	Units	Values
Nozzle diameter	mm	1.5
Exposure time	min	10
Temperature	°C	800
Impact angle(degrees)	degrees	30° and 90°
Powder feed rate	g/min	6
Erodent size	µm	60
Erodent powder	-	Aluminium oxide

3.5 ANALYSIS OF SLIDING AND EROSION PRODUCTS.

3.5.1 Sliding Wear Studies.

A high-temperature pin-on-disc tribometer was applied for tribological research under dry, unidirectional sliding circumstances. Before conducting wear & friction experiments, samples have been polished with sandpaper of various grit levels, lowering the Ra values for every sample to below 1 µm. The ASTM G99-04 guidelines were followed during the testing. Therefore, in the current experiment, the disc had been preheated with an induction heater to the desired test temperature. Using a pyrometer, the disc temperature was estimated. Based on the characteristic characteristics of a typical hot forming process, the wear & friction test parameters have been selected. The tests were run using the settings listed in **Table 3.3.** The pin samples used for the pin–on–disc sliding wear test are shown in **Fig.3.3.**

Table 3.3. The details of the various process parameters used for performing the pin-on-disc test at various conditions:

Parameters	Units	Values
Temperature	°C	400 and 800
disc Track diameter	Mm	80
Load	N	20,30
Speed	$m\ s^{-1}$	1
Sliding distance	M	2000

Fig. 3.3. The pin samples used for the pin–on–disc sliding wear test.

Friction was calculated using the strain gauge force transducer. The tribometer is supplied with automated data acquisition as well as a control system that allows it to regulate and monitor several element is shown in **Fig.3.4.** The surface morphology of all samples at different magnifications after performing the tribological testing (High-temperature solid air-jet erosion test, & Dry sliding wear) were analyzed by FE-SEM ("Make: JEOL, Japan; Model: JSM-6610LV") equipped with an EDS. A schematic illustration of the pin-on-disc facility utilized for performing testing as shown in **Fig.3.5.**

Fig. 3.4. Pin-on-disc tribometer.

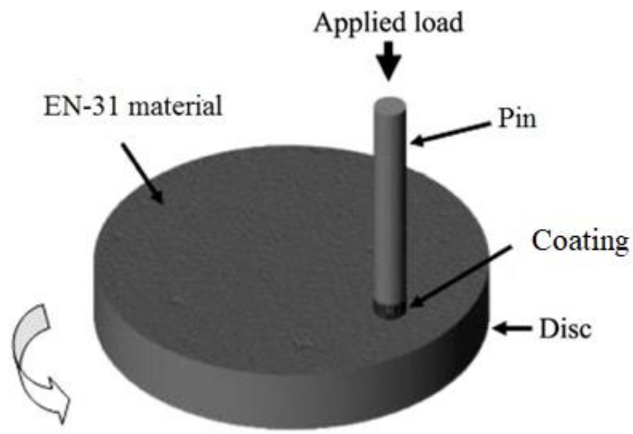

Fig. 3.5. A schematic illustration of the pin-on-disc facility utilized for performing testing.

3.5.2 XRD Analysis.

The XRD patterns of as-sprayed and uncoated GCI after exposure were taken to identify the phases formed on the coatings. XRD has been with a scanning rate of 1°/minute and a step range (2-θ range) of 10°-100° on Bruker AXS diffractometer. The radiation source of Cu-Kα generated at 40mA & 40 kV was used for the XRD. At the "Indian Institute of Technology" in Mandi, India, the XRD analysis was completed.

3.6.3 FE-SEM/EDS ANALYSIS.

3.6.3.1 Cross-sectional Analysis.

The specimens exposed to cyclic oxidation test were analysed from cross-section by FE-SEM ("Make: JEOL, Japan; Model: JSM-6610LV") with an EDS. The exposed specimens were initially silver pasted between the samples and stub for having conductivity, thereafter, gold coated for obtaining elemental maps for the analysis of various elements present. The effect of oxidation along the coated and uncoated samples cross-section was studied. The EDS analysis provides the elemental compositions (weight %) at the selected region in the form of point and line analysis were taken at any region of the coating across the cross-section. Samples were prepared according to procedure given in section 3.3.1.. EDS study was performed for the elemental composition across the cross-at various regions of the substrate, top coats, and bond coat as well. SEM/EDS study of the as-coated and uncoated sample was represented in Chapter 4 of the current research work study.

3.7 ANALYSIS OF EROSION TESTING.

3.7.1 Visual Observation

The visual inspection of the specimens includes the impression formed on the surface of the eroded specimens. This was performed to know the impact of different impact angles on the surface of the deposited coating. The visual inspection in the form of pictographs is given in chapter 6 of this research work. All deposited coating and uncoated GCI have been visualized to know the impressions formed on the specimens after exposure to the solid-particle erosion testing. Similarly, the oxidized samples during cyclic oxidation testing were seen from the surface to visualize the changes during and after the exposure to 50 cycles. The detail of oxidized samples has been discussed in Chapter 5 of this study.

3.7.2 FE-SEM Analysis

3.7.2.1 Surface Morphology

After being subjected to a high-temperature solid air-jet erosion test, the surface morphology of the eroded samples was examined at various magnifications using a FE-SEM ("Make: JEOL, Japan; Model: JSM-6610LV") fitted with an EDS.

Chapter 4

CHARACTERIZATION OF AS-SPRAYED AND POST-PROCESSED COATINGS

The chapter deals with the characterization of the deposited coatings on GCI substrate by the process of HVOF. The SEM/EDS analysis from surface and cross-section along with elemental mappings of the coatings are reported. The micro-hardness of all the deposited coatings was evaluated along the cross-sectional direction and porosity from the surface and from the cross-section is reported. The presented results are discussed concerning the available literature.

4.1 GCI SUBSTRATE.

4.1.1 Chemical Composition of Substrate

GCI has been chosen was chosen as substrate material and its composition has been examined with an optical spectrometer (Make: "Metal Vision, Model: 1008i"). The GCI compositions are provided in **Table 4.1.**

Table 4.1. GCI substrate's chemical composition.

Elements	Actual composition
C	3.5
Si	1.8
Mn	0.7
P	0.1
S	0.09
Fe	Bal.

4.2 SEM-EDS EXAMINATION OF SUBSTRATE, COATINGS, AND POST-PROCESSED COATINGS.

There were four different coatings that were deposited using the HVOF process on the GCI substrate. The various coatings used in the present work along with the designation system used are exhibited in **Table.2.** The coatings powders morphology (Alloy718 and alumina) was determined using SEM/EDS. A standard SEM micrograph that shows the morphology of the IN718 alloy powder is presented in **Fig. 4.1(a).** The EDS of the IN718 powder is presented in **Fig.4.1.**

Table 4.2 Designation system utilized for the coatings.

Sr. No	**Coatings**	**Designation System**
1.	Alloy718	**A718**
2.	Alloy718+10%Al_2O_3	**A718/10AL**
3.	Alloy718+20%Al_2O_3	**A718/20AL**
4.	Alloy718+30%Al_2O_3	**A718/30AL**

The image of SEM (**Fig. 4.1a**) makes it evident that the powder particles commonly have a spherical shape and have an average particle size of around 40 m. Cr, Ni, & Fe are the main alloying elements found in A718 powder, but Nb, Al, and Mo are also significant components. EDS analysis verified the existence of these elements, as presented **in Fig. 4.1. (b).** The morphology of alumina powder is different from the A718 powder and it shows a blocky appearance as shown in **Fig. 4.2(a).** The EDS of Al_2O_3 powder showed the existence of O and Al and therefore, it corresponds to the constituents existing in the feedstock powder as revealed in **Fig. 4.2(b).** The average powder particle size observed through SEM micrographs and the make of all powders are given in **Table 4.3.**

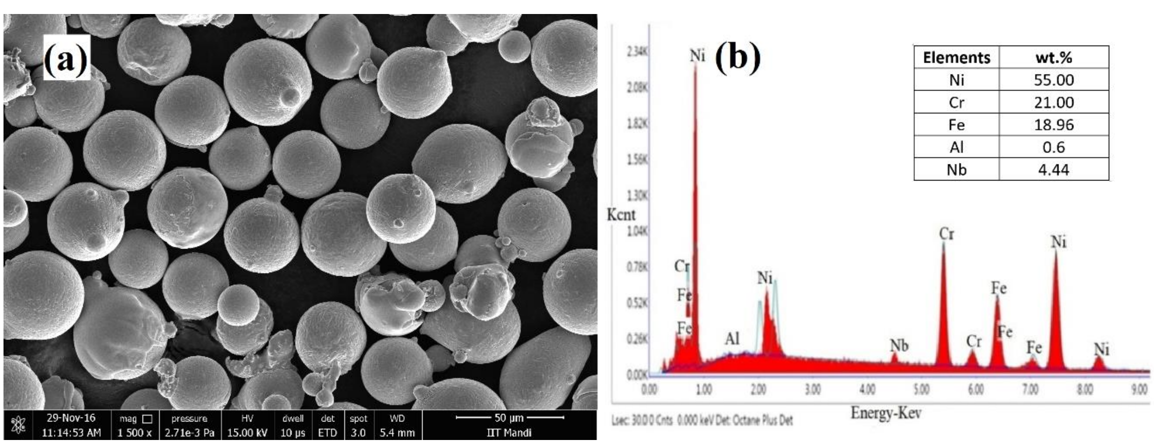

Fig. 4.1 (a). SEM micrograph of A718 powder, (b) EDS spectrum of A718 powder.

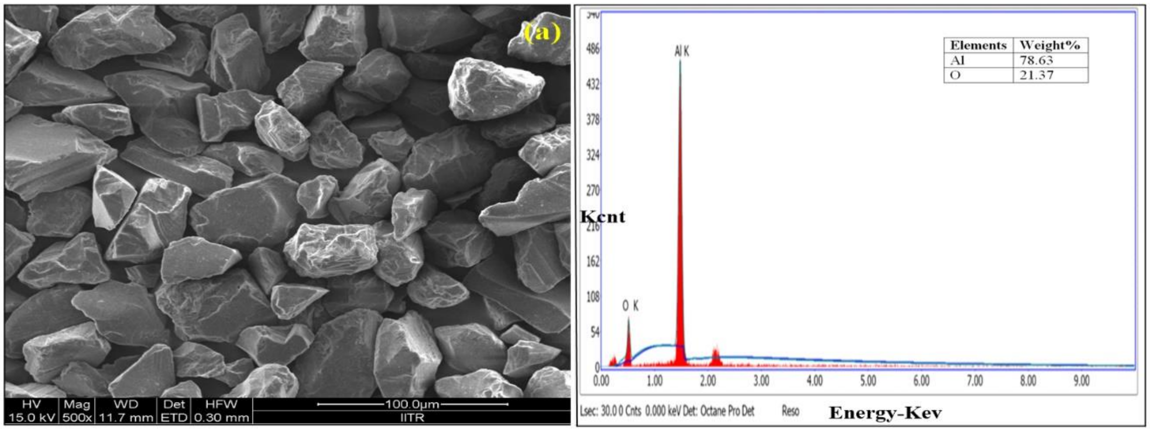

Fig. 4.2. (a). SEM micrograph of Al_2O_3 powder, and (b) EDS spectrum of Al_2O_3 powder.

The Al_2O_3 (alumina) powder utilized in the current study has a blocky/angular morphology with an APS of 40 µm and this size has been selected for proper blending of feedstock powders.

Table 4.2. Feedstock powders used in the current investigation

Coating powder	Make	Size
A718	Make M/s Metallizing Equipment Corporation Pvt. Ltd., Jodhpur, India.	about 40 µm
Al_2O_3	Amperit 587.090 H.C.Starck GmbH Made in Germany	40 µm

The A718 and alumina powder with a mean particle size of 40µm have been mechanically mixed in three proportions to get three combinations of micrometric coatings.

Both micron-sized alumina powders were mixed with A718 powder in 3 proportions before the deposition of coatings.

The XRD patterns of A718 and alumina are presented in **Fig.4.3.** The Spectra of IN718 powder showed the presence of Ni-Cr with FCC ("Face-Cantered Cubic") structure. It also demonstrated the dominant of γ (111) phases, which include a rich solid Ni-Cr solution with FCC structure (space group a=0.359 nm, Fm-3m). **Fig. 4.3(a)** displays the Alloy718 powder's XRD spectrum. The XRD spectra of aluminium oxide powder are revealed in **Fig. 4.3(b).** The peaks of alumina in this XRD are corresponding to the JCPDS reference code of 00-001-1243 which corresponds to the peaks of alumina. The chemical composition of powders is listed in **Table 4.3.**

Table 4.3. Chemical composition of feedstock powders.

	Elements (wt %)							
Material	**Ni**	**Cr**	**Fe**	**Nb**	**Mo**	**Al**	**C**	**Others**
A718	55.5	21.3	19.0	5.0	3.1	0.5	0.09	Bal.
Alumina	-	-	-	-	-	99.99	-	Bal.

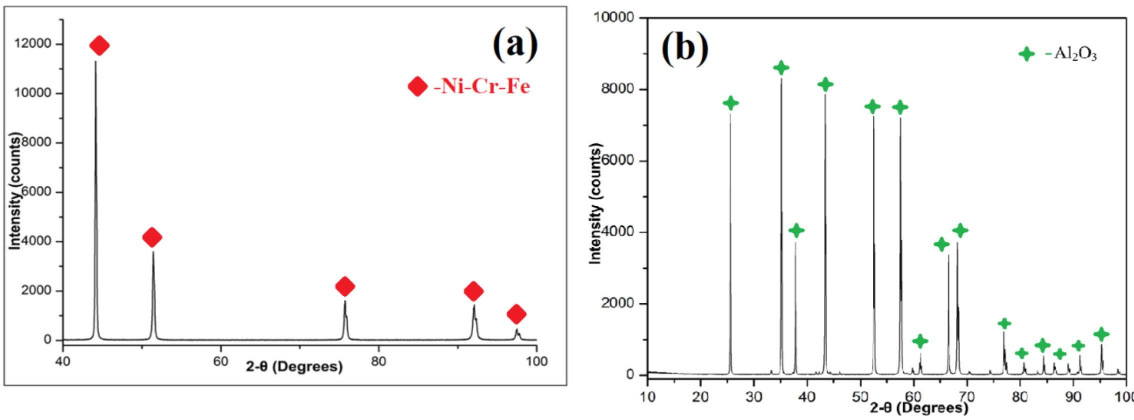

Fig.4.3. (a). XRD pattern of A718 powder, (b) XRD pattern of Al_2O_3 powder.

4.3 AS-SPRAYED COATINGS' FE-SEM/EDS ANALYSIS.

4.3.1 Surface Morphology/EDS Analysis.

FE-SEM morphologies along with EDAX analysis of the surfaces for the HVOF sprayed coatings on the GCI are shown in this section. **Fig.4.4** (a) and (b) represent a typical SEM micrograph showing the "surface morphology" of as-sprayed A718 coating on GCI substrate. The coating surface demonstrates the usual HVOF thermal spraying process features, such as the dispersion of partially melted, totally molten, and plastically deformed particles over the surface. There is a discernible boundary between the totally melted and partially melted powder particles.

Furthermore, When powder particles on a surface undergo sufficient plastic deformation, they do not break and do not splash around. The lower flame temperature of the HVOF process reduces thermal stresses, hence reducing the likelihood of crack production(Tellkamp et al., 1997).

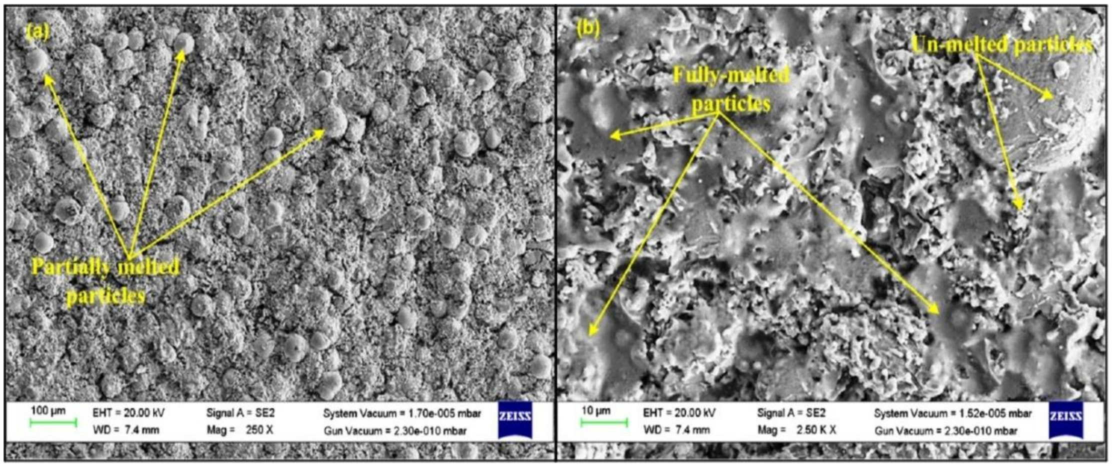

Fig.4.4. (a) GCI coated with A718 coating, and (b)GCI coated with A718 coating at higher magnification.

The SEM micrographs and EDS study of as-sprayed coatings with micrometric powders are shown in Figure 4.9. The melted, partially melted as well as unmelted particles show the typical characteristics of the HVOF process as shown in these figures. The micrographs indicate the partially melted & unmelted particles are embedded in the fully melted matrix. To examine the elemental structures of such particles; the EDS spectra were conducted corresponding to location 1 as revealed in Figs. From the EDS spectrum, it is clear that the "fully melted" particles are corresponding to the A718 matrix. The melting of A718 has occurred in the coatings process of deposition as the concentration of IN718 feedstock powder was higher and it has a considerably lower melting point (about 1456 °C) as compared to alumina (about 2200°C). Further, the flattened un-melted particles of alumina were formed owing to the high velocity of the HVOF process. These particles got deposited at some locations in the form of splats and separated by the interfaces of partially melted particles. The alumina particle distribution was observed to be almost uniform within the A718 matrix at a higher magnification micrograph. Moreover, with the rise in the content of alumina, the percentage area filled by un-melted articles (Al_2O_3) also increased as shown in **Fig. 4.5(a), (c) & 4.5(e).** The alumina particles seem to be well-bonded in the A718 matrix.

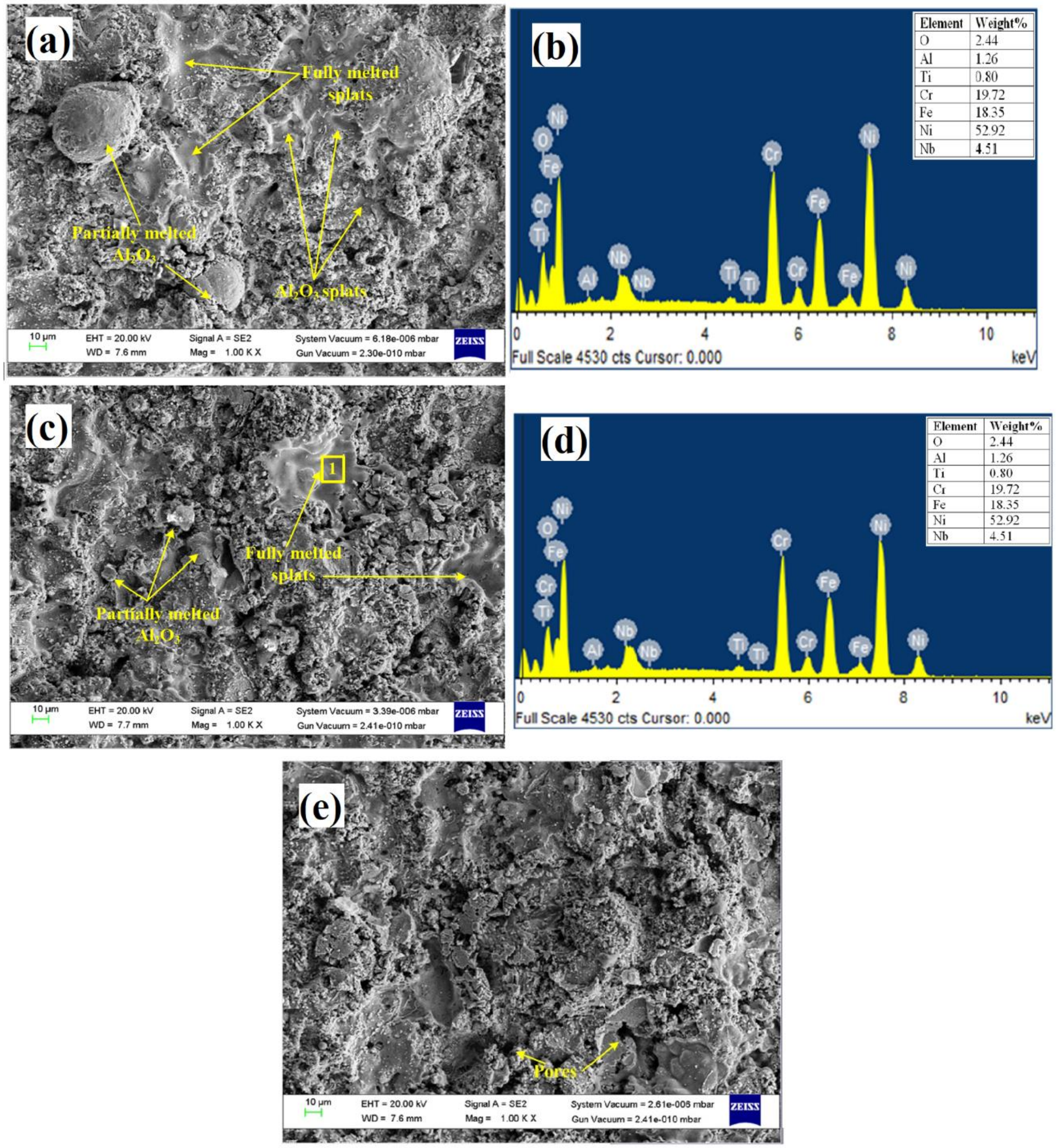

Fig.4.5. (a) GCI-coated SEM micrograph with A718-10 % Al_2O_3 coating, (b) EDS spectrum taken corresponding to IN718-10 % Al_2O_3 coating (c) GCI-coated SEM micrograph with A718-20 % Al_2O_3 coating, (d) EDS spectrum taken corresponding to A718-20 % Al_2O_3 coating, and (e) SEM micrograph of GCI coated with IN718-30 % Al2O3 coating.

The micrographs have also shown the incidence of some micro-voids (porosity) in the deposited coatings. The porosity (pores/voids) within deposited coatings were computed as designated in the above-mentioned section. The porosity in the coatings increased with the rise in the Al_2O_3 content in the feedstock powder. This is explained by the A718 significantly lower melting point temperature and greater plasticity than alumina. As a result, the A718 powder particles melted during the coating deposition process and underwent significant plastic deformation upon impact. This plastic nature of A718 covers most of the irregularities (pores/voids) in the coatings. A higher number of semi-melted as well as un-melted particles inside the coatings are displayed in Figure as a result of alumina's high melting point and high composition in the A718-30 percent Al_2O_3. Designation system used for the post-treated coatings are shown in **Table 4.4.**

Table 4.4 Designation system used for the post-treated coatings.

Sr.No	**Post Treated Coatings**	**Designation System**
1.	Alloy718	**PT-A718**
2.	Alloy718+10%Al_2O_3	**PT-A718/10AL**
3.	Alloy718+20%Al_2O_3	**PT-A718/20AL**
4.	Alloy718+30%Al_2O_3	**PT-A718/30AL**

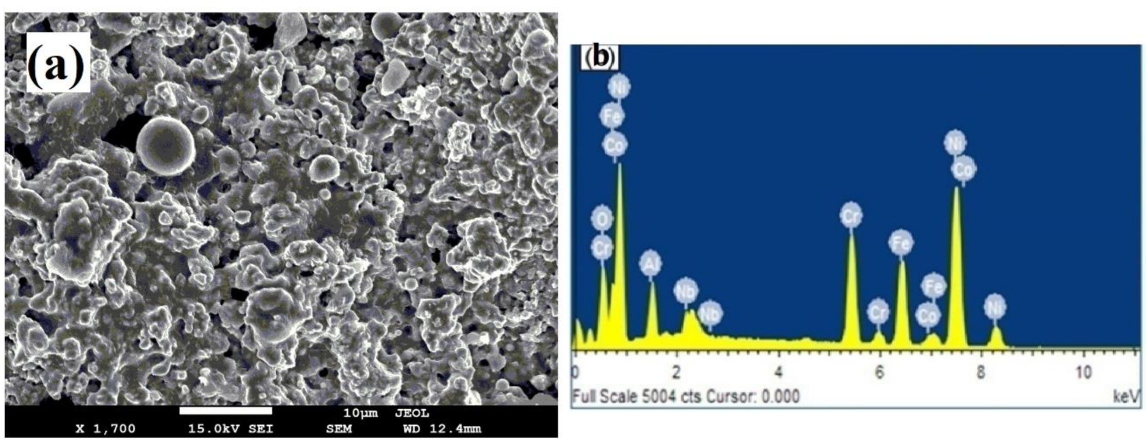

Fig. 4.6. (a)SEM micrograph of PT-A718 coating on cast iron at 1700x (B) EDS corresponds to SEM image of PT-A718**.**

The SEM/EDS analysis of PT-A718 coating on cast iron is shown in **Fig. 4.6.** The completely melted splats of the Ni-Cr matrix are shown in **Fig. 4.6 (a)** and the same is revealed by the EDS spectra. The micrograph has shown the melted and refined structure when subjected to heat treatment.

The SEM/EDS analysis of PT-A718/10AL coating on cast iron is shown in **Fig. 4.7.** This may be attributed to the presence of a maximum weight percentage of A718 alloy in the coating feedstock powder with 10% Al_2O_3. There is a considerable variation between melting points as well as thermal conductivities of A718 and Al_2O_3 feedstock material. The Ni-Cr matrix may absorb the excess heat Due to its higher thermal conductivity and lower melting point than Al_2O_3. This melted splats of Ni-Cr matrix and the retained alumina particles with angular morphology similar to nano-Al_2O_3 powder. The high flame temperature of the HVOF spraying technique, however, which ranged from 2500 to 3000°C, led to the partial melting of certain alumina particles during the deposition process (Oska et al., 2011). The formation of partially and completely melted particles is a typical characteristic of coating deposited by the HVOF process (Chen et al., 2014).

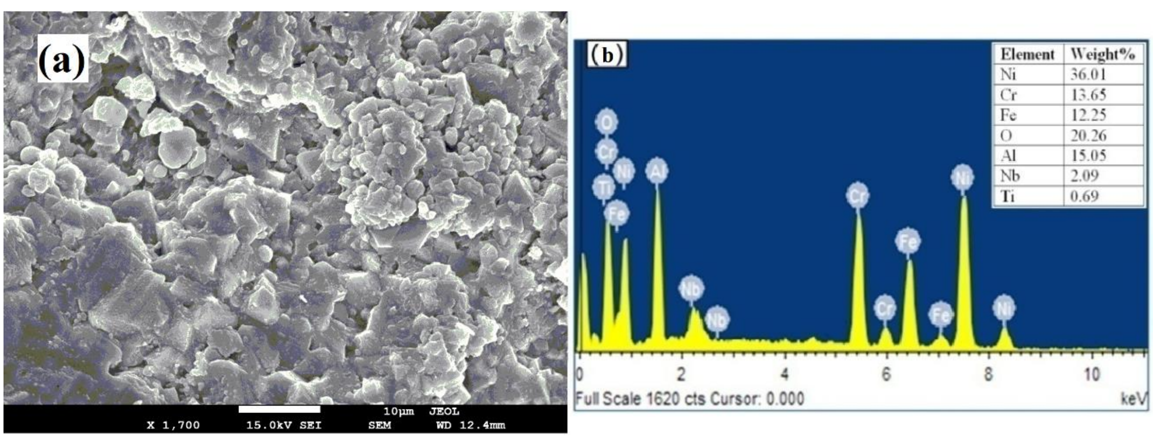

Fig. 4.7. (a)SEM micrograph of PT-A718/10AL coating on cast iron (b) EDS corresponding to 4.11a.

The SEM/EDS analysis of PT-A718/20AL coating on cast iron is exhibited in **Fig. 4.8.** The coating indicates the distribution of alumina particles and fewer melted splats. More melted and uniformly distributed microstructure can be seen after heat treatment. The increased content of 20% alumina in the feedstock powder when sprayed with a high velocity of the HVOF process, then gets dissociated and distributed on the coating surface.

The process of HVOF has a high velocity close to the CS technique and therefore the particles do have not enough time for meting down and they get deposited with a high impact on the substrate.

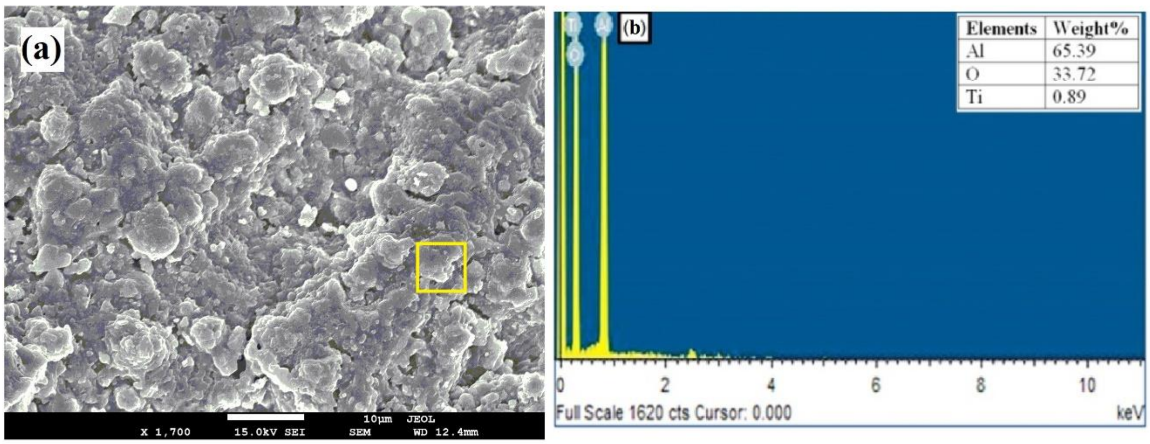

Fig. 4.8. (a)SEM micrograph of PT-A718/20AL coating on cast iron (b) EDS corresponding to 4.12a.

The SEM micrograph of PT-A718/30AL coating on cast iron revealed fewer melted splats along with Al_2O_3 particles as shown in **Fig.4.9.** The coating with 30% alumina also represented the healed and refined microstructure. The coating's porosity enhanced with the rise in alumina content in the coatings.

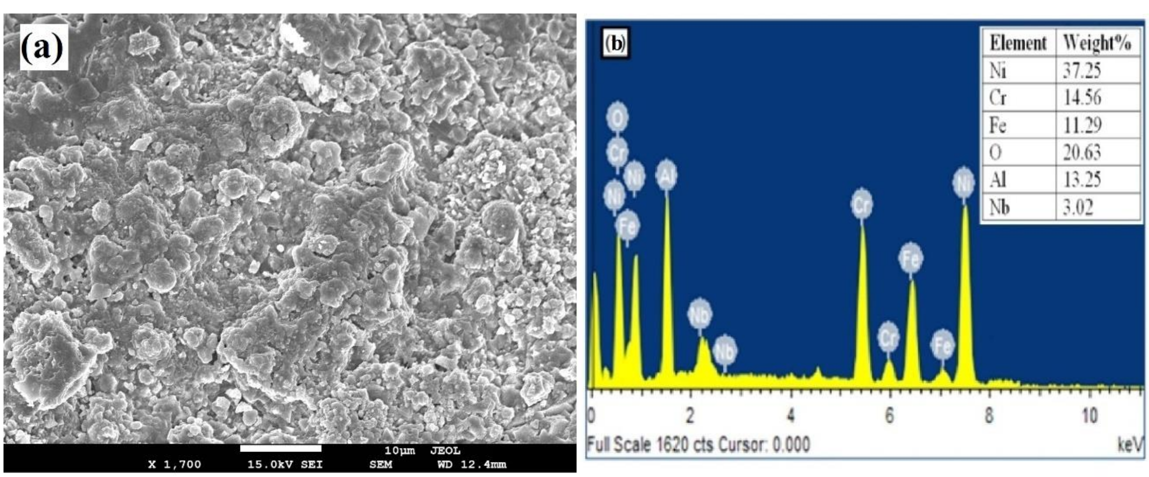

Fig. 4.9. (a)SEM micrograph of PT-A718/20AL coating on cast iron (b) EDS corresponding to 4.13a.

4.4 POROSITY ANALYSIS AND SURFACE ROUGHNESS.

The porosity value in the percentage of the deposited coatings is a surface property that has an important role to play in case of the development of high-temperature oxidation-resistant coatings. Due to high porosity, the corrosion products could penetrate the top and sub-substrate. Porosity in the deposited coating during thermal spraying is a dominant parameter and is a physical property that differs in the oxidation resistance provided by variants of TSC processes. The mean of five measurements was performed for all deposited coatings and is given in **Table 4.5.** The surface roughness (Ra) value of every coating has been determined by the "Surface roughness" tester (Model: SJ 201; Model: Mitutoyo, Japan) and reported in **Table 4.5.** To obtain *Ra* values, the center-line average method was adopted. It has been found that the surface roughness as well as porosity raised with the rise in the content of Al_2O_3 in the coatings. Furthermore, the porosity measurement showed fewer porosity values at the cross-section as compared to the as-sprayed surface of the coatings. The thickness of the deposited coating was kept around 250-300 µm. The thickness was measured by using *Image-J software package* from SEM micrographs taken across the cross-section of the deposited coatings. The SEM micrographs of coated samples from the cross-section clearly show the thickness of deposited coatings. In each SEM micrograph, the two interfaces between the bond coat, substrate, and top coats are shown.

Table 4.5 Average coating roughness, porosity, and thickness for various coatings under investigation.

Coating powders	Roughness (R_a)	Porosity (%)	
		As-sprayed	Post-treated
A718	0.5	0.85	-
A718/10AL	0.68	1.1	-
A718/20AL	0.79	1.5	-
A718/30AL	0.86	2.4	-
PT-A718	0.4	-	0.78
PT-A718/10AL	0.65	-	0.99
PT-A718/20AL	0.71	-	1.2
PT-A718/30AL	0.80	-	2.3

4.5 EVALUATION OF MICROHARDNESS

In high-temperature hostile environments, coatings may have to withstand the oxidation and erosion attack simultaneously. In these aggressive environments, the softer coatings may be more at risk of this oxidation and erosion attack at elevated temperatures.

The two interfaces have been presented along the coated substrate's cross-section. The cast iron substrate is generally 225 HV in hardness. The initial contact has seen an increase in the substrate's hardness. The polished substrate is subjected to the effects of virgin abrasive particles during the grit blasting process before the coatings are applied, and the increased hardness at the interface may be brought on by substrate work hardening (Grewal et al., 2012). The average microhardness of as-sprayed & post-processed coatings are shown in **Table 4.6.**

Table 4.6. Average microhardness of as-sprayed & post-processed coatings.

Coating powders	Microhardness (HV_
GCI	225±10
A718	560±10
A718/10AL	625±15
A718/20AL	735±15
A718/30AL	805±16
PT-A718	610±10
PT-A718/10AL	665±15
PT-A718/20AL	780±15
PT-A718/30AL	912±16

The hardness of the coatings was compared with the values noted in the literature. Miguel et al. (2003) noted an average hardness value of 610 for the NiCrSiB coating deposited by the PS coating process. S. Harsha et.al. (2008) found an average value of 511 HV for flame-sprayed coating with NiCrSiB+20%CrC powder. Wang et al. (2009) examine an average micro-hardness value of 410 HV forNiAl + 40% Al_2O_3 powder deposited by the process of HVOF. Koivuluoto et al. (2009) observed a micro-hardness value of 350 HV for cold spray coating with NiCr + 50% Al_2O_3 feedstock powder. Hu et al. (2011) observed a maximum micro-hardness of 225HV for Ni+40% Al_2O_3powder deposited with the cold spray process, while, Li et al. (2008) reported the highest micro-hardness of 173 HV for the cold sprayed coatings.

In the present study, it could be observed that the hardness of post-treated showed much better improvement in the hardness values as compared to the data of hardness for different coatings available in the literature. The higher value of coatings is due to the closely packed splats and eventually the lower porosity content. Moreover, higher hardness is attributed to the coatings deposition with the process of HVOF as this process is suitable for developing the Ni-based composite coatings.

4.6 XRD ANALYSIS

Fig. 4.10. represents the "XRD pattern" of as-sprayed coating, which confirms the existence of constituents of deposited feedstock powder. The NiO phase is also present with peaks of low intensity.

The XRD patterns of as-sprayed coatings as well as post-treated are indicated in **Fig. 4.11** and **Fig. 4.12**, respectively. The XRD analysis indicated the existence of the Ni-Cr matrix along with Al_2O_3 as the primary stages in the as-sprayed samples. Further, the peak intensity corresponding to alumina is rising with raise in alumina content in the "feedstock powder" (both in as-sprayed coatings and post-treated). In the coatings, certain NiO-related low-intensity peaks have also been observed. The existence of NiO shows that nickel underwent oxidation during the coatings' deposition. Additionally, the outcomes support earlier findings (Grewal et al., 2013). NbC ("Niobium Carbide") and the "γ-Ni-Cr solid solution" matrix were found in the coatings as they were being deposited, as well as Laves phases. During thermal spraying, the alloying components, which have been represented in the coating powder as a solid solution, interacted with one another in the "molten powder" layer. As a result, the new phases formed, as shown in the XRD pattern of the A718 coating. Due to the fact that they consume the alloying elements needed to reinforce the matrix, these novel phases have a substantial impact on the coating properties. The DA A718 coating's XRD spectrum shows that Laves phases coexist with the "γ-Ni–Cr (fcc) matrix", as seen by the coating's XRD pattern. The phase of laves is a brittle intermetallic compound that is denoted as "(Ni, Cr, $Fe)_2$(Nb, Mo, Ti)" in the interdendritic areas in the solidification of Alloy 718.

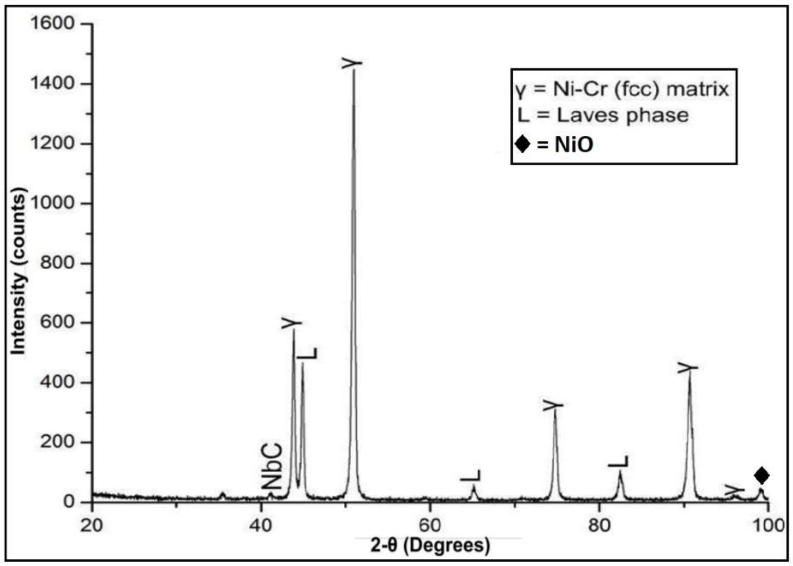

Fig. 4.10. XRD pattern of as-sprayed A718 coating on GCI.

X-ray patterns of all deposited coatings reveal the presence of constituents of used feedstock powders and include Ni-Cr matrix peaks with 2θ values of 43.45°,50.49°,74.33°,90.14° and 95.32° corresponding to the peaks of Inconel-718 feedstock powder along with alumina peaks.

4.7 CROSS-SECTIONAL ANALYSIS OF COATINGS.

FE-SEM images of the coated steels along the cross-section were collected, and EDAX analysis was also carried out at certain specifically chosen places of interest to determine the elemental composition (wt percent) across the coatings.

This section presents the FE-SEM/EDS analysis of all coatings that were HVOF-deposited on GCI substrates.

The creation of a lamellar structure in the deposited coatings was caused by the use of many sprays passes to achieve the desired coating thickness.

Metallographic investigations revealed that the coatings had a layered structure and that powder particles that had partially melted and melted completely had resolidified. The denser microstructure without any gaps or voids is seen in the FE-SEM image obtained throughout the coated cross-section.

It is evident from the BSE pictures of the cross-section of as-sprayed coatings that every coating has a consistent and dense microstructure.

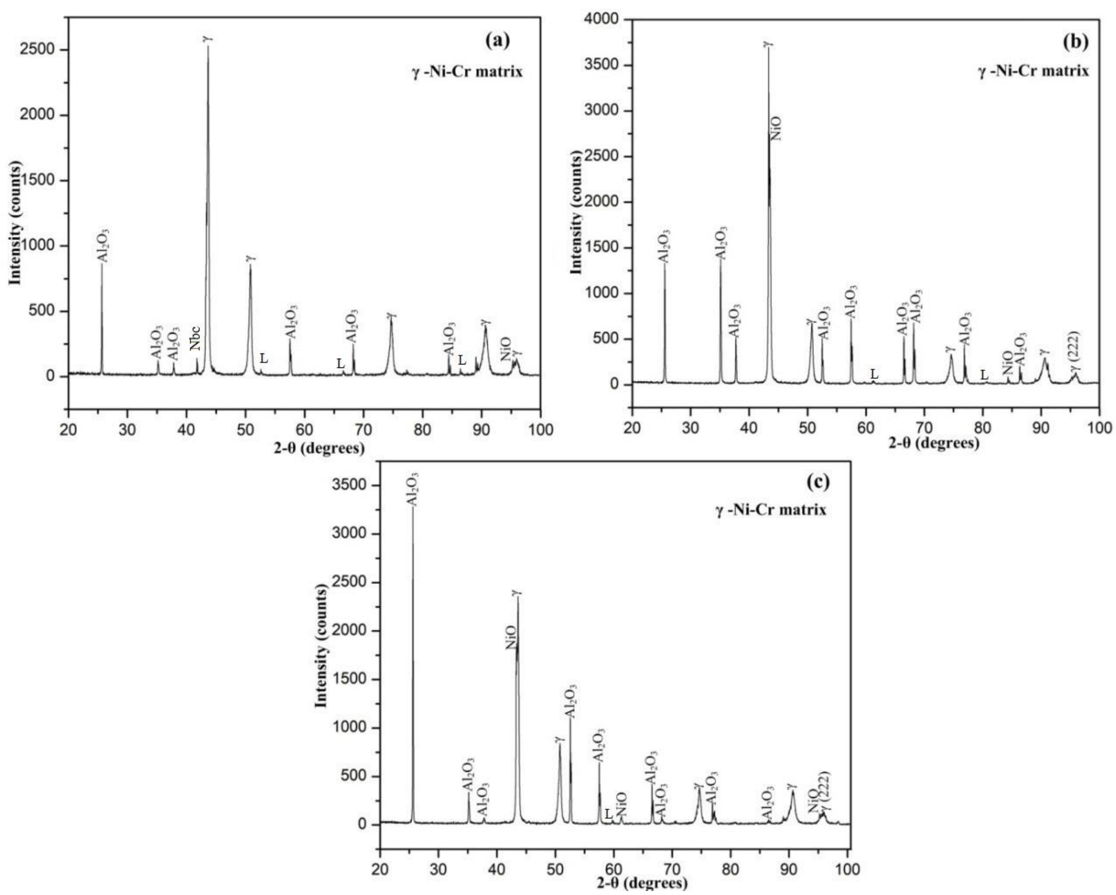

Fig. 4.11. XRD patterns of as-sprayed (a) A718/10AL, coating (b) A718/20AL coating, and (c) A718/30AL coating.

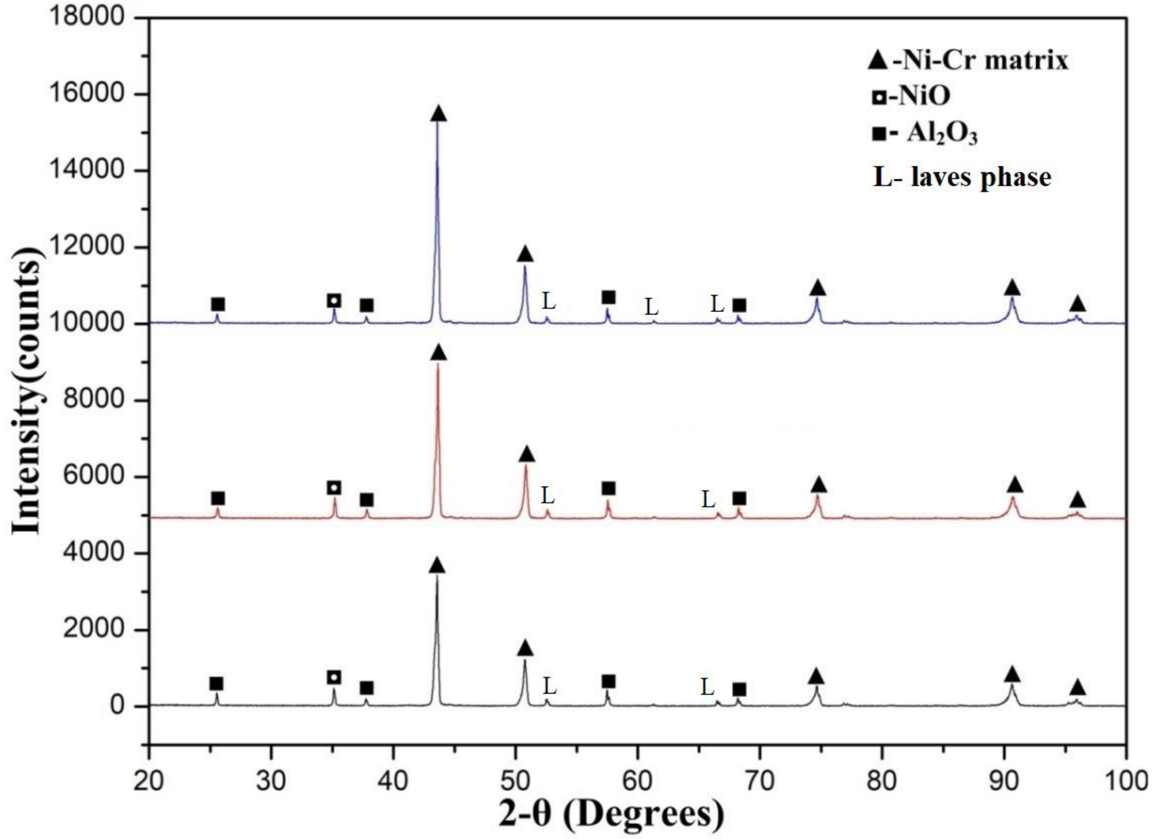

Fig. 4.12. (a)XRD patterns of as-sprayed PT-A718/10AL, (b) PT-A718/20AL, and (c) PT-A718/30AL.

Fig. 4.13 (a) represents a cross-sectional SEM image of a polished IN718 coating specimen whereas **Fig. 4.13** (b) cross-sectional SEM image of polished post-treated coating. It can also be observed that there is a proper interlayer bonding between GCI base metal and the layer of A718 coating without any interfacial cracks. The thermal process of spray produces a "lamellar splat" by splat formation of feedstock material in the process of deposition and the same could be found in the A718 coating. The HVOF method's high velocity produces effective mechanical anchoring for the layers. The coating had a tightly packed splat structure with no apparent voids or holes. In the coated specimen, it was discovered that the percentage porosity value was less than 1%. The main criterion for corrosion-resistant coatings is a lower % porosity value to prevent any kind of contact between the coated surface and external surroundings (Chen et al. 2014). The A718 coatings **(Fig.4.13(a))** have shown the well-bonded interface and lav phases present on the surface. The post-treated SEM micrograph has shown the distribution of laves phase as revealed in Figure 4.17(b).

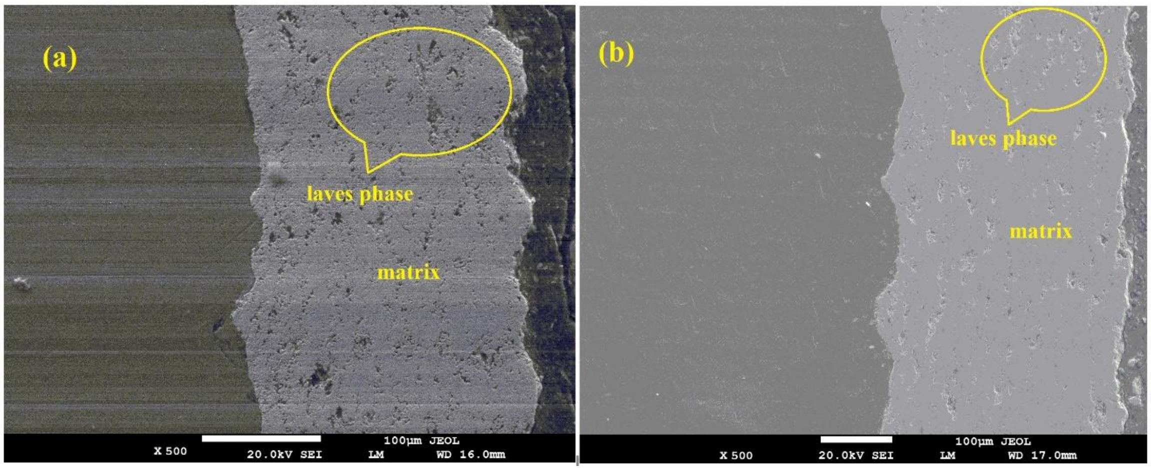

Fig.4.13 (a) Cross-sectional SEM micrograph of A718, (b) Cross-sectional SEM micrograph of PT-A718.

As shown in **Fig. 4.14**(a) and it has been observed that the black phase is the alumina present in the greyish matrix of Alloy718. The alumina content has increased in the A718/20AL coating as revealed in **Fig. 4.14(b).** The same trend has been found in the A718/30AL coating as shown in **Fig4.14(c).**

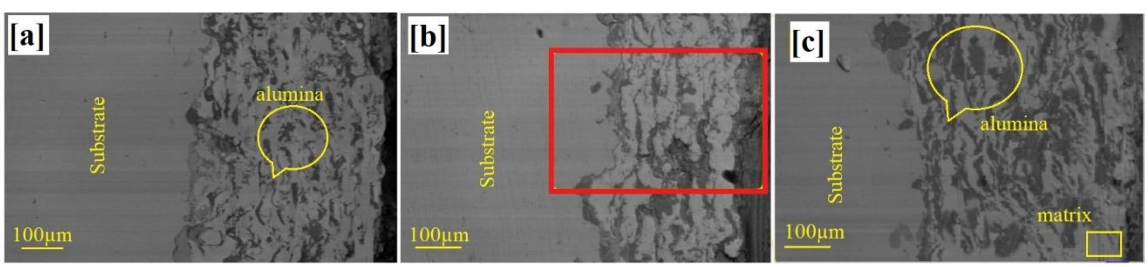

Fig.4.14 (a) Cross-sectional SEM micrograph of (a) A718/10AL, (b) A718/20AL, and (c) A718/20AL.

Fig. 4.15(a) is a cross-sectional SEM micrograph of PT-A718/10AL, in which the alumina, depicted in black, can be seen dispersed throughout the grey matrix of Alloy718. As can be observed in **FIg.4.15(b),** the alumina concentration in the PT-A718/20AL coating has grown. As can be seen in **Fig.4.15(c),** this pattern was also seen in the PT-A718/30AL coating. In all post-treated coatings, the refined and healed microstructure was observed as compared to the coatings without heat treatment.

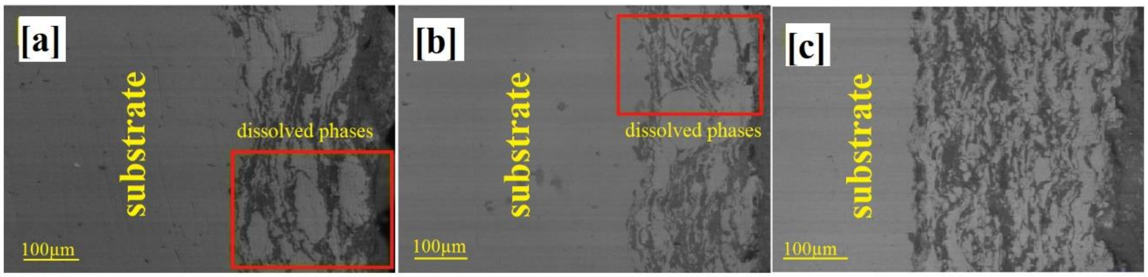

Fig.4.15 (a) Cross-sectional SEM micrograph of (a) PT-A718/10AL, (b) PT-A718/20AL, and (c) PT-A718/20AL.

4.8 DISCUSSION

The coating thickness of the deposited coatings has been determined along the cross-sections of samples and the range of 200-230µm has been found, which is near to the desired value for resisting high-temperature oxidation and similar to the analysis noted by Grewal et al. (2013); Espallargas et al. (2008); Roy et al. (2006); and Sidhu et al. (2005B and 2006B) for nickel-based coatings. The surface roughness is also associated with corrosion resistance, as the higher the surface roughness, the higher the possibility of corrosion attacks. HVOF coatings have a relatively smooth surface owing to the high effect energy of impinging particles, which causes better mechanical bonding and forms a homogeneous structure. A718+30% Al_2O_3 coating shows the maximum surface roughness, whereas minimum surface roughness is indicated by post-treated IN718+10% coating. The roughness of the coating is in good line with the findings noted by Yin et al. (2010); Espallargas et al. (2008); Fedrizzi et al. (2007); and Roy et al. (2004). The deposited coatings with dense microstructure provide better oxidation resistance than porous TSCs ("Thermally Sprayed Coatings"). The deposited coatings should possess minimum porosities as the porosity leads to the lower corrosion resistance of TSCs(Zhao et al, 2004 and 2005). The porosity of the coatings has been found to be less than 2.5% for all coatings. Further, coatings' post-treatment led to decreased porosity levels.

The high velocity in HVOF helps to deposit a coating having good inters plat bonding and mechanical anchorage to the substrate. Therefore, HVOF produces very hard and denser coatings. The mechanical property of the thermal spray coating that is most commonly cited is micro-hardness (Tuckeret al., 1994). In both the situations of micrometric and post-treated coatings, the HVOF sprayed coatings' micro-hardness has been discovered to be greater as compared to GCI. The coatings' micro-hardness values are found to be higher than those of the GCI substrates. As recommended by Verdon et al. (1998), Mingxi et al. (2004), and Hawthorne et al. (1999), the high thermal and kinetic energy acquired by the feedstock powder particles contributes to the high micro-hardness value and guarantees an excellent cohesion of powder particles, resulting in denser coatings along with homogeneous microstructure and the lack of unwanted oxides produced by the HVOF spray process. The research done by Kaushal et al. (2018), Praveen et al. (2015), Grewal et al. (2013), Sidhu et al. (2010), and Bin Yin et al. (2010), all show that the HVOF coating micro-hardness deposited in the current work is in excellent accord with those works.

Microstructures found in the present analysis are almost analogous to those reported by Kaur et al. (2011); Bala et al. (2010); Mahesh et al. (2009B); Sidhu and Prakash. (2006G); Sidhu et al. (2006D); Sundararajan et al. (2004); and Dent et al.(2001). The elements identified by the cross-sectional EDS maps are reported in the current study. The mappings indicate the rich incidence of Cr and Ni in each of the as-sprayed HVOF coatings. It was also found from the elemental mappings that the incidence of O and Al in the deposited combinations of powder and these elements showed increased concentration due to the addition of alumina content by 10, 20, and 30% in both micrometric and nanometric coatings.

CHAPTER 5

HIGH-TEMPERATURE EROSION AND DRY SLIDING WEAR STUDIES

The high-temperature erosion behavior of the bare GCI, as well as HVOF sprayed coatings, has been reported in this chapter. The uncoated & coated GCI were tested for solid erosion at 800 °C at various impingement angles. The eroded samples were examined using SEM micrographs at varying magnifications. Before erosion testing, the weight of the samples was determined, and the final weight was used to determine the erosive wear rate. After each test, the sample have been weighed and their weight alteration has been determined with a scale with a resolution of 0.01 mg.

5.1 RESULTS AND DISCUSSION

The high-temperature furnace described in the section was used in the present examination to examine the high-temperature erosion behavior of all samples (Chapter 4). The results that were obtained after various characterizations of test specimens are detailed in the following sections.

5.1.1 Uncoated GCI and A718 coated GCI

5.1.1.1 Erosion Rate

The size and shape of the impression left on both specimens' surfaces during erosion testing could be used to determine the erosion resistance of each specimen. In this chapter, the estimated and reported "erosive wear rates" (g/g) for uncoated GCI and A718 coated samples are discussed. Both the HVOF-coated samples and the GCI substrate were used to calculate the erosive wear rate (g/g), which is the ratio of wear loss of mass in grams to the erodent mass in grams. The macrographs offer useful data on the process of erosion behavior at 800 °C and of different impingement angles as presented in the upcoming sections. The uncoated GCI as well as A718 coated specimens underwent the high-temperature "solid particle erosion" test at 30° & 90° impact angles. **Fig.5.1a-d** displays the optical macrographs for both test angles. In both test angles, the A718 coating has sustained less damage than the GCI substrate that isn't coated. The **Fig.5.2** and **Fig.5.3** have shown in the pictographs of various as-sprayed and post-treated coatings, respectively.

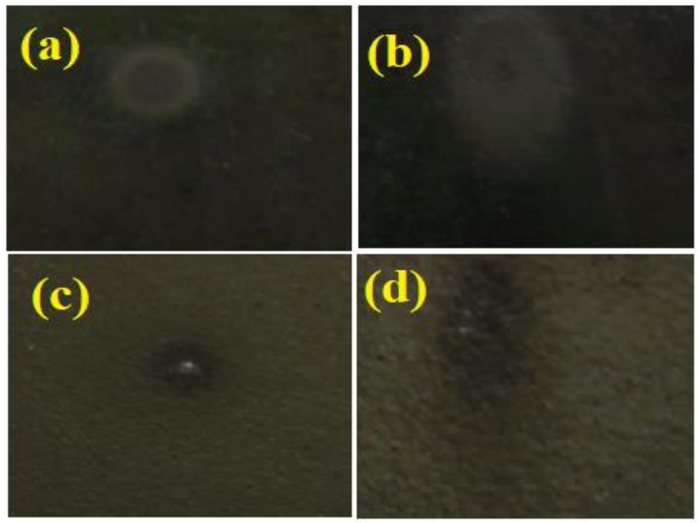

Fig.5.1. Macrographs of the GCI substrate and eroded A718 specimens at 30° and 90°

(a) Eroded GCI substrate attained after 90° impact angle, (b) Eroded GCI substrate attained after 30° impact angle, (c) Eroded A718 coated GCI specimen obtained after at 90° impact angle, and(d) Eroded A718 coated GCI specimen obtained at 30°impact angle, respectively.

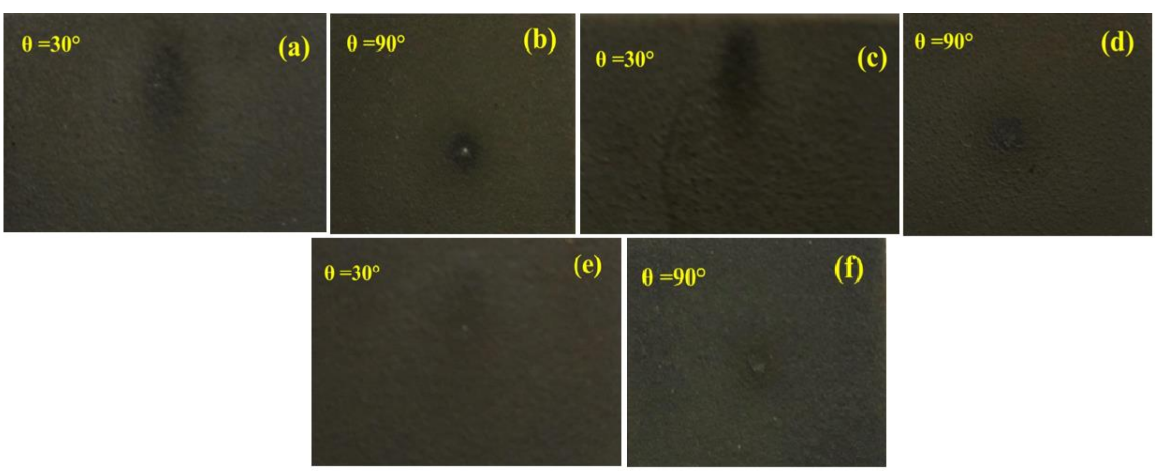

Fig.5.2. Photograph of the various A718+Al_2O_3 coated eroded samples at 30° & 90°angle of impacts (a) A718/10AL obtained after 30°, impact angle, (b) A718/10AL after 30° impact angle, (c) A718/20AL obtained after at 30°, (d) A718/20AL obtained at 90° (e) A718/30AL obtained at 30°, and (f) A718/30AL obtained at 90° impact angle, respectively.

The coatings at a 30° impact angle showed the elliptical mark formed in the erosion test and for a 90° impact angle the round marks were formed.

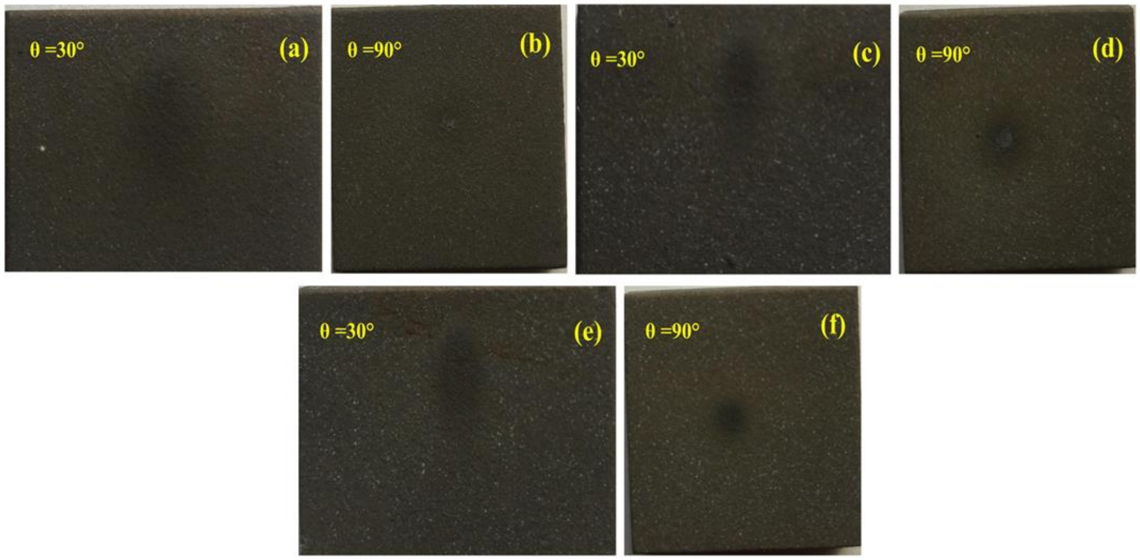

Fig.5.3. Photograph of the various PT- A718+Al_2O_3 coated eroded samples at 30° & 90°angle of impacts (a) PT-A718/10AL obtained after 30°, impact angle, (b) PT-A718/10AL after 30° impact angle, (c) PT-A718/20AL obtained after at 30°, (d) PT-A718/20AL obtained at 90° (e) PT-A718/30AL obtained at 30°, and (f) PT-A718/30AL obtained at 90° impact angle, respectively.

5.1.2 SEM Analysis

Due to the existence of small fissures and a few "erodent particles" embedded on the surface at a 90°impact angle, the surface of uncoated GCI substrates shows wear in Fig.5.4. SEM picture. These fractures developed as a result of the recurrent fatigue loading brought on by the many erodent effects that led to the GCI material's brittle fracture. The surface of the erodent is cracked from repeated impact; these fractures have grown larger and joined together, pulling material away and causing craters to develop in various places. Therefore, the material removal from the uncoated GCI substrate surface is caused by the brittle mode of erosion. Nevertheless, as seen in **Fig.5.4.**, the uncoated GCI substrate has some signs of micro-cutting brought on by the erodent's sharp edges impacting the surface at a grazing angle (at a 30° impact angle) (a). Additionally, at a 30° impact angle, a few tiny craters & cavities also developed on an uncoated GCI substrate. These characteristics have developed in a manner that is comparable to that found in the GCI sample that underwent erosion testing at a 90° angle of contact. The fatigue stress and production of tiny fractures that result in material pullout are caused by the vertical component of oblique impacts.

The GCI substrate formed several craters on its surface after being tested with air-jet erosion at a 30° angle, as illustrated in **Fig.5.4. (a).** In addition to micro-cutting marks, the cavities following erosion tests are visible on the surface. At a 90-degree impact angle, the GCI substrate surface exhibited pull-out and fissures. Because they repeatedly strike the GCI substrate at a normal angle, as demonstrated in **Fig.5.4. (b)**, the erodent particles adhere to the surface of the substrate. At a 90° impact angle, the direct impingement of the erodent particles results in fatigue, which leads to pull-out and the development of cracks from direct impacts.

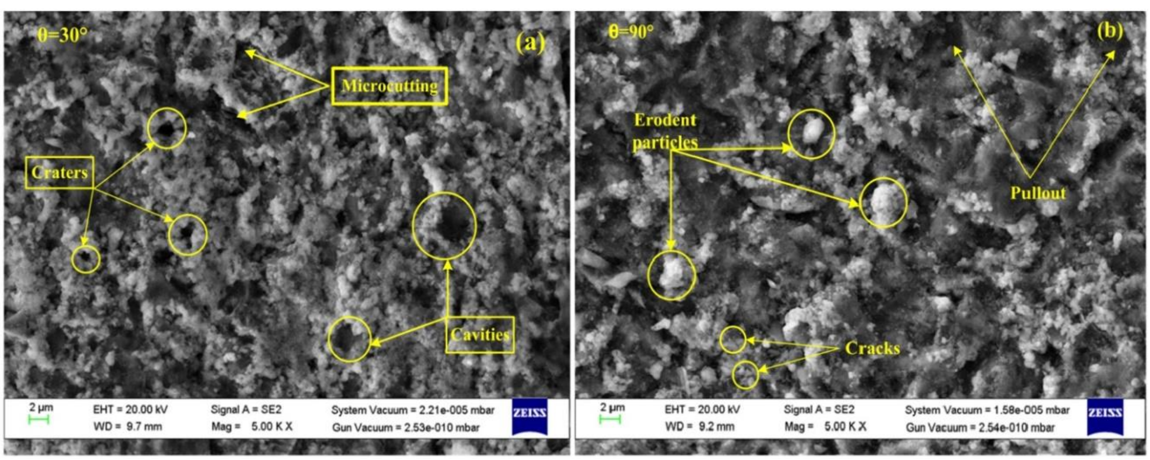

Fig.5.4. (a) Eroded surface's SEM micrographs of uncoated GCI substrate at 30°, and (b) at 90° angle of impacts.

However, as shown in **Fig.5.5,** the worn-out surface of A718 coated samples exhibits ploughing as well as plastic deformation of the material. When erosion testing was done at a 30° impact angle, a ploughing or cutting (abrasion)mark could be observed beside the strain-hardened material (lip) and plastically deformed. However, the A718 coating exhibited higher hardness at room temperature but at such high-temperature niobium carbide (NbC) and Ni_3Nb were formed and may act as a brittle phase. Therefore, the ploughing or cutting marks might have appeared on the coated surface. Furthermore, the higher erosion rate at a 30° angle of impingement confirms that the IN718-covered specimen is eroding in ductile mode (Wheeler et al., 2005; Finnie,1995 Finnie,1998)**.** The surface of the A718 coated sample was subjected to erosive wear tests at a 90° impact angle, which also indicated the development of lip around the edges of the craters. The numerous normal collisions of the erodent particles over the unmelted IN718 powder particles may have fatigued the powder, causing these craters to develop. The development of lips close to cavities demonstrates the splats strain hardening under repeated hits from erodent particles. The A718 and bare GCI substrate showed different impression marks formed during the erosion test at 30° & 90° impact angles.The micro-cutting of the A718 coating, which was applied using the HVOF technique to a GCI substrate, caused the coating to deform plastically. The coating displayed the ductile mode of erosion at a 30° impact angle. As seen in **Fig.5.5(a)**, the higher SEM micrograph demonstrates how the crater edges have developed a lip and distorted splats. When the A718 coating is hit at a 90° impact angle, fractures, and erodent particles are visible, which signifies the erosion brittle mode caused by the repeated impact of erodent during air-jet erosion testing.

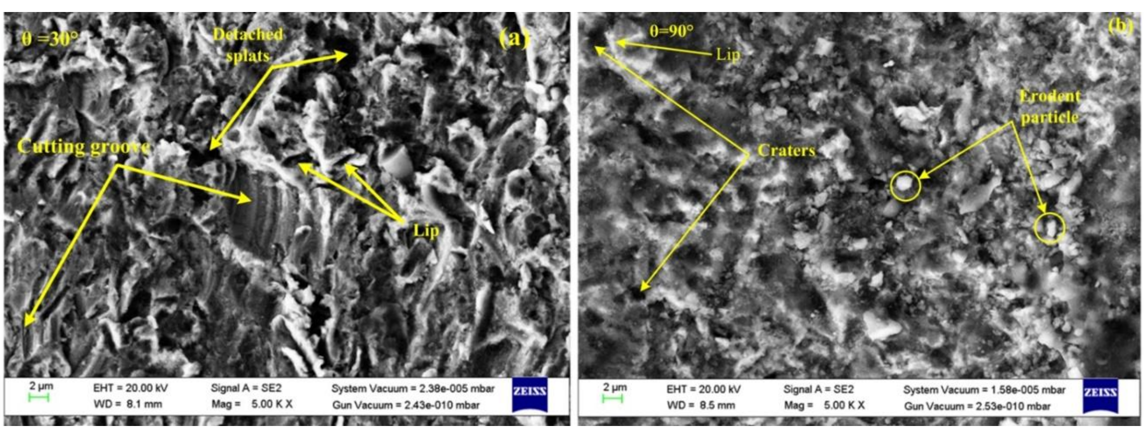

Fig.5.5. (a) SEM micrographs of the eroded surface of A718 coated GCI at 30°, and (b) at 90°angle of impacts.

In three quantities, Al_2O_3 (alumina) was mixed with the A718 alloy powder before being deposited on the GCI substrate using the HVOF method. The performance of high-temperature erosion of the A718/10AL has been evaluated and presented. The SEM micrograph of A718/10AL coatings showed the formation of cutting grooves and lip formation at a 30° impact angle as presented in **Fig.5.6(a)**. The coating showed the pullout and cracks along with erodent particles sticking on the surface at 90° as presented in Figure **Fig.5.6(b)**.

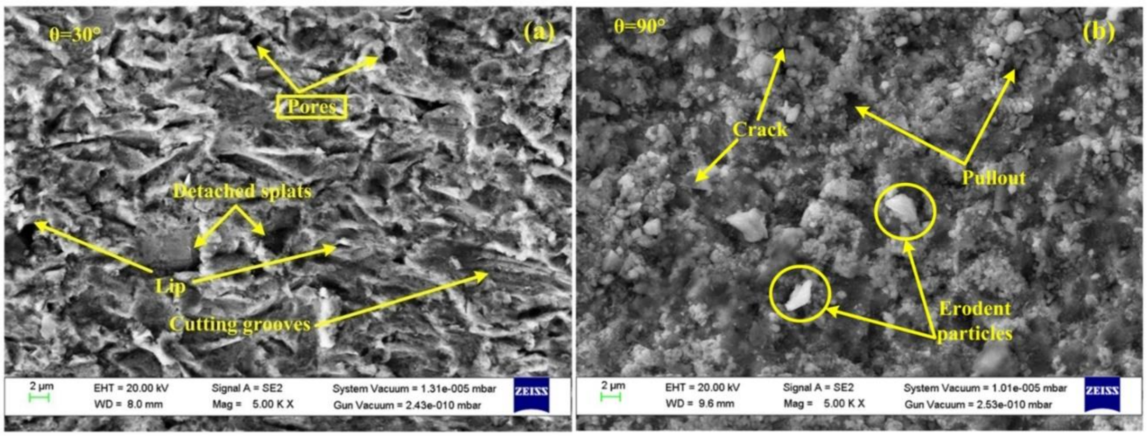

Fig.5.6. (a) SEM of eroded micrographs of A718/10AL coated GCI at 30°, and (b) at 90° angle of impacts.

The SEM micrograph of eroded A718/20AL coating showed ploughing marks and craters when impacted at a 30° impact angle as presented in **Fig.5.7(a)**. The ploughing marks are also present on the eroded coating's surface and a detached splat can be seen. However, the surface morphology of this coating seems in good condition as compared to the A718and A718/10AL coating. There are fewer cracks and impacted sites formed in A718/20AL coating at a 90° angle of impact as presented in **Fig.5.7(b)**.

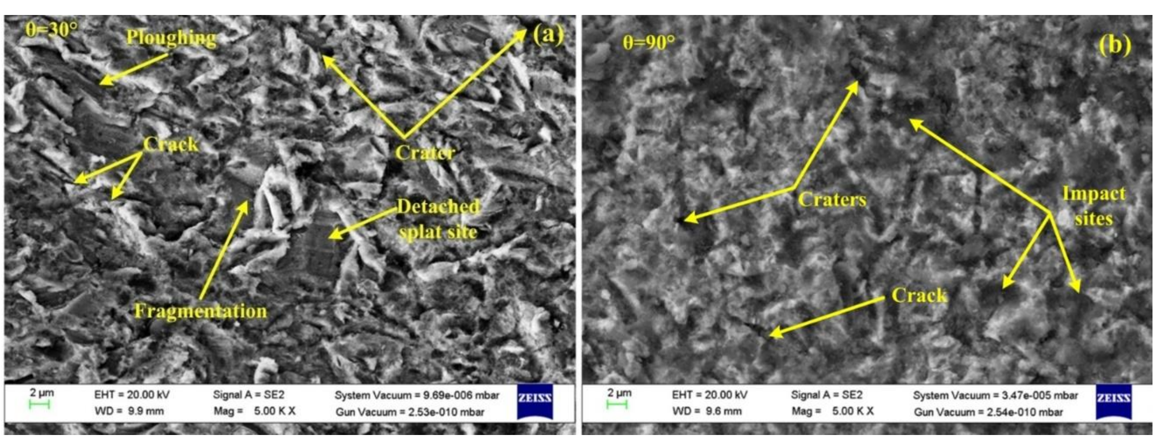

Fig.5.7. (a) SEM of eroded micrographs of A718/20AL coated GCI at 30°, and (b) at 90° angle of impacts.

The eroded A718/30AL coating's SEM micrograph showed abrasion marks on the surface and fewer lip formations at the edges of the craters at a 30° impact angle as presented in **Fig.5.8(a).**

The higher content of 30% micrometric Al_2O_3 in A718/30AL coating revealed the intense development of cracks and debonding of deposited coating as shown in **Fig.5.8 (b).** This has been attributed to the higher content of micrometric Al_2O_3 which is responsible for the excessive brittleness of the deposited coating.

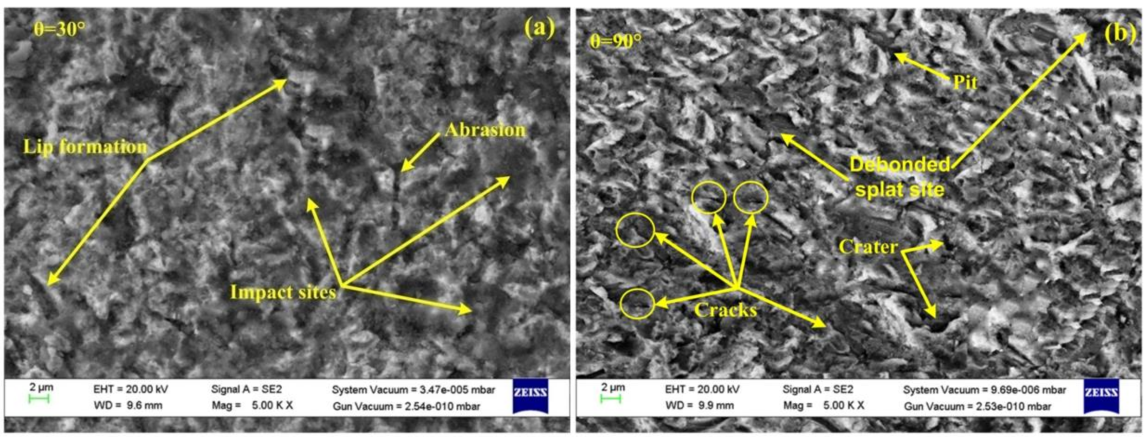

Fig.5.8. (a) SEM of the eroded surface of A718/30AL coated GCI at 30°, and (b) at 90° angle of impacts.

The post-processed PT-A718 has shown the pullout marks at 30° and some grooves at 90° angle of impacts as revealed in **Figs.5.9** (a) and (b), respectively.

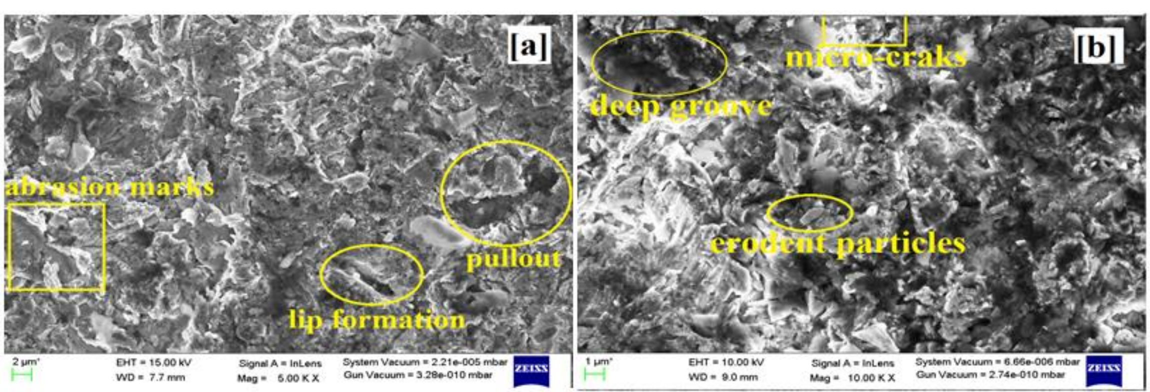

Fig.5.9. (a) SEM micrographs of the eroded surface of PT-A718 coated GCI at 30°, and (b) at 90°angle of impacts.

The performance of high-temperature erosion of the PT-A718/10AL has been presented. The eroded surface of PT-A718/10AL coatings presented fewer cutting grooves at a 30° impact angle as revealed in **Fig.5.10 (a)** and some impact sites &crack arrests as revealed in **Fig.5.10 (b).**

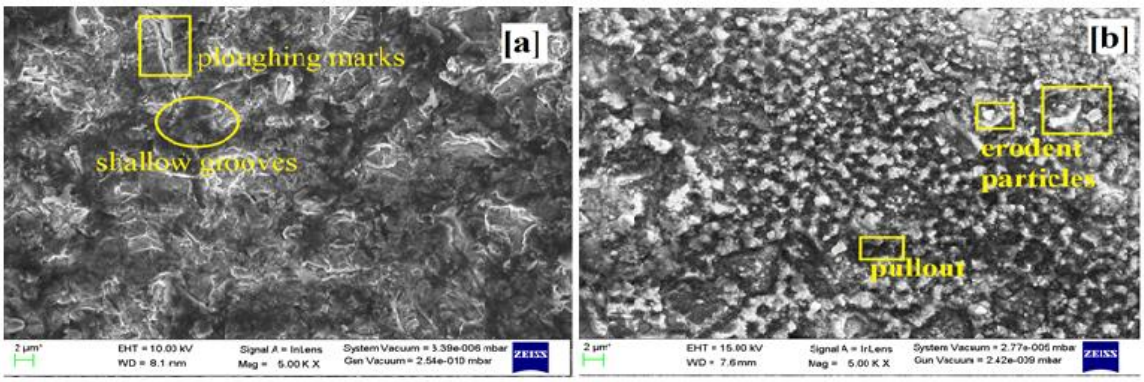

Fig.5.10. (a) Eroded surface's SEM of PT-A718/10AL coated GCI at 30°, and (b) at 90° angle of impacts.

The eroded PT-A718/20AL coating's SEM micrograph showed the retained identity of nanoparticles after exposure to air-jet erosion at 800°C and some abrasion marks along with less plastic deformation at impingement 30° angle as revealed in **Fig.5.11 (a).**

The tiny Al_2O_3 particles maintain the A718 matrix in place and prevent the applied coating from deforming. The PT-A718/20AL coating presented the development of fewer cracks but has been arrested as revealed in **Fig.5.11 (b).**

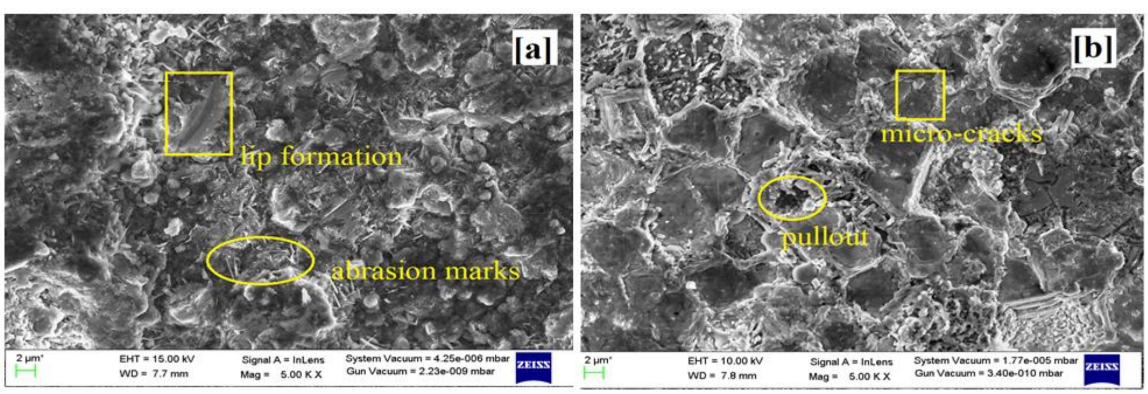

Fig.5.11. (a) SEM of the eroded surface of PT-A718/20AL coated GCI at 30°, and (b) at 90° angle of impacts.

The eroded PT-A718/30AL coating's SEM micrograph showed the retained microstructure of the coating and some cavities have been identified. These cavities are less distorted at a 30° impact angle than other deposited coatings, as seen in **Fig. 5.12 (a).** As illustrated in **Fig.5.12(b)**, there are minor impact sites on the degraded coating at an impact angle of 90 degrees.

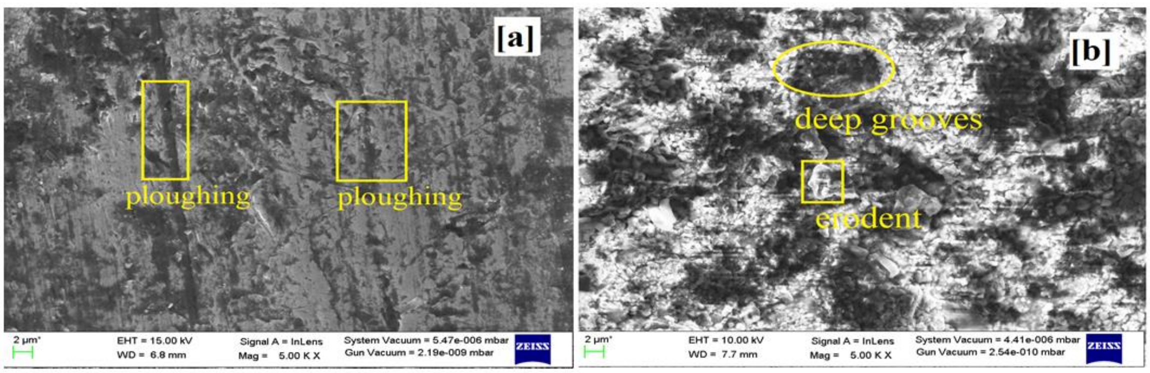

Fig.5.12. SEM of the eroded surface of PT-A718/30AL coated GCI at 30°, and (b) at 90° angle of impacts.

The erosive wear rate of the as-sprayed & post-treated coatings are presented in **Table 5.1.**

Table 5.1. Erosive wear rate of the as-sprayed & post-treated coatings.

Coating	**Erosion Rate (g/g)**	
	30º	**90º**
GCI	1.4×10^{-3}	2.1×10^{-3}
A718	5.2×10^{-4}	5.0×10^{-4}
A718/10AL	4.1×10^{-4}	5.9×10^{-4}
A718/20AL	3.5×10^{-4}	3.9×10^{-4}
A718/30AL	3.8×10^{-4}	4.0×10^{-4}
PT-A718	4.8×10^{-4}	4.7×10^{-4}
PT-A718/10AL	2.9×10^{-4}	3.1×10^{-4}
PT-A718/20AL	2.2×10^{-4}	2.8×10^{-4}
PT-A718/30AL	1.7×10^{-4}	2.0×10^{-4}

The erosive wear rate (g/g) for the uncoated and coated specimens showed nearly 4.7 times better erosion resistance of post-treated coatings when compared with uncoated cast iron and is shown in Table. On the contrary micrometric coatings showed 3.2 times better resistance to erosive wear than GCI substrate. Furthermore, post-treated coatings showed 1.4 times erosion resistance as compared to micrometric coatings.

5.2 DISCUSSION

There are two methods for deconstructing the erosion wear process. This comprises analyzing the erosion process based on the type of material being used and, secondly, based on the angles at which an erodent substance is impacting the material's surface. Firstly, the material removal mechanism owing to erosive wear takes into account the ductile and brittle character of the material. The two potential processes that might occur during erosive wear and cause surface deterioration are repeated plastic deformation and cutting. In the case of ductile materials, micro-cutting is the process responsible for material removal. It is followed by cutting the material from its surface. Contrarily, brittle materials break down due to a process called fatigue in which erodent repeatedly contacts the material's surface (Wheeler et al., 2005). These particles repeatedly and continuously transmit their energy to the surface, causing repeated collisions that eventually lead to fatigue failure. As a result, repeated impacts cause surface fissures and debonding of the splats reveals the coating's fragile nature. The impact angle is a key determinant of the material removal method, and the “impingement angle” of the erodent particles has a direct bearing on the erosion mechanism. The impact angle at where the working fluid enters the system and impacts the surface to produce a material deterioration of the component's working surface varies depending on the actual uses, such as gas turbines, rocketry components, heat exchangers, boilers, and hydrodynamic turbines. The material removal method changes depending on the change in the impact angles, which range from low to high. Cutting of the material as well as chip formation results in the removal of the material at low-impact angles. Higher erosion rates are seen at lower angles of 20° & 30° according to an analysis of the ductile process of erosion (Finnie et al., 1995). When the angle is at or near 90 degrees, erosion failure occurs. This entails the production of lips primarily for materials that deform more quickly. Platelets are removed when repeatedly impacting erodent particles. However, the materials with the lowest 90-degree erosive wear resistance fall into the brittle mode category (Flynn et al., 2001).

The erosive wear rate (g/g) has been computed for GCI substrate and coatings at 30° & 90° angles of impact. It displays that the post-treated coatings exhibited greater erosion resistance as compared with micrometric and uncoated cast iron. The erosion rate reduced with an increase in alumina content in the case of post-treated coating and on the other hand, A718/20AL coating alumina showed higher erosion resistance as compared to A718/30AL coating. This might be explained by the covering being more brittle and ductile. The base metal, Inconel-718, and as-sprayed coatings have experienced ductile and brittle modes of erosion with grooves, lip development, pullouts, and craters as prominent processes. The material takes place at low angles mainly due to micro-cutting caused by striking of erodent and lip formation followed by strain hardening are responsible for ductile fracture (Praveen et al., 2015). The coatings show the maximum loss through erosion at 90° in comparison to the lower angle of impact at30°.

The SEM images of GCI substrate and coated specimens reveal the craters produced due to impacts and the elongated lips around the periphery of craters. The micro-cutting, micro-plowing, and irregular indentations at 30° could be seen. For a 90° angle of impingement, erodent particles, cracks, and impact sites reveal the plastic deformation. The erosion process also indicates the elimination of splats at a 30° angle and this is due has caused as the tangential forces act directly by striking of erodent on the splats at the lower impact angle (Ramesh et al., 2011).

As far as the post-treated coatings are concerned, the brittle mode of failure has been suppressed owing to high hardness and less porosity. This results in superior erosion resistance than as-sprayed coatings.

Additionally, the grooves and abrasion marks, which is an indication of material removal by the action of micro-cutting as well as micro-plowing. Coatings showed better resistance to erosive wear at a 30° angle in comparison to a 90° angle of impact owing to the pinning impact of angular alumina having a high hardness value (Shreedhar et al., 2009).

At a 90° angle of impact, impact sites can be seen along with erodent particles on the eroded surface. The effect of shielding by alumina decreases at 90° and excessive brittleness in the case of A718/30AL coating leads to pullouts. This trend can be observed and the formation of cracks at a 90° angle occurred and A718/30AL coating failed to prevent erosion resistance as compared to PT-A718/30AL.

5.3 DRY SLIDING WEAR

The relative motion between two solid, smooth surfaces in contact when under load is what defines sliding. High local pressure between the contacting asperities causes plastic deformation, adhesion, and ultimately the local development of junctions. These junctions are ruptured by repeated sliding between the contacting surfaces, which also commonly results in material transfer from one surface to the other. Material loss occurs in the form of small particles which are usually transferred to the other surface or get dislodged from the candidate surface. One of the most frequent forms of tribal contact that engineering components like gears, cutting tools, and machine tool slides undergo is sliding. During sliding contact, tribochemical reaction, abrasion, adhesion, and surface fatigue may take place. While in abrasion, the material is removed as a result of the presence of hard particles on the counter surface, adhesion results in the formation of a welded junction with the surface. As a result of the tribochemical process, surfaces develop loose wear particles that function as abrasives. Numerous studies have been conducted in this field as a result of applications of sliding wear in engineering components (Deuis and Kailas, 2009). In the present study, pin-on-disc tribometers were used to measure the dry sliding wear performances of the substrate material, as-deposited, as well as heat-treated specimens. Additionally, the worn surfaces’ SEM micrographs and the wear results were correlated.

5.3.1 Wear Rate and Cumulative Weight Loss Characteristics

The approach described in Chapter 3 was followed to measure the abrasive wear (Pin on disc) performance of the as-deposited specimen and the post-heat-treated specimens. The overall specimens' cumulative weight loss characteristics and “abrasive wear coefficient” (substrate, as-sprayed as well as heat-treated coatings). The cumulative weight loss data indicated the substantial weight substrate loss followed by as-deposited A718 coating followed by A718/10AL, A718/20AL, and A718/30AL, respectively. It is observed that the heat-treated specimens (A718, A718/10AL, A718/20AL, and A718/30AL) exhibited minimum weight loss among all the tested samples. This was ascribed to the significant increase in hardness & strength of the post-heat-treated coatings owing to the creation of strengthening precipitates after the precipitation hardening heat treatment process. It is evident that all samples, including substrate GCI, as-sprayed, and heat-treated coating specimens, exhibit an abrupt rise in weight loss during the early run-in-wear phase. Archard's wear relation **(Eq. 5.1)** was applied to determine the coefficient of wear rate for all the examined specimens (substrate, as-deposited, and heat-treated).

$$Q = \frac{KW}{H} \qquad \textbf{(Equation-5.1)}$$

Here,

Q indicates Wear rate in g/m,

H represents the material’s hardness

W signifies Load in N.

K *denotes* dimensionless constant referred to as “abrasive wear coefficient”

After first contact with the disc, the wear rate of the substrate (GCI) steadily decreases. The major causes of wear in the substrate (GCI) were plastic deformation brought on by surface and sub-surface deformation, the creation of debris, material transfer, and environmental reactions. It was found that both the as-deposited & heat-treated samples had considerably lower wear rates. For each of the tested specimens (substrate, as-deposited, and heat-treated samples), the estimated value of the abrasive wear coefficient was determined. The cumulative weight loss vs substrate and coating sliding distance as shown in **Fig.5.13.** The calculations for the abrasive wear co-efficient [k] in case of substrate and as-sprayed coatings are presented in **Table.5.2**

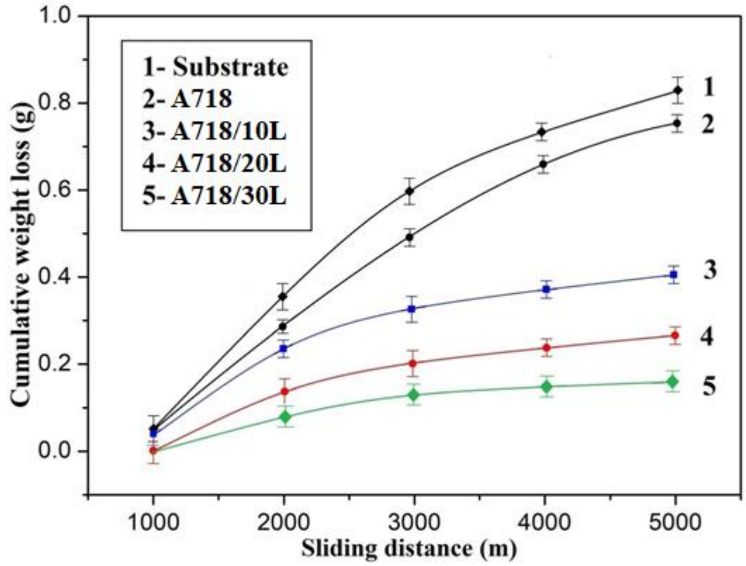

Fig.5.13. Cumulative weight loss vs coating sliding distance for substrate and coatings

The cumulative weight loss vs sliding distance for post-treated coatings are shown in **Fig.5.14.** The calculations of abrasive wear co-efficient [k] in case of post-treated coatings are shown in **Table 5.3.**

Table 5.2 Abrasive wear co-efficient [k] in case of substrate and as-sprayed coatings.

S.No	**Coatings/Substrate**	**Abrasive wear co-efficient [k]**
1.	GCI	1.0 x 10E-4 [MAXIMUM]
2.	**A718**	6.0 x 10E-5
3.	**A718/10AL**	3.9 x 10E-5
4.	**A718/20AL**	2.5 x 10E-5
5.	**A718/30AL**	1.7 x 10E-5 [MINIMUM]- 5.8 TIMES

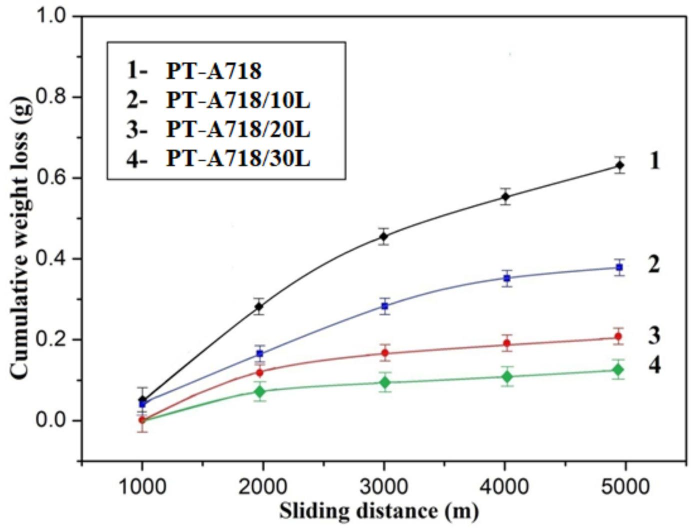

Fig.5.14. Cumulative weight loss vs sliding distance for post-treated coatings.

Table.5.3 Abrasive wear co-efficient [k] in case of post-treated coatings.

S.No	Coatings/Substrate	Abrasive wear co-efficient [k]
1.	**PT-A718**	4.5 x 10E-5
2.	**PT-A718/10AL**	2.5 x 10E-5
3.	**PT-A718/20AL**	1.9 x 10E-5
4.	**PT-A718/30AL**	1.2 x 10E-5 [MINIMUM- 8.3 times]

The PT-A718/30AL specimens showed a 78% minimum abrasive wear coefficient from the substrate (GCI) and a 60% minimum abrasive wear coefficient compared with as-deposited A718 Coating. The fact that a large amount of Laves phase became dissolved in the matrix and caused more Nb, Mo, and Ti elements to be utilized for the precipitation of “strengthening phases” (γ') within the matrix was the cause of the samples treated with the

PT-A718/30AL having the lowest possible abrasive wear coefficient. Thus, the PT-A718/30AL treatment resulted in a maximum rise in the hardness and strength of the matrix as compared to all heat-treated samples.

5.3.2 Worn Surfaces SEM Analysis.

All samples were investigated using SEM/EDS after the wear testing to examine the wear mechanisms of each specimen. Mostly plastic deformation and abrasion of the substrate's surface material occurred. The substrate material wore down due to adhesion, abrasion, and plastic deformation (GCI) as shown in **Fig.5.15.**

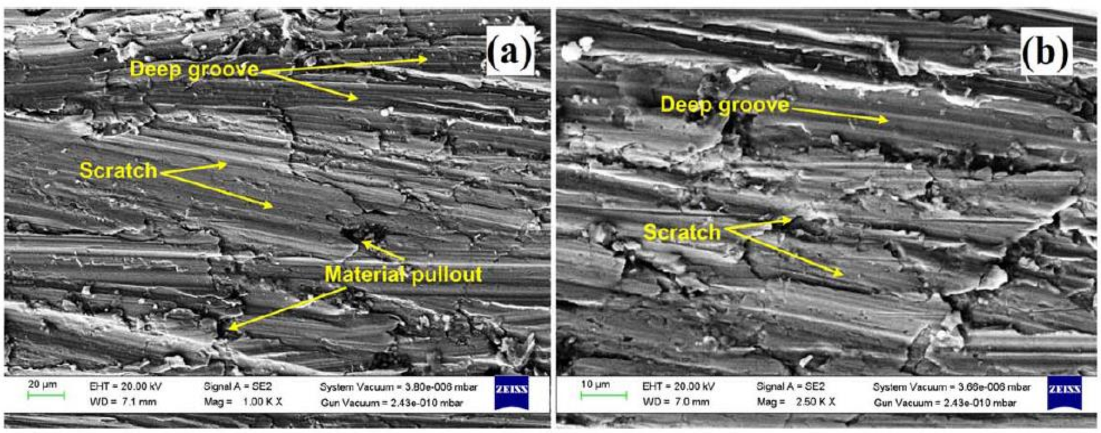

Fig.5.15. SEM micrograph of worn out (a), (b) uncoated substrates.

The adhesion between the counter disc and the substrate caused the material to come loose from the substrate, which caused the material to transfer and created craters in the worn surface. The surface developed deep scratches that show where the material was pulled out. On the worn-out substrate surfaces, considerable abrasion was also observed as a wear mechanism in the form of ploughing marks, deep grooves, craters, and scratches, as illustrated in the figures.

The surface of the worn-out specimen of as-sprayed A718 coating displayed abrasion marks and pit development. **Fig.5.16(a)** depicts the scratches generated during sliding wear. Furthermore, ploughing can be seen on the surface, and micro-cutting action can be seen in some places, as shown in figure **Fig.5.16(b).** The presence of un-melted particles on the as-sprayed surface may cause micro-cutting in the coating (sharma et, al

2010). During the ploughing motion, the interface of the melted and un-melted is sheared, resulting in micro-cutting lines on the surface.

The worn-out specimen of post-processed coating, on the other hand, displayed a depressed imprint of the counter surface, as illustrated in **Fig.5.16(c) &(d),** respectively (Zafar et al., 2014,2016).

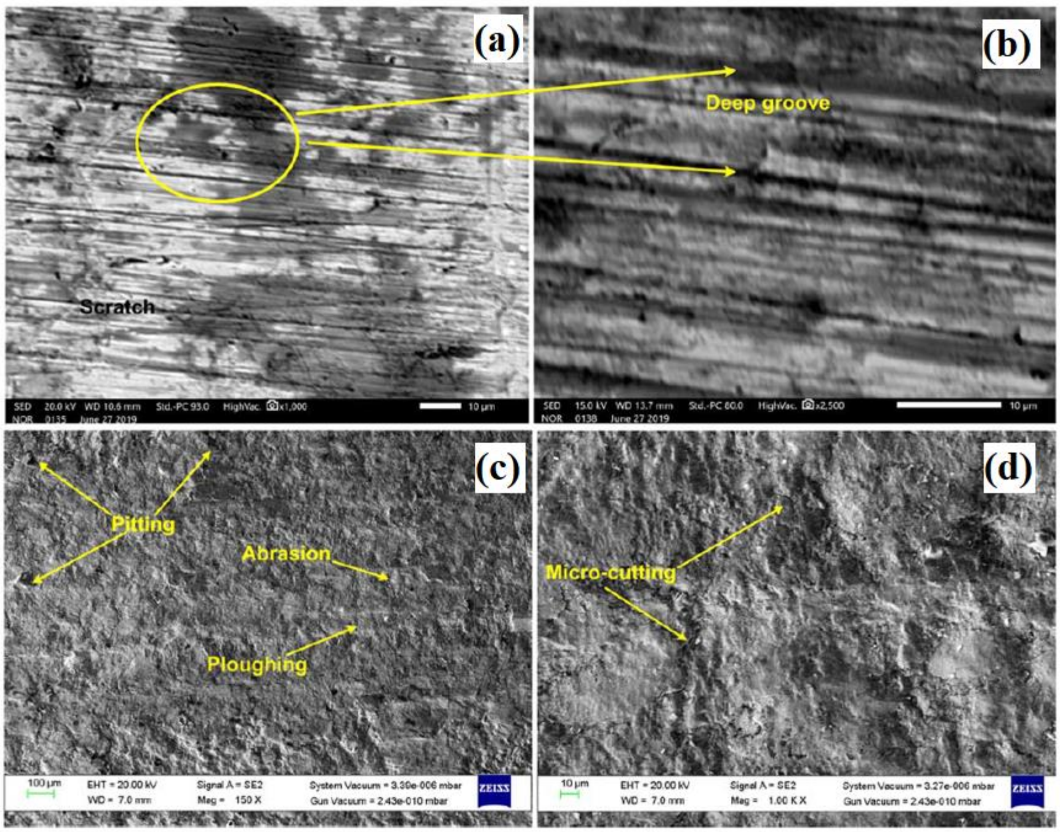

Fig.5.16. SEM micrograph of worn out (a), (b) as-sprayed A718 coating, and (c), (d) post-processed A718 coating

As illustrated in the SEM/EDS Figs, the worn-out surfaces of the as-deposited and post-treated samples had some deep grooves, craters, and material debonding had occurred. The surface also had abrasion marks with the creation of pits. At certain locations during the sliding, the scratches developed. Additionally, there is visible ploughing on the surface, and there is micro-cutting activity.

The worn surface of A718/10AL has shown in **Fig.5.17.** The surface has shown plastic deformation and shearing on the surface, that is attributed to the presence of major portion of matrix in the coating combination. However, few craters are also present on the surface, that may have shown the pull-out of the alumina particles from the surface. The HVOF coating process is not capable to completely melt hard phase present in the coating. However, due to increase in the hardness of A718/10AL has shown reduction in wear rate as compared to substrate and A718 coating, respectively. The mixed mode of wear was observed in A718/10AL coating.

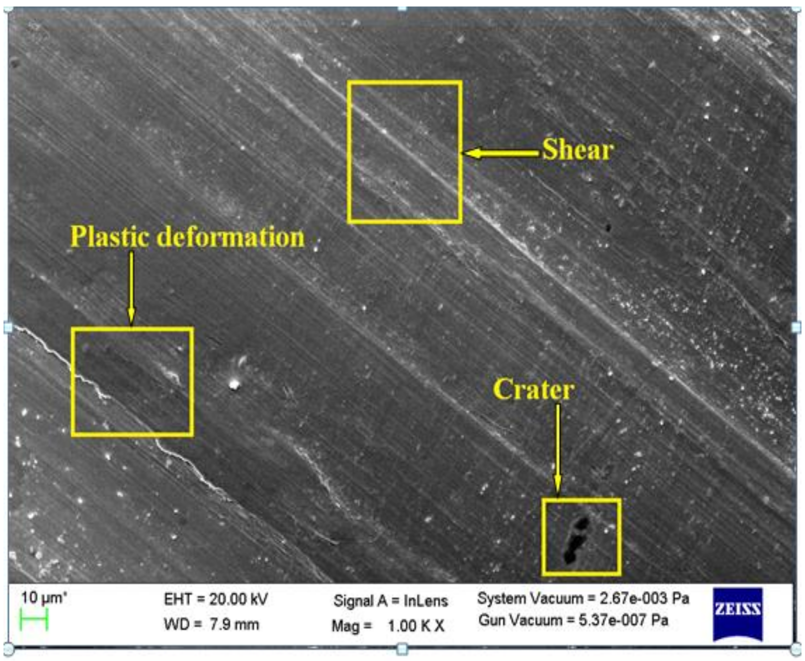

Fig.5.17. The worn surface of substrate A718/10AL may be seen in a typical SEM micrograph.

The Typical SEM micrograph of the A718/30AL's worn surface has been presented in **Fig.5.18.** The surface has shown the crater, groves and some de-bonded particles from the surface of A718/30AL coating. The A718/20AL coating has also shown the similar surface and to avoid the repetition in the reasoning, the SEM micrograph of A718/30AL coating has shown to understand the wear mechanism. These coatings have shown brittle mode of wear. The hard alumina particles have resisted ploughing and micro-cutting in these coatings. The abrasion caused on the surface was resisted by the hard reinforcement as compared to substrate, A718 and A718/10AL coating, respectively.

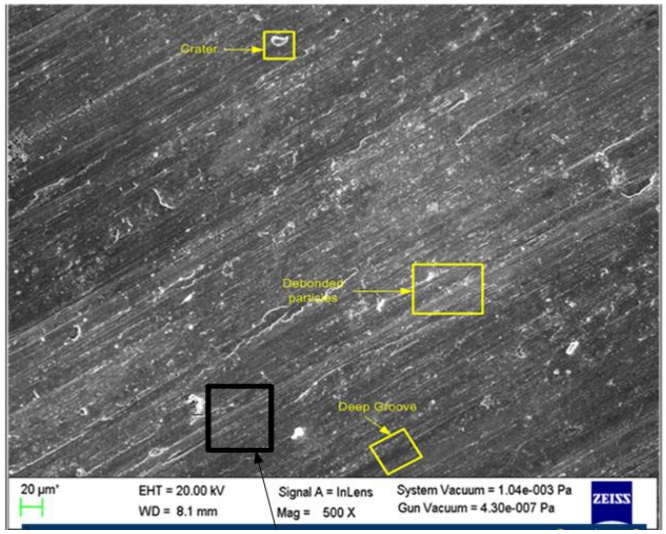

Fig.5.18. Typical SEM micrograph of the A718/30AL's worn surface.

It is observed that A718 treated samples suffered material loss owing to ploughing and pitting. On the other hand, there is no material pull-out or deep grooves were shown in PT-A718/10AL treated specimens as shown in **Fig.5.19.** The abrasion marks and ploughing has been shown by PT-A718/10AL treated coatings.

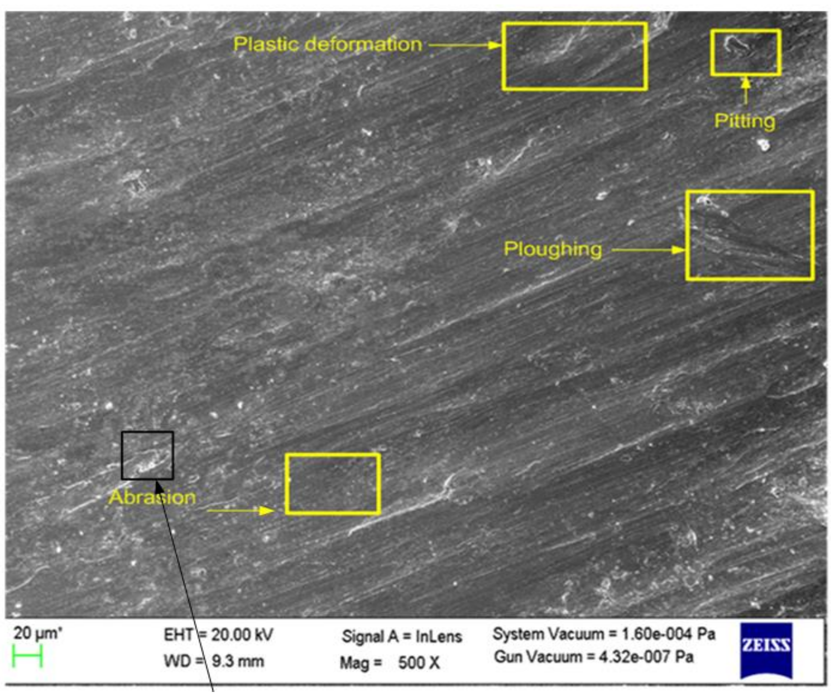

Fig.5.19. Typical SEM image of the PT-A718/10AL's worn surface.

The increased wear resistance of A718/20AL was due to the Laves phase being almost completely dissolved within a matrix and simultaneously formation of strengthening precipitates (γ') in the matrix as shown in **Fig.5.20.** The worn-out surface of the PT-A718/30AL specimen indicated the depressed and abrasion impression of the "counter surface" which shows enhanced wear resistance of the PT-A718/30AL specimen as shown in **Fig.5.21.**

More material was transferred and wear debris was produced as a result of the material detaching from the substrate due to adhesion between the counter disc and the substrate.

The surface developed deep scratches that show where the material was pulled out. In the forms of deep grooves, ploughing marks, and scratches, as illustrated in the figures, considerable abrasion has also been visible as a wear process on the "worn-out substrate" surfaces.

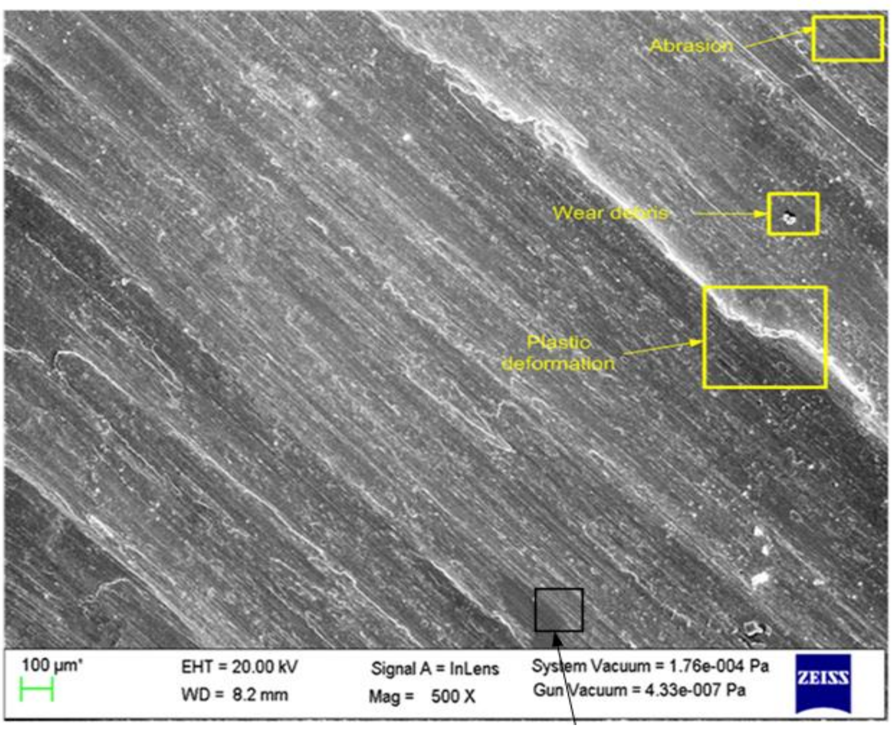

Fig.5.20. Typical SEM image of the PT-A718/20AL's worn surface.

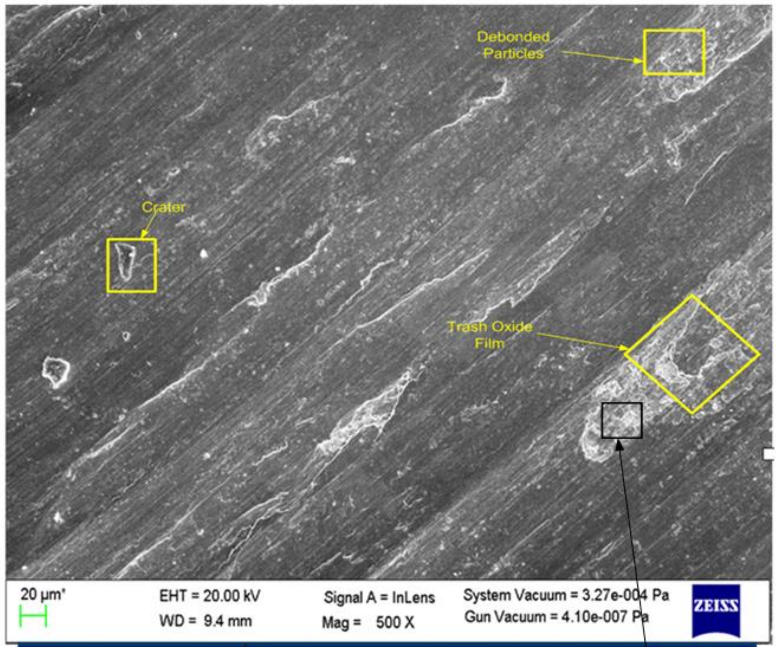

Fig.5.21. Typical SEM/EDS image of the PT-A718/30AL's worn surface.

5.4 SUMMARY

The tribological aspects of A718 coating and heat-treated specimens were discussed with suitable illustrations. The sliding wear rate for PT-A718/30AL was reduced by 3.2 times and 2.8 from the substrate and as-deposited coatings. Whereas in the case of the A718/30AL sample, it is reduced by 2.1, and 1.8 times compared with the substrate. The dry sliding wear rate of PT-A718/30AL specimens showed a 78% minimum abrasive wear coefficient from the substrate material. The PT-A718/30AL treated samples had the lowest possible abrasive wear coefficient as a consequence of a significant amount of Laves phase dissolving in the matrix as a result of heat treatment, which allowed for more Nb elements to be employed for the strengthening phases' precipitation.

Chapter 6

CONCLUSIONS AND FUTURE SCOPE

6.1 CONCLUSIONS

The following conclusions were obtained on the basis of experimental results obtained and their analysis in the current work.

1. HVOF-sprayed A718-based coatings with different proportions of nanometric and micrometric alumina content have successfully been deposited on GCI substrate. The deposited coatings showed homogenous, dense, crack-free, and uniform microstructure.
2. The EDS spectra of different coatings confirm the presence of major elements of feedstock powder used which improved the erosion and oxidation resistance. EDS maps of all coatings showed the proper distribution of Al_2O_3 in the deposited coatings and the incidence of major constituents Fe, Cr, and Ni of feedstock powder. The EDS spectra indicate that their chemical was no change observed in the base metal occurred.
3. The as-deposited coatings showed signs of Laves phases, “niobium carbide” (NbC), and the “γ-Ni-Cr (fcc) solid solution” matrix. The alloying components, which have been expressed in the coating powder as a solid solution, interacted with one another in the molten powder layer in thermal spraying. As a result, the new phases formed, as shown in the A718 coating's XRD pattern. As a result of consuming the alloying elements necessary for matrix reinforcement, these new phases significantly affect the coating qualities. The Spectra of the post-treated A718 coating, as revealed in the XRD pattern of A718 coating, show the existence of Laves phases in addition to the γ-Ni–Cr (fcc) matrix.
4. The microstructure analysis showed that the dispersion of alumina particles in post-treated coatings was significantly effective as compared to the as-sprayed coatings. However, the porosity level increased with an increase in Al_2O_3 content in the A718

matrix. Maximum porosity in order of 2.4% was observed in A718/30AL coating while the lowest porosity was found in the case of PT-A718 and PT-A718/10AL coatings on order of 0.78 and 0.99, respectively.

5. The micro-hardness analysis showed a trend of increased hardness with the addition of alumina content in A718. A higher hardness of 912±16 HV was found for PT-A718/30AL coating which is approximately 5.8 times higher than the hardness of uncoated GCI (225±10 HV). On the other hand, in the case of as-sprayed coatings, the maximum average micro-hardness value of 805±16 HV was obtained for the A718/30AL, which is about 3.56 times the hardness of the substrate.
6. PT-A718 coating has shown the least average surface roughness of about 0.40µm, whereas the highest surface roughness of 0.86µm has been observed for A718/30AL coating.
7. The PT-A718/30AL coated GCI showed the maximum resistance to erosive wear with approximately 4.7 times better performance as compared to uncoated GCI. It was found that the role of alumina content and dissolved laves phase has played a critical role in erosion resistance.
8. With the increase in Al_2O_3 content in A718 alloy, the erosion resistance significantly increased and a ductile mode of erosion was observed in the case of A718 coating, and for all A718/AL coatings, a brittle mode of erosion was observed.
9. Based on the erosive wear rate, the erosion rates for the uncoated and coated GCI at both impingement angles have been arranged in decreasing order in the following sequence:

   As-sprayed: A718/30AL > A718/20AL > A718/10AL> A718>GCI

   Post-treated: PT-A718/30AL > PT-A718/20AL > PT-A718/10AL> PT-A718
10. The sliding wear rate for PT-A718/30AL was reduced by 3.2 times and 2.8 from the substrate and as-deposited coatings. Whereas in the case of the A718/30AL specimen, it is reduced by 2.1, and 1.8 times compared with the substrate. The dry sliding wear rate of PT-A718/30AL specimens showed a 78% minimum abrasive

wear coefficient from the substrate material. The minimum abrasive wear coefficient in the PT-A718/30AL treated samples was due to the fact that after heat treatment, a great number of Laves phases got dissolved in the matrix which resulted in more Nb elements being used for the precipitation of strengthening phases. The sliding wear resistance has been observed in the following sequence:

As-sprayed: A718/30AL > A718/20AL > A718/10AL> A718>GCI

Post-treated: PT-A718/30AL > PT-A718/20AL > PT-A718/10AL> PT-A718

6.2 FUTURE SCOPE

1. Nano- A718 could be used instead of micron-sized A718 and other ceramics powders like TiO_2 may be used.
2. The post treatments like laser hardening of the deposited coatings can also be done to know the impact of "post heat" treatments on the performance of the coatings.
3. The electrochemical and hot-corrosion behavior of the coatings may also be performed for particular high-temperature applications like boiler tubes and turbine blades.

BIBLIOGRAPHY

1. Akdogan, A.N. and Durakbasa, M.N., (2008), “Thermal cycling experiments for glass moulds surface texture lifetime prediction – Evaluation with the help of statistical techniques” Measurement,Vol. 41, pp. 697–703.
2. Bala, N., (2010), “Investigations on the Hot Corrosion Behaviour of Cold Spray and HVOF Spray Coatings on T22 and SA 516 Steels,” Ph.D. Thesis, Mechanical Engineering Department, Punjab Technical University, Jalandhar, India.
3. Bala, N., Singh, H., and Prakash, S., (2009), “High Temperature Corrosion Behavior of Cold Spray Ni-20Cr Coating on Boiler Steel in Molten Salt Environment at 900ºC,” Journal of Thermal Spray Technology, Vol. 19, pp. 110-118.
4. Bala, N., Singh, H., Karthikeyan, J. and Prakash, S., (2012), “Performance of cold sprayed Ni-20Cr and Ni-50Cr coatings on SA 516 steel in actual industrial environment of a coal fired boiler,” Vol.14,pp. 568-580.
5. Bansal, P., Padture, N. P. and Vasiliev, A., (2003), “Improved interfacial properties of Al2O3-13wt%TiO2 plasma sprayed coatings derived from nanocrytalline powders”, Acta Materialia, Vol.51, pp.2959-2970.
6. Baskaran, T., & Arya, S. B., (2017), “Role of thermally grown oxide and oxidation resistance of samarium strontium aluminate based air plasma sprayed ceramic thermal barrier coatings”, Surface and Coatings Technology, 326, 299–309.
7. Brand, J., Gadow, R. and Killinger, A., (2004), “Application of diamond-like carbon coatings on steel tools in the production of precision glass components” Surface and Coatings Technology , Vol.180, pp. 213–217.
8. Cable, M., (1999), “Mechanization of Glass Manufacture” Journal of the American Ceramic Society, Vol.82, pp.1093–1112.
9. Callister, W.D., Rethwisch, D.G. and Balasubramaniam, R., (2017), Materials science and engineering, Chaudhary press, Delhi, India.
10. Chatha, S.S., Sidhu, H.S. and Sidhu, B.S., (2012A), “High temperature hot corrosion behaviour of NiCr and Cr_3C_2-NiCr coatings on T91 boiler steel in an

aggressive environment at 750°C," Surface Coating and Technology, Vol. 206, No. 19-20, pp. 3839-3850.

11. Chatha, S.S., Sidhu, H.S. and Sidhu, B.S., (2012B), "Characterisation and corrosion-erosion behaviour of carbide based thermal spray coatings," The Journal of Minerals and Materials Characterization and Engineering, Vol. 11, No. 6, pp. 569-586.
12. Chen, D., Jordan, E.H. and Gell, M., (2009), "Solution precursor high-velocity oxy-fuel spray ceramic coatings," Journal European Ceramic Society, Vol. 29, pp. 3349-3353.
13. Chen, S. F., Liu, S. Y., Wang, Y., Sun, X. G., Zou, Z. W., Li, X. W., & Wang, C. H., (2014), "Microstructure and properties of HVOF-sprayed NiCrAlY coatings modified by rare earth", Journal of Thermal Spray Technology, 23(5), 809–817.
14. Chidambaram, D., Clayton,C.R. and Dorfman, M.R., (2005), "Evaluation of the electrochemical behavior of HVOF-sprayed alloy coatings-II" Surface Coating and Technology, Vol. 192, No. 2-3, pp.178-283.
15. Choi, I.S. and Park, J.C., (2000), "The corrosion behaviour of TiAlN coatings prepared by PVD in a hydrofluoric gas atmosphere", Surface Coatings & Technology, Vol. 131, pp.383-385.
16. Cingi, M., Arisoy, F., Basman, G. and Sesen, K., (2002), "The effects of metallurgical structures of different alloyed glass mould cast irons on the mould performance" Materials Letters ,Vol. 55, pp. 360–363.
17. Delaunay, F., Berthier, C., Lenglet, M., & Lameille, J., (2000), "SEM-EDS and XPS Studies of the High Temperature Oxidation Behaviour of Inconel 718", Mikrochimica Acta, 132(2–4), 337–343.
18. Dent, A.H., Horlock A.J., Cartney D.G. M. and Harris S.J, (2001), "Microstructural characterisation of a Ni-Cr-B-C based alloy coating produced by high velocity oxy-fuel thermal spraying", Surface Coating and Technology,Vol. 139, pp. 244-250.
19. Espallargas, N., Berget, J., Guilemany, J.M., Benedetti, A.V. and Suegama, P.H.,

(2008), “Cr_3C_2–NiCr and WC–Ni thermal spray coatings as alternatives to hard chromium for erosion–corrosion resistance,” Surface Coating and Technology. Vol. 202, pp. 1405–1417.

20. Fedrizzi, L., Valentinelli, L., Rossi, S. and Segna, S., (2007), “Tribo Corrosion behavior of HVOF Cermet coatings,” Corrosion Science, Vol. 49, pp. 2781-2799
21. Feng, Q., Li, T., Teng, H., Zhang, X., Zhang, Y., Liu, C., & Jin, J., (2008), “Investigation on the corrosion and oxidation resistance of Ni-Al_2O_3nano-composite coatings prepared by sediment co-deposition”, Surface and Coatings Technology, 202(17), 4137–4144.
22. Firestone, G.C. and Yi, A.Y., (2005), **“**Precision compression moulding of glass micro lenses and micro lens arrays-an experimental study” Applied Optics, Vol. 29, pp. 6115-6122.
23. Gao, J., He, Y., & Wang, D., (2010), “Fabrication and high temperature oxidation resistance of ZrO_2/Al_2O_3micro-laminated coatings on stainless steel”, Materials Chemistry and Physics, 123(2–3), 731–736.
24. Ghaderi, A. R., Nili Ahmadabadi, M., & Ghasemi, H. M., (2003), “Effect of graphite morphologies on the tribological behavior of austempered cast iron”, Wear, 255(1–6), 410–416.
25. Ghriba, T., Tlilib, B., Nouveauc, C., Benlatrech, Y., Lambertin, M., Yacoubi, N. and Ennasr, M., (2009), “Experimental investigation of the mechanical micro structural and thermal properties of thin CrAIN layers deposited by PVD technique for various aluminium percentages” Physics Procedia, pp. 1327–1336.
26. Gil, L., and Staia, M.H., (2002), “Influence of HVOF parameters on the corrosion resistance of NiWCrBSi coatings” Thin Solid Films, Vol. 420 –421, pp. 446–454.
27. Goswami, D.Y., (2004), The CRC Handbook of Mechanical Engineering, CRC Press, New York, USA.
28. Grewal, H. S., Singh, H., & Agrawal, A., (2013a), “Microstructural and mechanical characterization of thermal sprayed nickel-alumina composite coatings”, Surface and Coatings Technology, 216, 78–92.

29. Grewal, H. S., Singh, H., & Agrawal, A., (2013b), "Understanding Liquid Impingement erosion behaviour of nickel-alumina based thermal spray coatings",Wear, 301(1–2), 424–433.
30. Griffith, J. D, (1975), United States Patent 1191, 5, 5–10.
31. Guilemany, J.M., De Paco, J.M., Miguel, J.R, Sanchez, J. and Smith, P., (1998), "Corrosion Resistance HVOF Coatings Based Upon TiC+ NiTiC and (Ti,W)C + Ni," Thermal Spray: Meeting the Challenges of the 21st, Century, C. Coddet, Ed., May 25-29, 1998 (Nice, France), ASM International, pp. 57-61.
32. Guilemany, J.M., Espallargas, N., Suegama, P.H. and Benedetti, A.V., (2006), "Comparative Study of Cr_3C_2-NiCr Coatings Obtained by HVOF and Hard Chromium Coatings," Corrosion Science, Vol. 48, pp. 2998-3013.
33. Hatate, M., Shiota, T., Takahashi, N., & Shimizu, K., (2001), "Influences of graphite shapes on wear characteristics of austempered cast iron", Wear, 250–251, 885–889.
34. Heath, G. R., Heimgartner, P., Irons, G., Miller, R. and Gustafsson, S., (1997), "An Assessment of Thermal Spray Coating Technologies for High Temperature Corrosion Protection," Material Science Forum, Vol. 251-54, pp. 809-816.
35. Hecht, R. L., Dinwiddie, R. B., & Wang, H., (1999), "Effect of graphite flake morphology on the thermal diffusivity of gray cast irons used for automotive brake discs", Journal of Materials Science, 34(19), 4775–4781.
36. Hemanth, J. (2000), "Wear characteristics of austempered chilled ductile iron" Materials and Design, Vol. 21, pp. 139-148.
37. Hidalgo, V. H., Varela J. B., Menéndeza A. C. and Martýnez S. P., (2001), "High temperature erosion wear of flame and plasma-sprayed nickel–chromium coatings under simulated coal-fired boiler atmospheres", Wear, Vol. 247, pp. 214–222.
38. Hidalgo, V. H., Varela, F. J. B. and Rico, E. F., (1997), "Erosion Wear and Mechanical Properties of Plasma-Sprayed Nickel- and Iron-Based Coatings Subjected to Service Conditions in Boilers," Tribology International, Vol. 30, No. 9, pp. 641-649.

39. Hidalgo, V. H., Varela, J. B., Calle, J. M. de la and Menendez, A. C., (2000), "Characterisation of NiCr Flame and Plasma Sprayed Coatings for Use in High Temperature Regions of Boilers," Surface Enginering, Vol. 16, No. 2, pp. 137-142.

40. Hock, M., Schaffer, E., Doll, W. and Klee, G., (2003), "Composite coating materials for the moulding of diffractive and refractive optical components of inorganic glasses "Surface and Coatings Technology, Vol. 163 –164 , pp. 689–694.

41. Hocking, M.G., (1993), "Coatings Resistant to Erosive/Corrosive and Severe Environments," Surface Coating and Technology., Vol. 62, pp. 460-466.

42. Holmberg, k. and Mathews, A., (2009), "Coatings tribology properties, mechanisms, techniques and applications in surface engineering" Elsevier Tribology and interface engineering series , Second edition , 56, Elsevier , Amsterdam, the Netherlands,2009.

43. Hones, P., Consiglio, R., Randall, N. and Levy, F., (2000), "Mechanical properties of hard chromium tungsten nitride coatings" Surface and Coatings Technology, Vol. 125, pp. 179–184.

44. Hu, H. X., Jiang, S. L., Tao, Y. S., Xiong, T. Y., & Zheng, Y. G., (2011), "Cavitation erosion and jet impingement erosion mechanism of cold sprayed Ni-Al_2O_3coating", Nuclear Engineering and Design, 241(12), 4929–4937.

45. Ishikawa, K., Seki, M. and Tobe, S., (1993), "Application of Thermal Spray Coatings to Prevent Corrosion of Construction in Japan," Proc. of the 5th Natioanal Thermal Spraying Conference, Anaheim, CA, USA, (1993), pp.679-684.

46. Istikamah, S., Fazira, M. F., & Talib, R. J., (2011), Atmospheric Plasma Spray of NiCrAlY Bond Coat with Different Feed Rates. Solid State Science and Technology, 19(1), 32–39.

47. Jiwang, Y., Takashi O., Tianfeng, Z. and Tsunemoto, K., (2009), "Precision machining of microstructures on electroless-plated NiP surface for moulding glass components", Journal of Materials Processing Technology, Vol.209, pp. 4802–4808.

48. Kalss, W., Reiter, A., Derfinger, V., Gey, C. and Endrino, J.L., (2006), "Modern coatings in high performance cutting applications", International Journal of Refractory Metals & Hard Materials, Vol. 24, pp 399-404.

49. Kamal, S. Jayaganthan, R., Prakash, S. and Kumar, S., (2008), "Hot Corrosion Behavior of Detonation Gun Sprayed Cr_3C_2-NiCr Coatings on Ni and Fe-based Superalloys in Na_2SO_4-60%V_2O_5 Environment at 900°C," Journal of Alloys and Compounds, Vol. 463, No. 1-2, pp. 358-372.

50. Kamal, S. Jayaganthan, R., Prakash, S. and Kumar, S., (2009A), "Evaluation of cyclic hot corrosion behaviour of detonation gun sprayed Cr_3C_2-25%NiCr coatings on nickel- and iron-based superalloys," Surface Coating and Technology., Vol. 203, pp. 1004-1013.

51. Karaoglanli, A. C., Altuncu, E., Ozdemir, I., Turk, A., & Ustel, F., (2011), "Structure and durability evaluation of YSZ+Al_2O_3composite TBCs with APS and HVOF bond coats under thermal cycling conditions", Surface and Coatings Technology, 205, S369–S373.

52. Kaur, M. and Singh, H., (2008), "A survey of the literature on the use of high velocity oxy-fuel spray technology for high temperature corrosion and erosion-corrosion resistant coatings," Anti-Corrosion Methods and Materials, Vol. 55, No.2, pp. 86–96.

53. Kaur, M., Singh, H. and Prakash, S., (2011), "Studies on Role of Detonation-Gun Sprayed WC-Co Coatings to Combat High Temperature Corrosion of Boiler Steel", International Journal of Surface Engineering & Materials Technology, Vol. 01, pp. 33-38.

54. Kaur, M., Singh, H. and Prakash, S., (2011), "Surface engineering analysis of detonation-gun sprayed Cr3C2–NiCr coating under high-temperature oxidation and oxidation–erosion environments" Surface & Coatings Technology ,Vol. 206,pp. 530–541.

55. Kaur, M., Singh, H. and Prakash, S., (2009A), "High Temperature Corrosion Studies of HVOF Sprayed Cr_3C_2-NiCr Coating on SAE-347H Boiler Steel,"

Journal of Thermal Spray Technology, Vol. 18, No. 4, pp. 619-632.

56. Kaur, M., Singh, H. and Prakash, S., (2011), "Surface engineering analysis of detonation-gun sprayed Cr_3C_2-NiCr coating under high-temperature oxidation and oxidation–erosion environments," Surface Coating and Technology., Vol. 206, pp. 530-541.
57. Kaur, M., Singh, H., & Prakash, S., (2011), Surface engineering analysis of detonation-gun sprayed Cr_3C_2-NiCr coating under high-temperature oxidation and oxidation-erosion environments. Surface and Coatings Technology, 206(2–3), 530–541.
58. Kaur, M., Singh, H., Singh, B. and Singh, B., (2009B), "Studies on the Sliding Wear Performance of Plasma Spray Ni-20Cr and Ni3Al Coatings," Journal of Thermal Spray Technology. Vol. 19, Nos. 1-2, pp. 3378-3383.
59. Kaur, N., Kumar, M., Sharma, S. K., Kim, D. Y., Kumar, S., Chavan, N. M.,Singh, H., (2015), "Study of mechanical properties and high temperature oxidation behavior of a novel cold-spray Ni-20Cr coating on boiler steels",Applied Surface Science, 328, 13–25.
60. Kaushal, G. Singh, H. and Prakash, S., (2011), "High Temperature Erosion-Corrosion Performance of HVOF Sprayed Ni-20Cr Coating in Actual Boiler Environment," Metallurgical and Materials Transactions. A, Volume 42,No. 7, pp. 1836-1846.
61. Kaushal, G. Singh, H. and Prakash, S., (2011), "High Temperature Corrosion Behavior of HVOF- Sprayed Ni-20Cr Coating on Boiler Steel in Molten Salt Environment at 900ºC," International Journal of Surface Science and Engineering, Vol. 5, No. 1, pp. 45-53.
62. Kaushal, G. Singh, H. and Prakash, S., (2011B), "Comparative High Temperature Analysis of HVOF Sprayed and Detonation Gun Sprayed Ni-20Cr Coating in Laboratory and Actual Boiler Environments," Oxidation of Metals, Volume 76, No.3-4, pp 169-191.
63. Kaushal, S., Gupta, D., & Bhowmick, H., (2017), "An approach for functionally

graded cladding of composite material on austenitic stainless steel substrate through microwave heating", Journal of Composite Materials, (Mmc), 2199831770597.

64. Khanna, A.S., (2002), "Introduction to High Temperature Oxidation and Corrosion," ASM International, Materials Park, Ohio.
65. Khanna, A.S., Kumari, S., Kanungo, S. and Gasser, A., (2009), "Hard Coatings Based on Thermal Spray and Laser Cladding," International Journal of Refractory Metals and Hard Materials, Vol. 27, pp. 485-491.
66. Kim, S., Cockcroft, S., L, Omran, A M. and Hwang, H., (2009), "Mechanical wear and heat exposure properties of compacted graphite cast iron at elevated temperatures' Journal of Alloys and Compounds, Vol. 487,pp. 253–257.
67. Kleer, G. and Doell, W., (1997), "Ceramic multilayer coatings for glass moulding applications" Surface and Coatings Technology, Vol. 94-95, pp. 647-651.
68. Koivuluoto, H., & Vuoristo, P., (2009), "Effect of ceramic particles on properties of cold sprayed Ni–20Cr + Al_2O_3 coatings", Journal of thermal spray technology, 18, 555–562.
69. Kong, G., Zhang, D., Brown, P.D., McCartney, D.G. and Harris, S.J., (2003), "Microstructural Characterisation of HVOF Thermally Sprayed Stellite 6," Mater. Sci. Technol., Vol. 19, pp.1003-1011.
70. Kuar, N., Kumar, M., Kumar, S., Joshi, S.V. and Singh, H., (2015), "Study of mechanical properties and high temperature oxidation behaviour of a novel cold-spray Ni-20Cr coatings on boiler steels", Applied surface science, Vol.328, pp. 13-25.
71. Kumar, M., Singh, H., Singh, N., & Joshi, R. S., (2015), "Erosion-corrosion behavior of cold-spray nanostructured Ni-20Cr coatings in actual boiler environment", Wear, 332–333, 1035–1043.
72. Labrecque, C., & Gagné, M., (1998), "Ductile Iron: Fifty Years of Continuous Development", Canadian Metallurgical Quarterly, 37(5), 343–378.
73. Lai, G Y, Pub. ASM International (1990) Chapter 3, 15.

74. Lee, C.H. and Min, K.O., (2000), "Effects of heat treatment on the microstructure and properties of HVOF-sprayed Ni-Cr-W-Mo-B alloy coatings", Surface Coating and Technology, Vol.132, pp. 49-57.
75. Lee, S.H., (2009), "High-Temperature Corrosion Phenomena in Waste-to-Energy Boilers," Ph.D Thesis, Gradual School of Arts and Sciences, Columbia University.
76. Lembke, M.I., Lewis, D.B. and Munz, W.D., (2000), "Localised oxidation defects inTiAlN/CrN superlattice structured hard coatings grown by cathodic arc/ unbalanced magnetron deposition on various substrate materials", Surface and Coatings Technology, Vol. 125, pp. 263–268.
77. Leushin, I.O. and Chistyakov, D.G., (2014), "Analysis of Cracking in Glass Moulds Made of Cast Iron" Russian Metallurgy (Metally), Vol.9, pp. 768–771
78. Levy, A.V., (1993), "The Erosion-Corrosion of Tubing Steels in Combustión Boiler Environments," Corrosion Science, Vol. 35, Nos. 5-8, pp. 1035-1043.
79. Li, C.J., Li, W.Y., (2003), "Effect of sprayed powder particle size on the oxidation behavior of MCrAlY materials during high velocity oxygen-fuel deposition", Surface Coating and Technology Vol.162, pp. 31–41.
80. Li, G.C., Li, C.J., Wang, Y.Y. and Li, W.Y., (2007), "Erosion Performance of HVOF sprayed Cr_3C_2-NiCr coatings", Journal of Thermal Spray Technology, Vol. 16, No. 4,557-565.
81. Liang, B. and Ding, C., (2005), "Thermal shock resistance of nano-structured and conventional zirconia coatings deposited by atmospheric spraying", Surface & Coating Technology journal, Vol.197, pp.85-192.
82. Limarga, A. M., Widjaja, S., & Yip, T. H., (2005), "Mechanical properties and oxidation resistance of plasma-sprayed multilayered Al_2O_3/ZrO_2thermal barrier coatings", Surface and Coatings Technology, 197(1), 93–102.
83. Lin, M.-B., Wang, C.-J., & Volinsky, A. A., (2011), "High Temperature Oxidation Behavior of Flake and Spheroidal Graphite Cast Irons", Oxidation of Metals, 76(3–4), 161–168.

84. Lin, X., Zeng, Y., Ding, C. and Zhang, P., (2004), "Effects of temperature on tribological properties of nanostructured and conventional Al_2O_3-3wt% TiO_2 coatings", Wear, Vol.256, pp. 1018-1025.
85. Liscano, S., Gil, L., Leon, O.A., Cruz, M. and Staia, MH., (2006), "Corrosion performance of duplex treatments based on plasma nitriding and PAPVD TiAlN coating", Surface Coatings & Technology, Vol. 201, pp. 4419-4423.
86. Liu, Y., Fischer, T. E. and Dent, A., (2003), "Comparison of HVOF and plasma-sprayed alumina/titania coatings-microstructure, mechanical properties and abrasion behavior", Surface Coating and Technology Vol. 167, pp. 68–76.
87. Lugschider, E., Herbst, C. and Zhao, L., (1998), "Parameter Studies on High Velocity Oxy-Fuel Spraying of MCrAIY Coatings," Surface Coating and Technology, Vol. 108-109, pp. 16-23.
88. Lyphout, C., Fasth, A., & Nylen, P., (2014), "Mechanical property of HVOF inconel 718 coating for aeronautic repair",Journal of Thermal Spray Technology, 23(3), 380–388.
89. Lyphout, C., Nylén, P., & Östergren, L., (2011), "Relationships between process parameters, microstructure, and adhesion strength of HVOF sprayed IN718 coatings", Journal of Thermal Spray Technology, 20(1–2), 76–82.
90. Lyphout, C., Nylén, P., Manescu, A., & Pirling, T., (2008), "Residual stresses distribution through thick HVOF sprayed inconel 718 coatings", Journal of Thermal Spray Technology, 17(5–6), 915–923.
91. Ma, K.J., Chien, H.H, Chuan, W.H, Chao, C. L. and Hwang, K.C., (2008), "Design of Protective Coatings for Glass Lens Moulding" Key Engineering Materials, Vol. 364-366, pp. 655-661.
92. Mahesh, R.A., Jayaganthan, R. and Prakash, S., (2009A), "Microstructural characterization and hardness evaluation of HVOF sprayed Ni–5Al coatings on Ni- and Fe-based superalloys," Journal of Material Processing and Technology, Vol. 209, pp. 3501-3510.

93. Mahesh, R.A., Jayaganthan, R., Prakash, S., (2009B), “Microstructural characteristics and mechanical properties of HVOF sprayed NiCrAl coating on superalloys,” Journal of Alloys and Compounds.,Vol. 468, pp. 392-405.

94. Mashloosh, K.M., (2015), “Wear resistance of different types of cast iron used in glass blow mould” Diyala Journal of Engineering Sciences, Vol. 08, pp. 3-12.

95. Masud, J., Yan, J., Zhou, T., Kuriyagawa, T. and Fukase, Y., (2011), “Thermally induced atomic diffusion at the interface between release agent coating and mould substrate in a glass moulding press” Journal of physics, Vol. 44, pp. 215-302.

96. Matthews, S., Hyland, M. and James, B., (2004), “Long-Term Carbide Development in High-Velocity Oxygen Fuel/High-Velocity Air Fuel Cr_3C_2-NiCr Coatings Heat Treated at 900°C,” Journal of Thermal Spray Technology, Vol. 13, No. 4, pp. 526-536.

97. Matthews, S.J., James, B.J. and Hyland, M.M., (2007), “Microstructural influence on erosion behaviour of thermal spray coatings,” Material Characterization, Vol. 58, pp. 59-64.

98. Mayrhofer, P.H., Kunc, F., Musil, J. and Mitter, C., (2002), “A comparative study on reactive and non-reactive unbalanced magnetron sputters deposition of TiN coatings” Thin Solid Films, Vol. 415, pp. 151–159.

99. Mayrhofer, P.H., Tischler, G. and Mitter, C., (2001), “Microstructure and mechanical/thermal properties of Cr-N coatings deposited by reactive unbalanced magnetron sputtering” Surface and Coatings Technology, Vol.142-144, pp. 78-84.

100. Metals Handbook, (1961), “Properties and Selection of Metals, 8th Edition,” Vol. 1, ASM Publication, Metals Park Ohio.

101. Miguel, J. M., Guilemany, J. M., & Vizcaino, S., (2003), “Tribological study of NiCrBSi coating obtained by different processes”, Tribology International, 36(3), 181–187.

102. Miguel, J.M., Guilemany, J.M., Mellor, B.G. and Xu, Y.M., (2003A), “Acoustic emission study on WC–Co thermal sprayed coatings,” Material Science Engineering A, Vol. 352, No. 1-2, pp. 55-63.

103. Mishra, S.B., Prakash, S. and Chandra, K., (2006),"Studies on erosion behaviour of plasma sprayed coatings on a Ni-based superalloy", Wear, Vol.260, pp.422-432.

104. Muhammad, R., Wahab, N. A., & Rakik, R., (2017), "Study on thermal behavior of Inconel 718 thermal cyclic behaviour",Wear,12(6), 1915–1921.

105. Nicholls, J.R., (2000), "Designing Oxidation-Resistant Coatings," JOM, pp.28-35.

106. Nishiyama, S., Takahashi, E., Iwamot, Y., Ebe, A., Kuratani, N. And Ogata, K., (1996), "Boron nitride hard coatings by ion beam and vapour deposition" Thin Solid Films, Vol. 281-282, pp. 327-330.

107. Pawlowski, L., (1995), "The Science and Engineering of Thermal Spray Coatings," Wiley, NewYork, 1995.

108. Prakash, S., Puri, D. and Singh H., (2005), "Hot Corrosion Behavoiur of Plasma Sprayed Coatings on a Ni-Based Superalloy in Na_2SO_4 -60% V_2O_5 Environment, "International Surface journal, Vol. 45, No. 6, pp. 886-895.

109. Prakash, S., Singh, S., Sidhu, B. S. and Madeshia, A., (2001), "Tube Failures in Coal Fired Boilers," Proc. National Seminar on Advances in Material and Processing, 9-10th Nov., IIT, Roorkee, India, pp. 245-53.

110. Prasad, A. and Gupta, D., (2013), "Microwave Cladding-Emerging innovative cladding process" Proc. Of Int. Conf. on Emerging Trends in Engineering and Technology, pp.506-510.

111. Praveen, A. S., Sarangan, J., Suresh, S., & Siva Subramanian, J., (2015), "Erosion wear behaviour of plasma sprayed NiCrSiB/Al_2O_3 composite coating.", International Journal of Refractory Metals and Hard Materials, 52, 209–218.

112. Priyantha, N., Jayaweera, P., Sanjurjo, A., Lau, K. and K. Krish., (2003), "Corrosion-resistant metallic coatings for applications in highly aggressive environment", Surface & Coating Technology, Vol. 163-164, pp. 31-36.

113. Priyantha, N., Jayaweera, P., Sanjurjo, A., Lau, K., Lu, F. and Krist, K., (2003), "Corrosion-Resistant Metallic Coatings for Applications in Highly Aggressive Environments," Surface Coating and Technology.Vol. 163-64, pp. 31-36.

114. Provot, X., Burlet, H., Vardayoulias, M., Jeandin, M. and Richard, C., (1993), "Comparative Studies of Microstructures, Residual Stress Distributions and Wear Properties for HVOF and APS WC-Co Coatings of Ti6Al4V," Proc. NTSC, Anahiem, USA, pp. 159-166.

115. Ramesh, C. S., Devaraj, D. S., Keshavamurthy, R., & Sridhar, B. R., (2011), "Slurry erosive wear behaviour of thermally sprayed Inconel-718 coatings by APS process", Wear, 271(9–10), 1365–1371.

116. Rieser, D., Spie, G. and Manns, G., (2008), "Investigations on glass-to-mould sticking in the hot forming process" Journal of Non-Crystalline Solids, Vol.354, pp. 1393–1397.

117. Roy, M., Pauschitz A., Polak R. and Franek, F., (2006), "Comparative evaluation of ambient temperature friction behaviour of thermal sprayed Cr_3C_2–25(Ni-20Cr) coatings with conventional and nano-crystalline grains," Tribology International, Vol.39, pp. 29-38.

118. Roy, M., Pauschitz A., Wernisch J. and Franek, F., (2004), "The influence of temperature on the wear of Cr_3C_2–25(Ni20Cr) coating comparison between nanocrystalline grains and conventional grains," Wear, Vol.257, pp. 799-811

119. Sarhadi, A., Hattel, J.H. and Hansen, H.N., (2014), "Evaluation of the visco-elastic behaviour and glass/mould interface friction coefficient in the wafer based precision glass moulding" Journal of Materials Processing Technology, Vol. 214, pp. 1427–1435.

120. Sidhu, B.S. and Prakash, S., (2003), "Evaluation of the corrosion behaviour of plasma sprayed Ni_3Al coatings on steel in oxidation and molten salt environments at 9000C", Surface & coatings technology, Vol.166, pp. 89-100.

121. Sidhu, B.S. and Prakash, S., (2003), "Evaluation of the Corrosion Behaviour of Plasma-Sprayed Ni_3Al Coatings on Steel in Oxidation and Molten Salt Environment at 9000C," Surface Coating and Technology,Vol. 166, No. 1, pp. 89-100.

122. Sidhu, B.S. and Prakash, S., (2006G), "Evaluation of the Behavior of Shrouded Plasma Spray Coatings in the Platen Superheater of Coal-Fired Boilers," Metals and Material Transactio A, Vol. 37a, pp. 19-27.
123. Sidhu, B.S. and Prakash, S., (2006H), "Evaluation of the Behavior of Shrouded Plasma Spray Coatings in the Platen Superheater of Coal-Fired Boilers," Metal Material Transaction A, Vol. 37A, pp. 1927-1936.
124. Sidhu, B.S., Puri, D. and Prakash, S., (2005A), "Mechanical and Metallurgical Properties of Plasma Sprayed and Laser Remelted Ni-20Cr and Stellite-6 Coatings," Journal of Material Processing and Technology., Vol. 159, No. 3, pp. 347-355.
125. Sidhu, H.S., Singh, B.S. and Prakash, S., (2006D), "The Role of HVOF Coatings in Improving Hot Corrosion Resistance of ASTM-SA210 GrA1 Steel in the Presence of Na_2SO_4–V_2O_5 Salt Deposits," Surface Coating and Technology,Vol. 200, No. 18-19, pp. 5386-5394.
126. Sidhu, T.S., Agarwal, R.D. and Prakash, S., (2006E), "Studies of the metallurgical and mechanical properties of high velocity oxy-fuel sprayed stellite-6 coatings on Ni- and Fe-based superalloys," Surface Coating and Technology Vol. 201, pp. 273-281.
127. Sidhu, T.S., Agarwal, R.D., Prakash, S., and Bhagat, R., (2009), "Erosion-corrosion behaviour of Ni-based superalloy Superni-75 in the real service environment of the boiler", Surface Coating and Technology, Vol. 34, No. 2, pp 299-307.
128. Sidhu, T.S., Agrawal, R.D. and Prakash, S., (2005B), "Hot corrosion of some superalloys and role of high-velocity oxy-fuel spray coatings—A Review," Surface Coating and Technology, Vol. 198, pp. 441- 446.
129. Sidhu, T.S., Prakash, S. and Agrawal, R.D., (2006), "Hot corrosion performance of a NiCr coated Ni-based alloy", Scripta Materialia, Vol.55, pp.179-182.
130. Sidhu, T.S., Prakash, S. and Agrawal, R.D., (2006A), "Performance of a High Velocity Oxy-fuel Sprayed Coatings on a Fe-Based Superalloy in Na_2SO_4-60%V_2O_5 Environment at 900 ºC, "Part I: Characterisation of the Coatings," Journal of Material Engineering and Performance, Vol. 15, No. 1, pp. 122 -129.

131. Sidhu, T.S., Prakash, S. and Agrawal, R.D., (2006B), "Characterizations and Hot Corrosion Resistance of Cr_3C_2-NiCr Coating on Ni-Base Superalloys in an Aggressive Environment," Journal of Thermal Spray Technology, Vol. 15, No. 4, pp. 811-816.

132. Sidhu, T.S., Prakash, S. and Agrawal, R.D., (2006C), "Evaluation of hot corrosion resistance of HVOF coatings on a Ni-based superalloy in molten salt environment," Material Science Engineering. A, Vol. 430, pp. 64-78.

133. Sidhu, T.S., Prakash, S. and Agrawal, R.D., (2006F), "Hot Corrosion Behaviour of HVOF Sprayed NiCrBSi Coatings on Ni- and Fe- Base Superalloys in Na_2SO_4-60%V_2O_5 Environment at 900°C," Acta Materialia, Vol. 54, No. 3, pp. 773-784.

134. Sidky, P.S. and Hocking, M.G., (1999), "Review of Inorganic Coatings and Coating Processes For Reducing Wear and Corrosion," British Corrosion Journal, Vol. 34, No. 3, pp. 171-183.

135. Singh, H., Bala, N., Kaur, N., Sharma, S. K., Kim, D. Y., & Prakash, S., (2015), Effect of additions of TiC and Re on high temperature corrosion performance of cold sprayed Ni-20Cr coatings. Surface and Coatings Technology, 280, 50–63.

136. Singh, H., Prakash, S., Puri, D. and Phase, D.M., (2006A), "Cyclic Oxidation Behavior of Some Plasma-Sprayed Coatings in Na_2SO_4-60%V_2O_5 Environment," Journal of Material Engineering and Performance, Vol. 15, No. 6, pp. 729-741.

137. Singh, H., Puri, D. and Prakash, S., (2005A), "Some Studies on Hot Corrosion Performance of Plasma Sprayed Coatings on a Fe-based Superalloy," Surface Coating and Technology, Vol. 192, No. 1, pp. 27-38.

138. Singh, H., Puri, D. and Prakash, S., (2005B), "Corrosion Behavior of Plasma-Sprayed Coatings on a Ni-Base Superalloy in Na_2SO_4-60 Pct V_2O_5 Environment at 900 °C," Metallic Material Transaction A, Vol. 36A, pp. 1007-1015.

139. Speidel, M. O., Hyatt, M. V, Speidel, M. O., & Hyatt, M. V., (2005), High-strength aluminum alloys.

140. Sreedhar, G., Alam, M. M., & Raja, V. S., (2009), "Hot corrosion behaviour of plasma sprayed YSZ/Al_2O_3 dispersed NiCrAlY coatings on Inconel-718 superalloy.

Surface and Coatings Technology, 204(3), 291–299.

141. Stliner, R., (1990), “Properties and selection of Irons, Steels and high performance Alloys” ASM Handbook, Ohio, USA.

142. Sundararajan, G. Sen, D. and Sivakumar., G., (2005), “The Tribological Behaviour of Detonation Sprayed Coatings: The Importance of Coating Process Parameters”, Wear, Vol. 258, pp.377-391.

143. Sundararajan, T., Kuroda, S., Itagaki, T. and Abe F., (2003A), “Steam Oxidation Resistance of Ni-Cr Thermal Spray Coatings on 9Cr-1Mo Steel. Part 1: 80Ni-20Cr,” ISIJ Int., Vol. 43, No.1, pp. 95-103.

144. Sundararajan, T., Kuroda, S., Itagaki, T. and Abe, F., (2003B), “Steam Oxidation Resistance of HVOF Thermal Sprayed Ni-Cr Coatings,” Thermal Spray 2003: Advancing the Science & Applying the Technology, (Ed.) C, Moreau and B. Marpie, pp. 495-502.

145. Sundararajan, T., Kuroda, S., Itagaki, T. and Abe, F., (2004), “Behaviour of Mn and Si in the Spray Powder during Steam Oxidation of Ni-Cr Thermal Spray Coatings,” ISIJ Int., Vol. 44, No.1, pp. 139-144.

146. Taheri, M., Valefi, Z., & Zangeneh-Madar, K., (2012), “Influence of HVOF process parameters on microstructure and bond strength of NiCrAlY coatings”, Surface Engineering, 28(4), 266–272.

147. Tellkamp, V. L., Lau, M. L., Fabel, a., & Lavernia, E. J., (1997), “Thermal spraying of nanocrystalline inconel 718”, Nanostructured Materials, 9(1–8), 489–492.

148. Thakur, L., & Arora, N., (2013), “A comparative study on slurry and dry erosion behaviour of HVOF sprayed WC-CoCr coatings”, Wear, 303(1–2), 405–411.

149. Thomas, A., El-Wahabi, M., Cabrera, J. M., & Prado, J. M., (2006), “High temperature deformation of Inconel 718”, Journal of Materials Processing Technology, 177(1–3), 469–472.

150. Tsai, Y.C., Hung, C., Hung, J.C., (2008), “Glass material model for the forming stage of the glass moulding process” Journal of materials processing technology, Vol. 201, pp. 751–754.

151. Uusitalo, M.A., Vuoristo, P.M.J., Mantyla, T.A., (2002), “High temperature corrosion of coatings and boiler steels in reducing chlorine-containing atmosphere,” Surface Coating and Technology, Vol. 161, pp. 275-285.

152. Viskanta, R. and Lim, J.M., (2001), “Theoretical Investigation of Heat Transfer in Glass Forming” Journal of the American Ceramic Society, Vol. 84, pp.2296–302.

153. W.Y. Li, Zhang, C., H. Liao, J. Li, Coddet, C., (2008), “Characterizations of cold-sprayed nickel–alumina composite coating with relatively large nickel-coated alumina powder”, Surface and coating technology, 202, 4855–4860.

154. Wadsworth, I., Smith, I.J., Donohue, L.A. and Miinz, W.D., (1997), “Thermal stability and oxidation resistance of TiAlNKrN multilayer coatings” Surface and Coatings Technology, Vol. 94-95, pp.315-321.

155. Wang, B. Q. and Shui, Z.R., (2002), “The hot erosion behavior of HVOF chromium carbide-metal cermet coatings sprayed with different powders,” Wear, Vol. 253, pp. 550-557.

156. Wang, B., & Lee, S. W., (2000), “Erosion-corrosion behaviour of HVOF NiAl-Al_2O_3 intermetallic-ceramic coating”, Wear, 239(1), 83–90.

157. Wang, B.Q. and Shui, Z.R., (2003), “Hot erosion behaviour of carbide-metal composite coatings”, Journal of Material Proceeding Technology, Vol. 143-144, pp. 87-92.

158. Wang, B.Q. and Verstak, A., (1999), “Elevated Temperature Erosion of HVOF Cr_3C_2/ TiC- NiCrMo Cermet Coating,” Wear, Vol. 233-235, pp. 342-351.

159. Wang, C.J. and Lin, J.S., (2002), “The oxidation of MAR M247 superalloy with Na_2SO_4 coating,” Materials Chemistry and Physics, Vol.76, pp. 123-129.

160. Wang, H.T., Ji G.C., Chen Q.Y., Du X. F. and Fu W., (2011), “The Microstructure and Erosion Wear Performance of HVOF-Sprayed Cr_3C_2-NiCr Coatings with Different Feedstock Powder,” Advanced Materials Research, Vol. 228-229, pp. 809-812.

161. Weck, M. Winterschlade, M. Pfeifer, T. Dorner, D. Brinksmeier, E. Autschbach, L. Riemer, O., (2005), “Manufacturing of Optical Molds using an Integrated Simulation and Measurement Interface” Proc. of SPIE,5252.

162. Yang, G.J., Li, C.J., Zhang, S.J., Li, C.X., (2008), “High-Temperature Erosion of HVOF Sprayed Cr_3C_2-NiCr Coating and Mild Steel for Boiler Tubes,” Journal of Thermal Spray Technology, Vol.17, No.5-6, pp.782-787.

163. Yang, Q., Senda,T. and Ohmori, A., (2003), “Effect of carbide grain size on microstructure and sliding wear behavior of HVOF-sprayed WC–12% Co coatings,” Wear, Vol. 254, No. 1-2, pp. 23-34.

164. Yin, B., Liu, G., Zhou, H., Chen, J. and Yan, F., (2010), “Sliding wear behavior of HVOF sprayed Cr_3C_2-NiCr/CeO_2 Composite coatings at elevated temperature upto 8000C,” Tribology Letter, Vol.37, pp. 463-475.

165. Zafar, S. and Sharma, A.K., (2016), “Abrasive and erosive wear behaviour of nanometric WC–12Co microwave clads”, Wear, Vol.46-47, pp-29-45.

166. Zafar, S., & Sharma, A. K., (2016), “Abrasive and erosive wear behaviour of nanometric WC-12Co microwave clads”, Wear, 389–400, pp-145-169.

167. Zhang, Y., Chen, Y., He, R., & Shen, B., (1993), “Investigation of tribological properties of brake shoe materials - phosphorous cast irons with different graphite morphologies”, Wear, 166(2), 179–186.

168. Zhao, L. and Lugscheider, E., (2002 B), “Influence of the spraying processes on the properties of 316L stainless steel coatings”, Surface Coating and Technology, Vol. 162, pp. 6-10.

169. Zhao, L. and Lugscheider, E., (2002A), “High Velocity Oxy-Fuel Spraying of a NiCoCrAlY and an Intermetallic NiAl-TaCr Alloy,” Surface Coating and Technology ,Vol. 149, pp. 230-235.

170. Zhao, W.M., Wang, Y., Dong, L.X., Wu, K.Y. and Xue, J., (2005), “Corrosion Mechanism of NiCrBSi Coatings Deposited by HVOF,” Surface Coating and Technology ,Vol. 190, pp. 293-298.

171. Zhao, W.M., Wang, Y., Han, T., Wu, K.Y. and Xue, J., (2004), "Electrochemical Evaluation of Corrosion Resistance of NiCrBSi Coatings Deposited by HVOF," Surface Coating and Technology,Vol. 183, pp. 118-125.
172. Zhong, D., Mateeva, E., Dahan, I., Moore, J., Mustoe, G.W., Ohno, T., Disamc, J. And Thiel, S. (2000), "Wettability of NiAl, Ni-Al-N, Ti-B-C, and Ti-B-C-N films by glass at high temperatures" Surface and Coatings Technology, Vol. 133-134,8-12.
173. Sharma AK and Krishnamurthy R (2010), "Sliding wear characterization of microwave-glazed plasma-sprayed ceramic composites", Proc.Inst. Mech. Eng. 224 497-51.
174. Zafar S and Sharma AK (2014), "Development and characterisations of WC– 12Co microwave clad", Materials Characterization. Vol. 96 pp241-249.
175. Zafar S and Sharma AK (2016), Investigations on flexural performance and residual stresses in nanometric WC-12Co microwave clads, Surface Coating and Technology, Vol. 291 pp.413-22.
176. Sidhu T S, Prakash S and Agrawal R D 2005 State of the art of HVOF coating investigations: a review Mar. Technol. Soc. J. 39 53–64.
177. Lee C H and Min K O 2000 Effects of heat treatment on the microstructure and properties of HVOF-sprayed Ni-Cr-W-Mo-B alloy coatings Surf. Coat. Technol. 132 49–57.
178. Guilemany J M, Fernandez J and Delgado J 2001 Influence of thermal treatments in the corrosion behaviour of HVOF Cr_3C_2-NiCr coatings ed C C Berndt and K A Khor Thermal Spray 2001: New Surfaces for a New Millennium, (ASM International: Materials Park, Ohio) 1165-1169.
179. Guilemany J M, Miguel J M, Vizcaıno S, Lorenzana C, Delgado J and Sanchez J 2002 Role of heat treatments in the improvement of the sliding wear properties of Cr_3C_2–NiCr coatings Surf. Coat. Technol. 157 207-13.

180. Praveen A S, Sarangan J, Suresh S and Subramanian J S 2015 Erosion wear behaviour of plasma sprayed NiCrSiB/Al_2O_3 composite coating Int. J. Refract. Met. Hard Mater 52 209-218.
181. Grewal H S, Singh H and Agarwal A 2013 Understanding liquid impingement erosion behaviour of nickel-alumina based thermal spray coatings Wear 301 424-433.
182. Bala N, Singh H and Prakash S 2017 Performance of cold sprayed Ni based coatings in actual boiler environment Surf. Coat. Technol. 318 50-61.
183. Afzal M, Ajmal M, Khan A N, Hussain A and Akhter R 2014 Surface modification of air plasma spraying WC–12% Co cermet coating by laser melting technique Opt. Laser Technol. 56 202-206.
184. Sidhu B S, Puri D and Prakash S 2005 Mechanical and metallurgical properties of plasma sprayed and laser remelted Ni-20Cr and stellite-6 coatings J. Mater. Process. Technol. 159 347-355.
185. Zafar S and Sharma A K 2017 Microstructure and mechanical properties of microwave post-processed Ni coating J. Mater. Eng. Perform. 26 1382-1390.

LIST OF PUBLICATIONS

1. **K. Sunitha** and H. Vasudev, "A short note on the various thermal spray coating processes and effect of post-treatment on Ni-based coatings," Materials Today: Proceedings, Volume 50, Part 5, 2022, Pages 1452-1457.**(Elsevier, Scopus Indexed).**
   a. https://doi.org/10.1016/j.matpr.2021.09.017

Contents lists available at ScienceDirect

Materials Today: Proceedings

journal homepage: www.elsevier.com/locate/matpr

A short note on the various thermal spray coating processes and effect of post-treatment on Ni-based coatings

Sunitha K., Hitesh Vasudev *

School of Mechanical Engineering, Lovely Professional University, Phagwara, Punjab 144411, India

ARTICLE INFO

Article history:
Received 15 August 2021
Received in revised form 29 August 2021
Accepted 2 September 2021
Available online xxxx

Keywords:
HVOF
Cold spray
Thermal spray
Flame spray
Arc spray
Post heat treatment

ABSTRACT

In the fabrication of equipment and device components that require surface qualities such as corrosion, oxidation and wear resistance, metal surface coating is an efficient and secure method. The main purpose of the coating application could be decorative, functional, or both. Functional coating can be used forimproving surface properties for example wear resistance, oxidation, corrosion, and adhesion. In contrast, cosmetic coatings, such as paints by designers, have been applied to render the product/material more desirable. Nowadays, various coating methods are being implemented to obtain the required practical or cosmetic properties. Some of the most effective and desirable approaches for preserving/protecting fresh machine parts from tear, heat corrosion and oxidation is the thermal spray coating technique. A concise description of the various spraying methods, their basic concepts, disadvantages and implementations is included in this article. In addition to these characteristics, the properties of the coating processes and the various methods used to avoid corrosion are easily identified.

Selection and peer-review under responsibility of the scientific committee of the 2nd International Conference on Functional Material, Manufacturing and Performances

LOVELY FACULTY OF TECHNOLOGY AND SCIENCES

[Under the Aegis of Lovely Professional University, Jalandhar-Delhi G.T. Road, Phagwara (Punjab)]

Certificate No. 233256

Certificate of Presentation

This is to certify that Dr./Mr./Ms. **K.Sunitha** *has Authored/Presented research paper titled* **A short note on the various thermal spray coating processes and effect of post treatment of Ni-based coatings**

in **"2nd International Conference on Functional Materials, Manufacturing and Performances (ICFMMP - 2021)"** *held on 17th to 18th September, 2021 organized by School of Mechanical Engineering at Lovely Professional University, Punjab.*

Date of Issue : 01-10-2021
Place of Issue: Phagwara (India)

Prepared by (Administrative Officer-Records) | Convenor | Conference Chairman

2. **K. Sunitha** and H. Vasudev (2022). Microsrtructural and Mechanical Characterization of HVOF-Sprayed Ni-Based Alloy Coating. *International Journal of Surface Engineering and Interdisciplinary Materials Science (IJSEIMS), 10*(1), 1-9. http://doi.org/10.4018/IJSEIMS.298705 **(IGI Global, Scopus Indexed).**

International Journal of Surface Engineering and Interdisciplinary Materials Science
Volume 10 • Issue 1

Microsrtructural and Mechanical Characterization of HVOF-Sprayed Ni-Based Alloy Coating

Sunitha K, Lovely Professional University, India
Hitesh Vasudev, Lovely Professional University, India*
https://orcid.org/0000-0002-1668-8765

ABSTRACT

The various engineering components works under aggressive environments include the furnace parts, sliding parts in lathe machine, and exhaust manifolds. Cast iron is used in these applications, and the important intention of this research work is to study enhancing the useful period of life. HVOF (high velocity oxy-fuel) sprayed Alloy-718 coatings on cast iron were analysed. Coatings were characterised by field emission scanning electron microscopy (FE-SEM), optical microscope (OM), and x-ray diffraction for its microstructural analysis. Energy dispersive spectroscopy (EDS) of the bare and coated samples was used to confirm the elemental details of the powder and the coating. Porosity measurements were taken and showed 1.6% for Alloy-718 coating. Microhardness investigation was conducted for the Alloy-718 coating, and it was resulted as 560±20 HV. The bare material has a hardness of 225±10, and there is a substantial difference of hardness found as 2.5 times higher. The fracture toughness was found to be 4.0 MPa.m1/2.

KEYWORDS

Alloy-718, HVOF (High Velocity Oxy-Fuel), Thermal Spray Coatings

3. **K. Sunitha** and H. Vasudev (2022). Study of sliding wear and erosion wear of HVOF sprayed alloy 718 and Al_2O_3 composite coating on GCI substrate, National conference on trends in science, engineering and management, Gulzar group of Institutions, Ludhiana, 31st May 2022.

4. **K. Sunitha** and H. Vasudev (2022). Study of sliding wear and erosion wear of HVOF sprayed alloy 718 and Al_2O_3 composite coating on GCI substrate, 3rd International conference on Functional, Manufacturing and Performances (ICFMMP-2022, Lovely Professional University, Punjab 29-30th July, 2022.

LOVELY PROFESSIONAL UNIVERSITY
Transforming Education Transforming India

Certificate No.253352

Certificate of Presentation

This is to certify that **Dr./Mr./Ms. Sunitha.K** of **School of Mechanical Engineering, Lovely Professional University- Phagwara** has presented a paper on **Study of Sliding Wear and Erosion wear of HVOF sprayed Alloy 718 and Al2O3 composite coating on GCI substrate** in the **"3rd International Conference on Functional Materials, Manufacturing and Performances (ICFMMP-2022)"** held on July29-30th, 2022, organized by **Division of Research and Development, Lovely Professional University, Punjab.**

Date of Issue: 30-08-2022
Place: Phagwara (Punjab), India

Prepared by (Administrative Officer-Records) | Dr. Hitesh Vasudev, Convenor | Dr. Pranav Kumar Prabhakar, Organizing Secretary | Dr. Chander Prakash, Conference Secretary

DSIR | CSIR-CSIO | SERB INDIA | MINISTRY OF SCIENCE AND TECHNOLOGY